TRACE AMINE-ASSOCIATED RECEPTOR 1 AS A NOVEL IMMUNOMODULATORY TARGET IN MULTIPLE SCLEROSIS

by

David A. Barnes

A dissertation submitted to the School of Graduate Studies in partial fulfillment of the requirements for the degree of Master of Science in Biochemistry

Department of Biochemistry

Memorial University of Newfoundland

August 2022

St. John's Newfoundland

ABSTRACT

TAAR1 is a previously established neuroregulator with emerging evidence suggesting a role in modulation of the immune response. Multiple sclerosis is an immune-mediated demyelinating disease of the central nervous system (CNS). This study investigated expression of TAAR1 in immune cells relevant to MS pathophysiology in both the periphery and CNS of MS patients. RT-qPCR analyses of TAAR1 mRNA levels in peripheral immune cells from MS patients shared a statistically significant decrease in TAAR1 mRNA in MS patient monocytes compared to controls. TAAR1 expression at the protein-level was visualized in both peripherally-derived and CNS-resident macrophages bordering an MS lesion. Additionally, this study attempted to characterize a function of TAAR1 within the immune system that is relevant to MS neuroinflammation. Effects of TAAR1 agonist treatment on cytokine secretion and on the metabolic profile of pro-inflammatory macrophages from the periphery indicated a potential anti-inflammatory function, however, TAAR1 agonists had no effect on cytokine secretion from macrophages resident to the CNS. This study effectively demonstrates the potential for a novel link between TAAR1 and MS pathophysiology and establishes critical preliminary research towards elucidating the function of TAAR1 in peripheral and CNS-resident macrophages.

Keywords: Multiple sclerosis; neuroinflammation; trace amine-associated receptor 1; trace amines; cytokine

GENERAL SUMMARY

Multiple sclerosis (MS) is a disease where a person's immune cells attack the nerve cell connections in their brain, leading to impaired muscle, cognitive, and sensory function. There is currently no cure for MS. Trace amines are naturally occurring compounds found in the body at very low levels. For the body to use these compounds, cells must detect and respond to their presence. Proteins present in cells that detect compounds and cause a response are known as receptors. In certain cells throughout the body a specific receptor known as trace amine associated receptor one, or TAAR1, is responsible for detecting trace amines. TAAR1 influences the release of hormones, blood sugar levels, mood states, and has recently been suggested to play a role in how the immune system responds. This project investigated whether TAAR1 plays a role in causing MS and if drugs that interact with TAAR1 can help people with MS.

ACKNOWLEDGEMENTS

First and foremost, I would like to acknowledge my co-supervisors, Dr. Mark D. Berry and Dr. Craig S. Moore for their trust, guidance, patience, and endless support throughout the project. Both went out of their way to answer every question and offer expert critique, and in turn, foster an excellent learning environment for me. Additionally, I would like to thank my supervisory committee members, Dr. Sherri L. Christian and Dr. Rodney S. Russell, for their continuous advice and constructive criticism. From my first day in the lab, to my thesis revisions, I can confidently say that the time spent on this project were some of the best years of my life and because of the world-class supervision I received, I finish the program not only a better scientist, but a better person in general.

Next, I would like to acknowledge the wonderful current and previous staff of the Moore lab: Tangyne Berry, Neva Fudge, Brad Williams, and Lesly Berghuis, for their expert assistance, lessons in the lab, and support throughout my experimentation. Whether they were helping me finish replicates of my best experiments, or troubleshoot my worst, they were always kind and supportive. The value of their work in the lab cannot be overstated, and I believe that every individual that has the opportunity to work with them shares my sentiment.

Furthermore, I would like to thank the students of both the Berry Lab and the Moore Lab for their encouragement and help. In the Berry Lab: Shreyasi Sarkar Mrunal Dayma, and Jenna Caines and in the Moore Lab: Dylan Galloway, Stephanie Blandford, Rochelle Benoit, Jordan Osmond, Riley Moores, and Tamara Spearing. Each and every one of these people were a pleasure to work with and made the days in the lab something I looked forward to, and without a doubt, will miss in the future. Specifically, I would like to thank Shreyasi Sarkar for her kindness

and patience as a co-worker and friend, as well as Dylan Galloway for his instruction and support; both were role models for me in the lab and taught lessons I will never forget.

Additionally, I would like to thank Dr. Marius C. Hoener (Hoffman-La Roche, Switzerland) for providing key reagents used throughout this study. Also, I would like to acknowledge the funding agencies for the project: the Natural Sciences and Engineering Research Council and the Canada Research Chairs Program.

Lastly, I would like to thank my close group of friends, and of course, my parents, Alana & Dave Barnes, for their continued unconditional support with any of my educational endeavours. While this was my project in the lab, completed with the aid of many experts, my people on the outside helped just as much.

TABLE OF CONTENTS

LIST OF FIGURES

LIST OF TABLES

LIST OF ABBREVIATIONS

AADC	Aromatic L-amino acid decarboxylase
ADP	Adenosine 5'-diphosphate
ANOVA	Analysis of variance
ATP	Adenosine 5'-triphosphate
BMDM	Bone marrow-derived macrophage
cAMP	3',5'-Cyclic adenosine monophosphate
CD	Cluster of differentiation
CIHR	Canadian Institutes of Health Research
CLP	Common lymphoid progenitor
CNS	Central nervous system
DAMP	Damage-associated molecular pattern
DAPI	4',6-Diamidino-2-phenylindole
DMEM	Dulbecco's Modified Eagle Medium
DMT	Disease-modifying therapy
DMSO	Dimethyl sulfoxide
DS	Dissection solution
EAE	Experimental autoimmune encephalomyelitis

ECAR	Extracellular acidification rate
ELISA	Enzyme-linked immunosorbent assay
FACS	Fluorescence-activated cell sorting
FBS	Fetal bovine serum
GAPDH	Glyceraldehyde 3-phosphate dehydrogenase
GirK	G protein-coupled inwardly rectifying potassium
GM-CSF	Granulocyte-macrophage colony-stimulating factor
GPCR	G protein-coupled receptor
IF	Immunofluorescence
IFN-γ	Interferon-γ
IL	Interleukin
LPS	Lipopolysaccharide
MACS	Magnetic-activated cell sorting
M-CSF	Macrophage colony-stimulating factor
MDM	Monocyte-derived macrophage
MHC	Major histocompatibility complex
MS	Multiple Sclerosis
NAWM	Normal-appearing white matter

NIND	Non-inflammatory neurological disorder
NK	Natural killer
NLRP3	NOD-like receptor family pyrin domain containing 3
NOD	Nucleotide-binding and oligomerization domain
OCR	Oxygen consumption rate
PAMP	Pathogen-associated molecular pattern
PBMC	Peripheral blood mononuclear cell
PBS	Phosphate buffered saline
PCR	Polymerase chain reaction
PPMS	Primary progressive multiple sclerosis
PRR	Pattern recognition receptor
RPMI	Roswell Park Memorial Institute
RRMS	Relapse-remitting multiple sclerosis
SEM	Standard error of the mean
SPMS	Secondary progressive multiple sclerosis
TAAR	Trace amine-associated receptor
T_c	Cytotoxic T cells
TCR	T cell receptor

TGF-β	Transforming growth factor beta
T_h	Helper T cells
TLR	Toll-like receptor
TNF	Tumor necrosis factor
T_{reg}	Regulatory T cell

I. INTRODUCTION

1.1 The Immune System

The human immune system is comprised of physiological barriers, circulating proteins, and cellular components responsible for protecting and repairing the body (1). These elements work independently and in conjunction with each other to initiate and regulate inflammation; the vast network of processes in which the immune system responds to invading pathogens or endogenous danger signals (1). The immune system can generally be divided into two branches: the adaptive immune system and the innate immune system (1). The innate immune system forms the first line of defense and is includes a variety of cells, including eosinophils, basophils, mast cells, dendritic cells, NK cells, monocytes, and macrophages (1). The adaptive immune system provides a robust antigen-selective protection through natural killer (NK) cell, B cell, and T cell activation via independent response and crosstalk with the innate immune system. The adaptive and innate immune systems must be strictly regulated since an overactive, self-reactive, or ineffective immune response can result in hypersensitivity reactions, autoimmunity, or immunodeficiency, respectively (2). The severity of immunopathologies can range from the simple local hypersensitivity reactions seen at the site of an injection, to the demyelination and deterioration of the central nervous system as noted in multiple sclerosis (MS) (2). While the range in clinical manifestation is incredibly wide, disorders of the immune system often result from the malfunctioning of the cells within our own adaptive and innate systems.

1.1.1 Cells of the Adaptive Immune System

The cellular components of both the innate and adaptive immune systems are derived from hematopoietic stem cells in the bone marrow (1). Hematopoietic stem cells develop further to form the common lymphoid progenitor (CLP) and common myeloid progenitor cells, which differentiate to form the leukocytes of the adaptive and innate immune systems, respectively (1).

The adaptive immune system consists of the B cell-controlled humoral response and the T cell-controlled cell-mediated response. CLP cells designated to become B cells differentiate in the bone marrow and mature within peripheral lymphoid tissue following exposure to antigen with contributions from T cells via both direct co-stimulatory interaction and cytokine signaling (1,3). Following activation, B cells differentiate into antibody secreting plasma cells, which are a significant contributor to humoral immunity. Additionally, B cells are heterogeneous in their cytokine secretion profiles and populations. Cytokines are the molecular language of the immune system and are secreted proteins used by various immune and non-immune cells to communicate in either an autocrine, paracrine, or endocrine manner (1). The microenvironment in which B cells reside can shape their phenotype towards secretion of either pro-inflammatory, inflammation-promoting, cytokines such as tumor necrosis factor (TNF) or granulocyte/macrophage-colony stimulating factor (GM-CSF) or anti-inflammatory, inflammation-inhibiting, cytokines such as interleukin (IL)-10 (3).

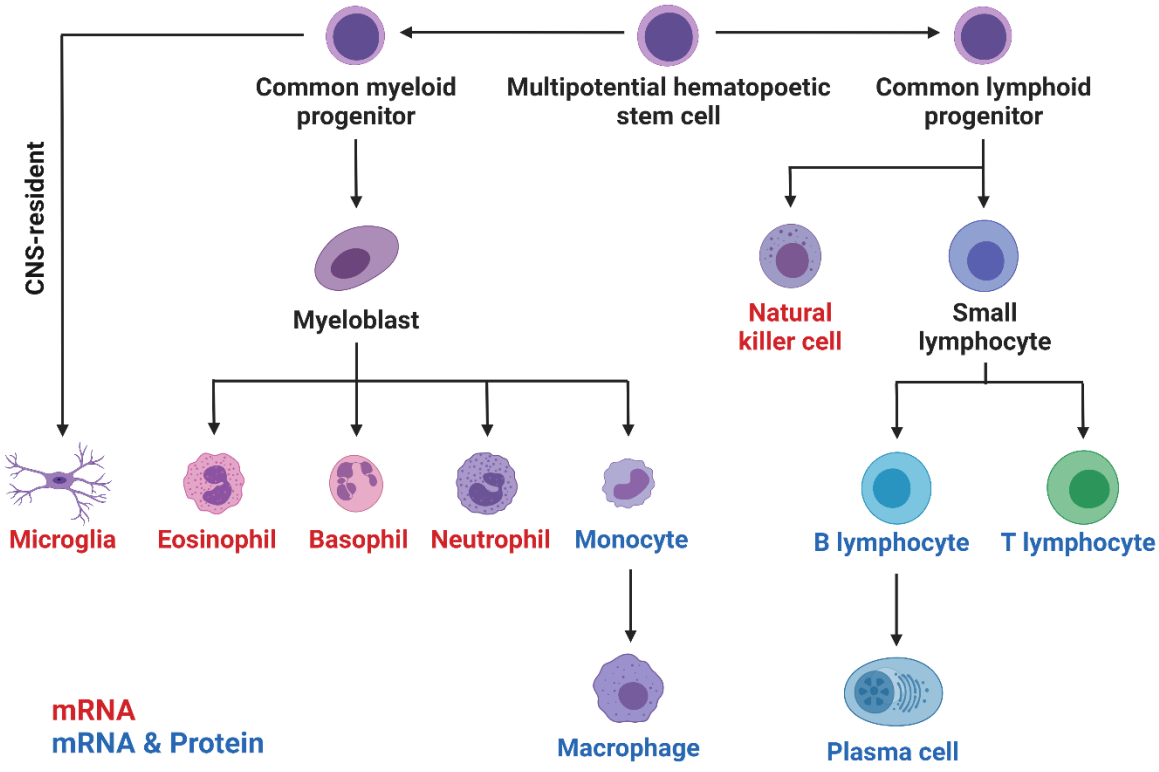

Figure 1.1: Immune cell lineage and reported TAAR1 expression. A flow chart representing the origin of certain human immune cells with reported TAAR1 mRNA and protein expression.

CLP cells that are committed to T cell differentiation also originate in the bone marrow prior to transportation to the thymus for maturation. As they move through the compartments of the thymus, expression of the T cell receptor (TCR) and the specific cluster of differentiation (CD) surface proteins occurs. CD3 as well as CD4 or CD8 provides the most general of many T cell phenotypic divisions (4). TCR and CD3 are expressed on all T cells and both are functionally involved in antigen recognition (4). CD8 is expressed on cytotoxic T cells (T_c cells), which are responsible for neutralizing infected or damaged host cells through interaction with major histocompatibility (MHC) class I molecules that have been loaded with antigen (1). CD4 is the marker associated with helper T cells (T_h cells) that are responsible for regulating the other cells involved in the immune system via activation following interaction with the MHC class II molecules that are commonly expressed on professional antigen presenting cells (1).

T_h cells are further differentiated into a wide array of effector cells, some of which are: T_h1, T_h2, regulatory T cells (T_{reg} cells) and T_h17 cells, depending on the cytokines present within their microenvironment as well as the type of cytokines they secrete in response (5). T_h1 and T_h2 cells aid in facilitating pro-inflammatory and anti-inflammatory responses respectively. The T_h1 response is characterized by pro-inflammatory cytokine secretion and promotion of cell-mediated immunity via cytolytic activity. The cytokine IL-12 is secreted following pro-inflammatory stimulation of the innate immune system and causes naïve T_h cells to differentiate into T_h1 cells, which then secrete additional pro-inflammatory cytokines such as IL-2 and interferon-γ(IFN-γ), further contributing to the associated inflammatory cascade (5). In contrast, T_h2 differentiation is induced by the anti-inflammatory cytokine IL-4, a cytokine produced within the microenvironment of an injury, and leads to the release of additional IL-4 as well as

other anti-inflammatory cytokines such as IL-13, polarizing the innate immune cells of the microenvironment towards phenotypes that counter-balance T_h1 responses and initiate repair (5).

While T_h1 and T_h2 function through facilitating pro- or anti-inflammatory processes, T_{reg} cells primarily contribute to the immune response through regulating inflammatory cellular phenotypes, preventing autoimmunity. T_{reg} cells primarily function from within the thymus during T cell development or within the periphery during inflammation (5). Finally, T_h17 are the T cell subset primarily characterized as inducing and propagating autoimmunity, leading to their association with immunological disorders such as rheumatoid arthritis and MS (5). T_h17 differentiation occurs following exposure to the cytokines IL-6 and transforming growth factor β (TGFβ) and results in the secretion of the characteristic cytokine IL-17. IL-17 functions through the induction of chemokine production, in which the chemokines are responsible for further immune cell recruitment (6). Dysregulated T_h17 differentiation results in increased IL-17 expression and has been closely associated with the induction and propagation of autoimmunity, wherein the treatment options for autoimmune disorders focus on the blockade of IL-17 signaling with monoclonal antibodies against the cytokine itself, or its receptor (5,6). In all cases, T cells are heavily involved in responding to, and further directing, the front line of defense: the innate immune system (1).

1.1.2 Cells of the Innate Immune System

Common myeloid progenitor cells are derived from hematopoietic stem cells within the bone marrow for development into the cellular component of the innate immune system. The cells of the innate immune system function through interaction with pathogen-associated or damage-associated molecular patterns (PAMPs/DAMPs) (7). PAMPs include molecules

associated with the exterior of common pathogens such as the lipopolysaccharide (LPS) found in the outer membrane of gram-negative bacteria, while DAMPs originate from host cells and mostly consist of common intracellular metabolites like adenosine 5'-triphosphate (ATP) or adenosine 5'-diphosphate (ADP) that are primarily only found in the extracellular milieu following cell death (7). Following exposure to these molecular patterns, the different cells of the innate immune system clear and process the associated pathogens, signal towards the adaptive immune system, and remove the remains of damaged cells (1).

The circulating innate immune cells are comprised of three main classes of leukocytes: granulocytes, NK cells, and monocytes. Granulocytes comprise the largest percentage of circulating leukocytes at up to 80%, and consist of neutrophils, basophils, and eosinophils. Granulocytes exert their functions within the immune system via a process known as degranulation, where, upon activation, they release granules of compounds with cytotoxic or signaling activity (1). Neutrophils are the most abundant granulocyte, consisting of up to 70% of the circulating leukocyte pool (1). Neutrophils are inactive in circulation, however, following interaction with chemokines, cytokines, or cell adhesion molecules, they are recruited to sites of infection where they assist in pathogen clearance via phagocytosis and degranulation (1). Activated neutrophils are also associated with up-regulated production and release of pro-inflammatory cytokines such as TNFα, IL-12, and IL-1β which differentiate naïve T cells and resting macrophages towards their pro-inflammatory phenotypes (1). Basophils constitute fewer than 1% of circulating leukocytes and, following allergy associated activation, release a large amount of histamine, IL-4, and IL-13 (1). Histamine leads to degranulation of eosinophils and the generation of a pro-inflammatory environment, while IL-4 and IL-13 work to mediate the reaction and prevent immunopathology (1). Eosinophils comprise less than 5% of circulating

leukocytes and are associated with defense against large multicellular parasites or fungi (1). Eosinophils are also closely associated with allergic reactions because they express histamine receptors and release cytotoxic proteins via degranulation (1).

NK cells are a powerful cellular component of the innate immune system making up 15% of circulating lymphoid-derived cells, however, due to their lymphoid lineage and a more robust response on second exposure to a pathogen, they blur the lines between the adaptive and innate immune systems (8). The primary function of NK cells is to eliminate cells that have lost expression of MHC class I molecules, often due to viral infection or malignancy (1). NK cell activation is dependent on a pro-inflammatory microenvironment containing IL-2, IFNα, IL-12, IL-15, IL-18, or IL-21 providing sufficient crosstalk with other cells of the innate and adaptive immune systems(1). Activated NK cells induce cytotoxicity and promote further cytokine production (1).

Dendritic cells are another important component of the innate immune system and are key partners of NK cells due to their production of IL-2, IL-12, IL-15, and IL-18 (1). While aiding the activation of NK cells is one function of dendritic cells, their primary function is antigen presentation to T cells, making them a key contributor to the interaction between the innate and adaptive immune systems. Immature dendritic cells are present throughout the periphery and are highly phagocytic in order to facilitate accumulation of large amounts of antigen. They, however, lack the ability to present antigens effectively (1). Following the completion of phagocytosis, dendritic cells mature and express proteins that facilitate antigen presentation. Mature dendritic cells are classified as professional antigen presenting cells , meaning they express MHC class II molecules and can therefore present degraded antigens to T_h

cells leading to T cell activation and the associated cascade of cytokine release and immune response activation (1).

1.1.2.1 Monocytes and Macrophages

Monocytes and macrophages are the final members of the cellular component of the innate immune system. Monocytes are derived from Common myeloid progenitor cells and account for up to 7% of the circulating leukocytes (1). More specifically, they constitute 10-20% of the peripheral blood mononuclear cells, the rest of which are made up of the circulating lymphocytes (1). Monocytes within the circulation and macrophages within tissues, play critical roles in antigen presentation as well as innate and adaptive immunomodulation (1). Monocytes were historically regarded as a bridge between the common myeloid progenitor cells and the resident macrophages and dendritic cells of the human body (9). In contrast, recent research links tissue-resident macrophages and dendritic cells to specific bone marrow precursor cells, while the monocyte represents the precursor for distinct monocyte-derived macrophages or dendritic cells, both of which have unique functions compared to their tissue-resident relatives (9).

Human monocytes can be classified as either classical, intermediate, or non-classical based on the relative amounts of CD14 and CD16 protein, where 80-90% of monocytes are $CD14^{+}CD16^{-}$ and are regarded as classical, while the remaining 10-20% are either intermediate with double positive expression or non-classical with $CD14^{low}CD16^{+}$ expression(9). CD14 acts as a pattern recognition receptor (PRR) for LPS, an established PAMP, acting as a co-receptor with Toll-like receptor (TLR) 4, where activation leads to downstream transcription of IFN-α and an associated pro-inflammatory cellular cascade (10). CD16, also known as $F_c\gamma RIII$, is a receptor responsible for interacting with the F_c portion of an antibody and mediates antibody

dependent cellular cytotoxicity by NK cells (11). In monocytes, however, CD16 expression can lead to a loss of both phagocytic ability and pro-inflammatory cytokine secretion (11). Classical, intermediate, and non-classical monocytes have functions in circulation prior to their differentiation into macrophages following migration into tissue throughout the periphery (12). This demonstrates how the inflammatory phenotype of monocytes is dependent on the expression of CD14 versus CD16 and how they contribute to immune system homeostasis, independent of their macrophage successors (12). The differential inflammatory phenotype continues following monocyte differentiation into macrophages (12). Classical macrophages primarily secrete pro-inflammatory cytokines such as TNF and IL-1β, non-classical macrophages secrete anti-inflammatory cytokines such as IL-10 and TGFβ, while intermediate macrophages are not primarily associated with cytokine secretion (12).

The primary role of macrophages is to phagocytose and destroy invading microorganisms, however, they also act as professional antigen presenting cells, secrete cytokines that modulate the adaptive immune response, and assist in injury repair and homeostasis (1). The transition of macrophage phenotype from pro-inflammatory to anti-inflammatory, or somewhere in between, allows them to carry out this wide range of functions (13).Previously, macrophage phenotype was described as either M1 (pro-inflammatory) or M2 (anti-inflammatory), however, the current understanding is that macrophages exist on a spectrum of inflammatory activity that is a function of their microenvironment (14). This spectrum of function exists between the three different categories previously described: classically activated macrophages, regulatory (intermediate) macrophages, and wound healing (non-classical) macrophages (14). It is important to note that the M1/M2 classification of macrophage

phenotype is still widely used for *in vitro* macrophage research, where the microenvironment can be more tightly controlled than *in vivo* (15).

Classically activated macrophages on the end of the M1 spectrum function as the first line of defence within the immune system, which takes place within hours to days; the M2 side of the spectrum functions during wound healing and inflammatory regulation that takes place during inflammatory resolution in the weeks following (14). These differences in function are also clearly reflected in the cells' metabolic profile (16). M1 macrophages prioritize glycolysis for fast energy production and retool the mitochondria and Krebs cycle intermediates such as succinate, fumarate, and malate for synthesis of inflammatory factors and induction of pro-inflammatory genes (16). On the M2 side of the spectrum, the cells' metabolic profile is shifted towards β oxidation of fatty acids and the subsequent use of oxidative phosphorylation to fund the exacerbated energetic costs of functions such as tissue repair (16). This shift in metabolic profile can be used to indicate macrophage shift between pro and anti-inflammatory function.

Classically activated macrophages function with high microbicidal activity and are induced by pro-inflammatory cytokines such as IFN-γ, a cytokine released by active T_h1 cells and NK cells, or TNF, a cytokine released by other activated antigen presenting cells (14). Classically activated macrophages with pro-inflammatory functions secrete reactive oxygen species and a variety of different cytokines such as IL-1, IL-6, and IL-23 (14). Prolonged elevated levels of these cytokines are associated with T_h17 differentiation, which as previously described, can lead to autoimmunity (14). Classically activated macrophages also balance T_h1 differentiation through secreting IL-12 to favor T_h1 differentiation and IL-27 to inhibit T_h1 differentiation (14).

Regulatory macrophages are induced by IL-10 released by T_{reg} cells or by interacting with other elements of their microenvironment such as apoptotic cells, glucocorticoids, prostaglandins, or a variety of other ligands for G protein-coupled receptors (GPCR) (14). In contrast to classically activated macrophages, regulatory macrophages exhibit anti-inflammatory activity, producing additional IL-10 to aid in T_h2 differentiation and losing most of their antigen presenting abilities (14). The activated T_h2 cells secrete IL-4 and IL-13, both of which give rise to the third category of macrophages, wound-healing macrophages (14). As such, regulatory macrophages work to transition the microenvironment towards healing following inflammation (14). In addition to T_h2 cells, granulocytes also act as a source of IL-4 for macrophage differentiation towards the wound-healing phenotype (14). As their name suggests, the primary function of wound healing macrophages is tissue repair (14). While T_h cell differentiation is terminal, macrophages have been reported to maintain plasticity following differentiation, where wound-healing macrophages that were primed with IL-4 can subsequently re-differentiate to a phenotype that releases higher amounts of IL-10 following exposure to LPS, thus behaving like regulatory macrophages and being identified as hybrid macrophages (14).

1.1.2.1.1 Microglia

In addition to the above described monocyte-derived macrophages, certain types of specialized macrophages are resident within specific tissues. Microglia, which are resident within the central nervous system (CNS), are one such example (14).

Microglia were the first cells of the innate immune system shown to be independent of bone marrow-derived replenishment from migrating monocytes (17). Microglia, acting in conjunction with macroglial cells (astrocytes and oligodendrocytes), make up the neuroimmune

system and fulfil two main functions in the adult human CNS: homeostatic maintenance and immune defence (18). With respect to immune defence, microglia function via cytokine production, phagocytosis, and antigen presentation, much like that of peripheral monocyte-derived macrophages (19). Depending on the molecular patterns of the microglia microenvironment, they take on similar M1-like or M2-like polarization states, representing pro and anti-inflammatory phenotypes (19). M1-polarized microglia can also be induced through interaction with GM-CSF, LPS, or IFN-γ, and secrete the pro-inflammatory cytokines TNFα, IL-6, IL-12 and IL-1β in addition to reactive oxygen species. M1 polarized microglia are involved in pro-inflammatory processes such as antigen presentation, tissue remodeling, cytotoxicity, or neurodegeneration (19). Polarization towards the anti-inflammatory M2 state results from microglia exposed to macrophage colony-stimulating factor (M-CSF), IL-4, or IL-13, and leads to secretion of the anti-inflammatory cytokines TGFβ, IL-10, or IL-13 (20). M2 microglia carry out anti-inflammatory processes such as immunoregulation, phagocytosis, and tissue regeneration (20).

1.1.3 Neurotransmitter regulation of the immune system

As discussed previously, cytokines are the primary agents of how immune cells within both the adaptive and innate immune systems signal in either a paracrine, autocrine, or endocrine fashion. With respect to the CNS, established neurotransmitters such as dopamine and adenosine function as critical immunomodulators and provide crosstalk between both systems (21).

1.1.3.1 Purinergic Regulation of the Immune System

Adenosine exerts its functions within the immune system via purinergic receptors, which are subdivided based on their ligands and class. P1 receptors are GPCRs that are activated by adenosine, while P2 receptors are activated by nucleotide variants featuring the adenosine ring such as ATP or ADP and are further subdivided as either P2X (ligand-gated ion channels) or P2Y (GPCRs) (22). The currently understood role of P1 receptors in the immune system is they are primarily associated with induction of cytokine secretion from both peripheral and CNS-resident immune cells (23), while P2 receptors have been implicated in a much wider range of functions including cytokine secretion, chemotaxis, differentiation, transcription factor activation, and pro-inflammatory cell death, i.e. pyroptosis (24).

As ATP research has progressed, understanding has evolved from being regarded as exclusively the primary energy currency of cells, to an established extracellular, non-adrenergic, non-cholinergic neurotransmitter (25). In recent years, it has been elucidated that ATP as well as its close molecular relative, ADP, play essential roles in immunomodulation of both the peripheral immune system and the neuroimmune cells of the CNS (25,26). As previously discussed, ATP and ADP act as DAMPs for immune cells, leading to pro-inflammatory activation via plasma membrane receptors such as ionotropic P2X receptors and metabotropic P2Y receptors, or via intracellular nucleotide-binding and oligomerization domain (NOD)-like receptors (7,24). For P2X receptors, activation has been implicated in cytokine secretion and NOD-like receptor family pyrin domain containing 3 (NLRP3) inflammasome activation associated with pyroptosis (24). More specifically, P2X receptor activation has been shown to induce T cell, B cell, macrophage, and microglia activation with the secretion of the characteristic pro-inflammatory cytokines from each cell type (27). Additionally, ATP has been

shown to be a critical immunomodulator of reactive astrocytes, maintaining homeostasis within the CNS through P2X receptors (28). Although P2Y activation has been implicated in cytokine and chemokine release as well as cell proliferation, the functions of G protein-coupled purinoceptors remain far less elucidated in comparison to P2X (24).

1.1.3.2 Dopaminergic Regulation of the Immune System

In addition to the established immunomodulatory functions of adenosine and the purinergic receptors, dopamine and its receptors also represent an important neurotransmitter regulator of the immune system. The five subtypes of dopamine receptors (D_1, D_2, D_3, D_4, and D_5, encoded by *DRD1*, *DRD2*, *DRD3*, *DRD4*, and *DRD5*, respectively) mediate the functions of dopamine throughout the body and are broadly classified as either D_1-like (D_1 and D_5) or D_2-like (D_2, D_3, and D_4). D_1-like receptors couple to stimulation of cyclic adenosine monophosphate (cAMP) production whereas D_2-like receptors inhibit cAMP production (29). In addition to the established role of dopamine as a neurotransmitter in the CNS, it also has an immunoregulatory role through the modulation of lymphocyte, granulocyte, macrophage, and NK cell function (30,31). More specifically, D_2-like receptor expression has been confirmed in T_{reg} cells, B cells, and monocytes (32) with activation of T cell D_2-like receptors shown to stimulate IL-10 secretion (33) and integrin expression (34), as well as inducing T_h2 differentiation (35). Additionally, activating D_2 and D_3 receptors with quinpirole inhibits bone-marrow derived M1 macrophages, reducing IL-1β and IL-18 secretion, and promoting differentiation towards the M2 phenotype (36). Taken together, these studies suggest that activating D_2-like receptor signaling could drive T cells and macrophages towards anti-inflammatory phenotypes.

Reflective of this, dopamine receptor-directed therapeutics have been tested for potential beneficial effects in autoimmune disorders (37,38). The D_2-like dopamine receptor agonist bromocriptine has been shown to improve the clinical course of experimental autoimmune encephalomyelitis (an animal model of T cell mediated demyelination) by down regulating T_h17-directed cytokine secretion (37,38), suggesting that pharmacologically targeting the dopaminergic system has potential for positively modifying immune-mediated demyelinating disorders.

1.2 Multiple Sclerosis

MS is defined as a demyelinating inflammatory and degenerative disease of the CNS characterized by inflammatory lesions disseminated in time and space (39). The current epidemiology indicates an average disease onset at approximately 30 years of age, with MS occurring in at least twice as many females (69%) as males (31%) (39). The global prevalence of MS is 1:3000 people, whereas in Canada, it is among the highest in the world at 1:400 (39). MS is a heterogeneous disease and is traditionally categorized into three defined subtypes based on clinical course: relapse-remitting MS (RRMS), primary-progressive MS (PPMS), and secondary-progressive MS (SPMS) (40). The majority of patients present with RRMS, which is a clinical course defined as symptoms manifesting and relapsing over time as a result of demyelination and remyelination, where each relapse is associated with progressively worsening neurodegeneration (41). Progressive MS is defined as a steady worsening of symptoms as a result of chronic neurodegeneration, and either occurs from disease onset (PPMS) or advancement from RRMS (SPMS). The majority of MS patients follow a transitioning RRMS to SPMS clinical course (42).

A currently understood mechanism of MS pathogenesis is that it results from a dysfunction of immunotolerance, involving an extravasation of immune cells from the peripheral circulation, through the blood-brain barrier, and into CNS tissue, however, the etiology of MS requires further elucidation. Due to myelin and neuronal antigen recognition, these infiltrating immune cells result in demyelination and axonal damage, manifesting as the chronic neurologic disability characteristic of MS. Additionally, the activated infiltrating immune cells secrete pro-inflammatory cytokines, resulting in the activation of resident CNS immune cells such as microglia (43,44). Established factors that increase the risk of developing MS include an individual's genetic susceptibility within the immune system, diet, or previous exposure to environmental immune triggers such as herpesvirus infection (45). The initiating cause of MS, however, remains unknown. Current research towards understanding MS pathophysiology at the cellular level is often focused on examining the cells involved *ex vivo*, or through the use of animal models of demyelination.

1.2.1 In vivo models of MS pathophysiology

Experimental autoimmune encephalomyelitis (EAE) is an established and commonly used animal model for studying the immunopathological and neuropathological mechanisms in MS (46). EAE involves directly sensitizing either the adaptive or innate immune system of mice to proteins found in the myelin of CNS neurons by harvesting dendritic cells and incubating with peptides generated from myelin, such that following reintroduction to the animal, the dendritic cells will present the peptides as antigens and trigger an immune attack against myelin, resulting in CNS demyelination (46). The generation and introduction of myelin-specific CD4+ T cells is another commonly used method of EAE induction (46). Following induction and symptom

manifestation, EAE also allows for study of remyelination and CNS repair (46). Recently, the generation and intravenous injection into Lewis rats of β-synuclein (a protein highly expressed throughout the brain) sensitive T cells has been shown to induce neuronal destruction and brain atrophy, and therefore has been proposed as an alternative model to EAE for studying the grey matter-related effects of MS (47). It is important to recognize that while the specific antigens are known in animal models, they remain unknown in MS, meaning there is likely key differences in the priming and activation of the adaptive immune system between the model systems and clinical cases.

1.2.2 The Adaptive Immune System in MS

The role of the adaptive immune system in MS has been extensively studied and established as a critical element of the underlying pathogenesis. CD4+ and CD8+ T cells have been identified within the inflammatory lesions of the CNS in MS patients and communicate with B cells, microglia, and other immune cells through the formation of germinal centers, or large clusters of activated immune cells and antibody-secreting B cells (48). MS lesions contain T_h cells deep within lesion cores, with T_c cells along the edges (49,50). In the context of T_h cells, both T_h1 and T_h17 cells have supported roles in MS pathogenesis, while pharmacologically inducing T_h2 differentiation has been shown to have therapeutic benefits (48). The administration of IFN-γ, previously described as one of the primary cytokines secreted by T_h1 cells, was shown to significantly exacerbate symptoms in MS patients (51). In contrast, targeting IL-17, the hallmark cytokine of T_h17 cells, with the anti-IL-17 antibody, secukinumab, reduced lesion formation (52). T_h2 differentiation within the CNS has been shown to be therapeutically

beneficial, in that polarizing T_h cells towards T_h2 with glatiramer acetate reverses EAE in mice and reduces the relapse rate of patients with RRMS (53).

B cells are hypothesized to play a role in antigen presentation to T cells in MS due to their ability to cross the blood-brain barrier and form germinal centers, or ectopic lymphoid follicles, functionally resembling lymph nodes within the CNS (46). An additional role of B cells in MS can be linked to cytokine secretion from dysfunctional pro-inflammatory B cells of unknown origin. B cells from MS patients were found to secrete higher amounts of GM-CSF and lower amounts of IL-10 than healthy subjects (54). As previously described, GM-CSF induces an M1 polarization in microglia and associated secretion of IL-6 and IL-12, which are respectively responsible for T_h17 and T_h1 differentiation and sequential neuroinflammation. Evidently, the effects of the adaptive immune system in MS can be dependent on interaction with the innate immune system.

1.2.3 The Innate Immune System in MS

As previously described (Section 1.2.1.2), microglia are the resident innate immune cells of the CNS and have a wide range of functions, some of which are analogous to peripheral monocyte-derived macrophages and some of which are unique. Microglia have been implicated in MS through their colocalization with T cells and resultant antigen presentation and soluble factor crosstalk (55). In terms of antigen presentation, MHC class II, as well as co-stimulatory molecules, were shown to be up regulated in MS patient microglia, clearly supporting their interaction with T_h cells (56). It is additionally important to note, however, that healthy microglia are incapable of initiating T_h1 proliferation *in vitro*, even following stimulation with IFN-γ or LPS (57), an established characteristic of peripheral antigen presenting cells. This suggests that

there is likely an undiscovered interaction required for the antigen presentation occurring in the CNS during MS pathophysiology. In terms of soluble factors, activated M1 microglia secrete pro-inflammatory cytokines that can propagate inflammation and immune cell infiltration. M1-polarized microglia have been previously confirmed present in active lesions of MS patients (58), and can exacerbate demyelination and neuronal death through secretion of reactive oxygen species, glutamate, and various proteases (55).

Pro-inflammatory peripheral monocytes are also thought to play a role in MS pathophysiology. Monocytes can be recruited into the CNS during MS inflammatory episodes and differentiate into macrophages, with functions unique from microglia (55). In EAE mice, microglia primarily assist in debris clearance, while CNS-infiltrating monocyte-derived macrophages do not assist the resident microglia population, and instead initiate demyelination (59,60). Further research is required to determine how monocyte derived macrophages uniquely contribute to the neuroinflammation of MS and could prove to be a valuable target for MS therapeutics since these treatments may not be required to cross the blood-brain barrier if the monocyte form can be targeted (55).

1.2.4 Current MS Therapeutics

Approved MS disease modifying therapies (DMT) in Canada can be placed into three different categories: injectable, oral, and infusion. As extensively reviewed by Baecher-Allan *et al.* in 2018 (48), there are currently seven injectable DMTs available for MS treatment in Canada. The most prescribed is IFN-β which functions by inhibiting T cell division, extravasation across the blood-brain barrier, and pro-inflammatory cytokine production. There are five different versions of IFN-β available, three of which are produced in mammalian cell

culture (IFNβ-1a -Avonex®, Rebif®, and Plegridy®) and two of which are produced in bacteria culture (IFNβ-1b - Extavia® and Betaseron®). Adverse events associated with IFNβ treatment include flu-like symptoms following injection as well as neutralizing antibody generation eventually reducing efficacy. Glatiramer acetate, available under the brand names Copaxone® and Glatopa®, is another approved DMT for MS, which functions through promoting T_h2 differentiation by inducing anti-inflammatory monocyte polarization and increasing IL-4 and IL-10 secretion. Adverse events associated with glatiramer acetate treatment include permanent scarring and a depression at the site of injection due to lipoatrophy and lymphadenopathy. Both IFNβ and glatiramer acetate have been shown to reduce the rate of relapses in RRMS.

Approved oral DMTs consist of siponimod, fingolimod, cladribine, teriflunomide and dimethyl fumarate (48). Fingolimod (Gilenya®) and siponimod (Mayzent®) both function via sequestering lymphocytes to the lymph nodes by inhibiting extravasation out of lymph node tissue, and therefore they severely immunocompromise the patient (48). Cladribine (Mavenclad®) depletes immune cells by inducing apoptosis and results in a sustained decrease in CD4+ and CD8+ T cells, as well as a transient reduction in B cells, also inducing a state of immunocompromise (48). Teriflunomide (Aubagio®) functions by directly inhibiting pyrimidine synthesis in T cells, thus preventing cytokine secretion and immune cell activation in general. In addition to the loss of T cell function, adverse effects of teriflunomide include hair loss and gastrointestinal dysfunction (48). Lastly, dimethyl fumarate (Tecfidera®) functions by activating the Nrf2 transcriptional pathway, an established antioxidant pathway, thus protecting cells from secreted reactive oxygen species. Side effects of dimethyl fumarate include gastrointestinal dysfunction, flushing, and rare cases of progressive multifocal leukoencephalopathy (48). As with the injectable compounds, all of the described oral DMTs are used to reduce RRMS relapse.

All infused monoclonal antibody-based medications are associated with the development of infusion reactions such as severe cases of rash, nausea and vomiting, fever and flushing (48). Due to the nature of monoclonal antibody treatment targeting specific elements of the immune system, patients are also left in an immunocompromised state, with increased risk of infection and developing various malignancies (61). The infused antibody treatments approved for use in Canada consist of alemtuzumab, ocrelizumab, and natalizumab. Alemtuzumab (Lemtrada®) is a humanized monoclonal antibody that targets CD52, a protein found on the surface of T cells and B cells and therefore completely depletes B and T cells via antibody dependent cellular cytotoxicity and complement-mediated lysis (48). This therapy has been found to increase the risk of autoimmune disorders such as immune thrombocytopenia purpura or glomerulonephritis. Ocrelizumab (Ocrevus®) targets CD20+ B cells, depleting them and reducing B cell mediated antigen presentation. Adverse effects for ocrelizumab include increased risk of breast cancer and a low risk of progressive multifocal leukoencephalopathy. Lastly, natalizumab targets VLA4, an integrin, or protein required for migration, found on T cells and B cells, therefore blocking migration across the blood-brain barrier and into the CNS. Some patients treated with this drug experienced reactivation of human polyomavirus 2, which is associated with the often fatal development of progressive multifocal leukoencephalopathy in the CNS (48). All infusion treatments are used to reduce relapse in RRMS patients, while ocrelizumab is the only drug approved for use in PPMS patients.

With the established DMTs for MS resulting in either an immunomodulatory and/or immunocompromised state, the search for new MS therapeutics is ongoing. Targeting the dopaminergic system is an alternative method that has been explored. In animal models, inhibiting D_1-like receptor signaling or depleting dopamine in dendritic cells used to induce EAE

was shown to significantly reduce the severity of EAE (62). *DRD5* expression has been suggested to be increased in non-classical monocytes from MS patients, indicating potential dysregulation of myeloid dopamine signaling in MS patients (62). In addition to this, the D_2-like dopamine receptor agonist bromocriptine improves the clinical course of EAE by down regulating T_h17-directed cytokine secretion (37,38,63). In a small-scale clinical trial, however 14/15 MS patients treated with bromocriptine still showed disease progression at one year of treatment (64). While these results show that bromocriptine was not successful in preventing disease progression, treating MS through targeting GPCR-mediated signaling systems remains an active area of research and potential way of avoiding the harsh side effects associated with current DMTs.

1.3 Trace Amines

Trace amines and their respective GPCRs are traditionally recognized for their involvement in psychiatric conditions, however with recent advances, they are an emerging topic of interest within GPCR-signaling in the immune system (65). The term "trace amine" was first used to differentiate a group of endogenous vertebrate monoamines from the more abundant compounds of similar structure such as catecholamine neurotransmitters (66). Trace amines have since been defined as an amine that is endogenously present in vertebrate tissues and/or bodily fluids at concentrations less than 50 ng/g of tissue and selectively binds to one or more trace amine-associated receptors (TAAR) at these concentrations (67).

Trace amines are classically regarded as comprising of 2-phenylethylamine, *p*-tyramine, and tryptamine, which are products of the decarboxylation of L-phenylalanine, L-tyrosine, and L-tryptophan by the enzyme aromatic L-amino acid decarboxylase (AADC; EC 4.1.1.28), as well

as *p*-octopamine, the product of the hydroxylation of *p*-tyramine by dopamine-*β*-hydroxylase (EC 1.14.17.1). These pathways are similar to those for synthesis of the established monoamine neurotransmitters dopamine, norepinephrine, and serotonin (67). In addition to their endogenous formation, trace amines also enter the body through enriched food sources such as aged cheeses, fermented meats, red wine, soy products and chocolate (68) or from being produced by the host's microbiota (67). Research into trace amines was limited prior to 2001 (69), but interest increased after the identification of a family of GPCRs with a high selectivity for trace amines (70). These receptors were later named TAAR (71).

1.3.1 Trace Amine-Associated Receptors

The identification of TAARs supported a role for trace amines as *bona fide* neuroactive metabolites (70). Many different TAARs have been identified since their initial discovery, however, there remains no consensus ligand for the entire family of receptors. Twenty-eight TAAR sub-families have been characterized in aquatic vertebrate species, most without any identified ligand or function (67). In terrestrial vertebrates, primary amines activate TAAR1-TAAR4, tertiary amines activate TAAR5-TAAR9, while a putative binding pocket for diamines has been identified in TAAR6 and TAAR8 (72,73). In addition to the previously described classical trace amines the thyroid hormone metabolite 3-iodothyronamine (74) (TAAR1), the catecholamine neurotransmitter metabolites 3-methoxytyramine (75,76) and normetanephrine (75,76) (TAAR1), trimethylamine (TAAR5) (72,73), isoamylamine (72,77) and isobutylamine (72,77) (TAAR3), as well as the polyamines putrescine (78) and cadaverine (78) (TAAR6, TAAR8) have been identified as selective agonists for various members of the TAAR family

(67). TAAR1, TAAR2, TAAR5, TAAR6, TAAR8, and TAAR9 are functionally expressed in humans, with TAAR3, TAAR4, and TAAR7 as pseudogenes (79).

With the wide range of ligands identified for TAARs, research into the function of TAARs within the human CNS has led to the identification of links to various psychiatric conditions (70,75). The characterization of the *TAAR* family localized the family of the nine receptor genes to a 108-kb region on human chromosome 6q23.2, a putative susceptibility locus for schizophrenia and mood disorders (70,75). While this has brought forth interest surrounding the entire TAAR family, TAAR1 still remains the only deorphanized TAAR, and as such TAAR1 is the most studied TAAR in humans (67) and is detailed in subsequent sections. More recently TAAR5 has been implicated in murine sensorimotor function (80) and dopaminergic neurotransmission (81), while human transcriptome analysis suggests expression within the brain (82). All TAARs other than TAAR1 were shown to additionally function as a novel class of olfactory receptor (77).

1.3.2 Trace Amine-Associated Receptor 1

TAAR1 is 1020 bp in length, lacks introns, can contain single-nucleotide polymorphisms, and codes for a 339 amino acid protein (83). The functional relevance of polymorphisms within the *TAAR1* gene was validated through a clinical trial that showed that methamphetamine-dependent individuals with the V288V polymorphism had increased drug craving (84). Expression of the TAAR1 protein in humans has been observed in pancreatic β-cells (85-88), the stomach (85,89), the intestines (85,88-90), various types of leukocytes (91-93), and throughout the brain (70,94-96). Functionally, TAAR1 has established roles in the CNS through regulation of reward circuits (88,97), mood states (98), movement control (99), and sleep (100).

In the periphery, TAAR1 has been implicated in glucose-induced insulin secretion (85) and body weight (88), and while functions of TAAR1 in immune cells have also been proposed, they lack systematic validation (67). As opposed to the common localization of a GPCR in the outer membrane of a cell, reports of TAAR1 protein expression describe an intracellular localization (71,75,85,88,101). Validated synthetic ligands (102-104) have paved the way for increased research into the function and therapeutic implications of TAAR1 throughout the body.

The applications of pharmacologically targeting TAAR1 have mostly been focused on CNS disorders. Extensive study of TAAR1 knockout mice have established TAAR1 as a potent modulator of dopaminergic neurotransmission (67), where studies using various TAAR1 agonists support the role of TAAR1 in dopaminergic activity through mediation of pre-synaptic dopamine release (96,105,106) as well as post-synaptic dopamine receptor sensitivity(107,108). The full TAAR1 agonist RO5256390 blocks cocaine-induced inhibition of dopamine clearance in murine nucleus accumbens slices, through a mechanism consistent with heterodimerization with D_2-like dopamine receptors (109). Additionally, the partial TAAR1 agonist RO5263397 was shown to attenuate cue-induced and self-administered cocaine intake in rats, while the selective full TAAR1 agonist, RO5166017, reduced reinstatement of cocaine-seeking behaviour (97). In humans, targeting TAAR1 as a therapy for schizophrenia has recently been supported via clinical trials verifying TAAR1 as a viable therapeutic target. Ulotaront (SEP-363856), a TAAR1 and $5HT_{1A}$ receptor agonist, has successfully been used in phase II clinical trials for treatment of schizophrenia (103,104).

1.3.2.1 TAAR1 Signaling

TAAR1 has been shown to interact with multiple signal transduction cascades. Following activation by an agonist, TAAR1 functions as a classical G_s protein-coupled receptor, primarily signaling through the production of cAMP via adenylyl cyclase (EC 4.6.1.1) stimulation, resulting in the accumulation of cAMP, the activation of protein kinase A, and the associated phosphorylation of downstream effectors (70). Additionally, TAAR1 can signal through the activation of G protein-coupled inwardly rectifying potassium (GirK) channels (105). Lastly, TAAR1 interacts with D_2-like dopamine receptors through heterodimerization, with TAAR1 activation reducing the recruitment of β-arrestin 2, subsequently inhibiting the activation of glycogen synthase kinase 3β-associated pathways (95,110). This range of signaling cascades have been associated with the previously discussed variety of functions of TAAR1 throughout the CNS and periphery (67).

1.3.2.2 TAAR1 in the Immune System

Expression of TAAR1 has been reported at the mRNA and protein level in most cells of the immune system (Figure 1). *TAAR1* mRNA is present in peripheral blood mononuclear cells and is up-regulated in response to pro-inflammatory activation (92,111). TAAR1 protein has subsequently been identified in both malignant and normal human B cells (93). In primary human B cells and immortalized B cell lines, TAAR1 protein levels are increased following activation (93,112). In mouse bone marrow-derived macrophages, *TAAR1* mRNA has been shown to increase following treatment with *p*-tyramine, as well as under pro-inflammatory polarization induced by LPS, an effect mirrored by the mRNA levels of the pro-inflammatory cytokines: IL-6, IL-1β, and TNF (113). In contrast, TAAR1 has also been implicated in anti-

inflammatory immune responses (91). A TAAR1-mediated chemotactic migration of granulocytes towards trace amines has also been reported, as well as induction of immunoglobulin E secretion from B cells and IL-4 secretion from T cells (91). These results suggest a TAAR1-mediated promotion of T_h2 differentiation, consistent with TAAR1 being a target for promoting anti-inflammatory responses (91).

Even fewer studies have investigated the role of TAAR1 in CNS-resident neuroimmune cells. TAAR1 agonists have been shown to influence key astrocytic responses following viral infection, such as glutamate clearance, and thus the excitability and survival of nearby neurons (114-116). Additionally, a retrospective meta-analysis indicated TAAR1 expression at low levels in microglia (117), however this requires confirmation. Given the potential for TAAR1 as a regulator of both peripheral and CNS-resident immune cell function, as well as the established interplay of both in MS, investigation of TAAR1 as a novel immunomodulatory target in MS represents an unexplored avenue in the fields of TAAR and MS research.

II. HYPOTHESIS & OBJECTIVES

2.1 Hypothesis

TAAR1 is expressed in human immune cells at both the mRNA and protein level, and pharmacologically targeting TAAR1 in myeloid cells elicits a response relevant to the neuroinflammation driving MS pathophysiology.

2.2 Objectives

1. Investigate *TAAR1* mRNA levels in human immune cells and determine whether differential expression occurs in MS patients.
2. Investigate TAAR1 protein expression in human immune cells relevant to MS pathophysiology.
3. Determine the effects of TAAR1 agonism in mouse and human macrophages and microglia.

III. METHODS & MATERIALS

3.1 Mouse Primary Bone Marrow-Derived Macrophages

All animal procedures and protocols were approved by the Memorial University Animal Care Committee in accordance with the Canadian Council on Animal Care guidelines (File ID: 20210522, Animal Care ID: 20-01-CM). A mix of male and female wild-type C57BL/6 mice (Charles River) aged 6 to 9 weeks were anaesthetized with CO_2 and euthanized by cervical dislocation. Mice were disinfected with 70 % ethanol prior to removal of the hind limbs at the hip flexor muscles. Muscle and adipose tissue were carefully removed from the hind limb. The cleaned bones from each animal were placed in a separate 50 mL conical tube with ice-cold phosphate buffered saline (PBS; 10 mM KH_2PO_4, 137 mM NaCl, pH = 7.4, consistent throughout all studies). Instruments were sterilized with 70 % ethanol between each dissection. Tibias and femurs from each animal were isolated and transferred to sterile petri dishes such that any remaining tissue could be removed using a scalpel. The cleaned bones were then cut at the knee and ankle joints to separate the tibia and femur, following which, the ends of the bones were removed with surgical scissors to expose the bone marrow. Repeated washing with 1 mL of ice-cold PBS via a 21.5 gauge needle was used to flush the bone marrow from the bones. The bone marrow was then transferred to a 15 mL conical tube with 3 mL of ice-cold 0.8% ammonium chloride (StemCell) and left on ice for 10 minutes to lyse the red blood cells. To dilute the ammonium chloride, 10 mL of ice-cold PBS was added to the tube prior to centrifugation at 450 x *g* for 10 minutes at 4 °C. The supernatant was removed and the pellet was resuspended in 2 mL of macrophage medium consisting of Dulbecco's Modified Eagle Medium (DMEM; Thermofisher/Life Technologies; pH = 7.4), 10% heat-inactivated fetal bovine serum

(HI FBS; USA Sourced, Corning, USA), 1x GlutaMAX (Thermofisher/Life Technologies), 1x penicillin/streptomycin (Thermofisher/Life Technologies), and 10 ng/mL of M-CSF. For cell counting and viability check via the Countess™ II Automated Cell Counter (Applied Biosystems), 10 µL of cell suspension was added to 10 µL of trypan blue (Sigma Aldrich). Cells were plated at 5 x 10^5 live cells/mL in a 10 cm petri dish with 10 mL of macrophage medium. Cells were incubated at 37 °C with a 5% CO_2 atmosphere for 6 – 7 days prior to cryopreservation or plating for experimentation.

Following the 6 – 7 day incubation, macrophage medium was removed, and cells were washed with 5 mL of sterile ice-cold PBS and incubated at 4 – 8 °C for 15 minutes. Adherent macrophages were collected by scraping with a sterile cell lifter (Thermofisher/Life Technologies) and centrifuged (450 x *g* for 5 minutes at 4 °C). The supernatant was removed, and the cells resuspended in macrophage medium lacking M-CSF for another cell count and viability check. Cells were then either plated in the experimental vessel of choice at 2.5 x 10^5 cells/mL or cryopreserved in 1 mL of freezing medium consisting of 75 % macrophage medium, 20 % FBS, and 5 % dimethyl sulfoxide (DMSO). For cryopreservation, the cell suspension was transferred to a cryovial and placed in a room temperature cryofreezing container, which was stored overnight at -80 °C. Cryovials were transferred to liquid nitrogen for long-term storage. After thawing, the same protocol was followed for incubation and plating as previously described in this section.

3.2 Mouse Primary Microglia and Mixed Glia Cultures

A mix of male and female C57BL/6 mouse pups aged postnatal day 1 (P1) to P4 were euthanized by decapitation and dissected to obtain cortical tissue for preparation of mixed glial

cell cultures (3 pups per culture). Prior to beginning this process, astrocyte medium (pH = 7.4) consisting of DMEM, 10% HI FBS, 1x penicillin/streptomycin, and 1x GlutaMAX was prepared and pre-warmed in a 37°C water bath. The following solutions were prepared prior to dissection and placed on ice: Dissection solution (DS) consisting of sterile Hank's Balanced Salt Solution (HBSS; 10 mM) (Thermofisher/Life Technologies) and digestion solution consisting of 0.625 % trypsin (Thermofisher/Life Technologies) and 0.05 mg/mL DNase I (Sigma Aldrich) in DS. Separate surgical instruments and solutions were used for each independent culture throughout the procedure to prevent cross-contamination.

Following decapitation, the brain was removed and transferred to a sterile petri dish containing 5 mL of DS. The meninges were then carefully removed from the cortex with forceps and cortices were isolated and transferred to a separate petri dish containing 5 mL of DS. The cortices were then checked for remaining meninges, diced into smaller pieces with a scalpel, and transferred to a 15 mL conical tube via a transfer pipette. A separate 15 mL conical tube was used for each independent culture preparation (3 pups). DS (approximately 9 mL) was carefully removed prior to the addition of 3 mL of digestion solution followed by gentle trituration with a transfer pipette. Conical tubes were then transferred to a 37°C incubator and nutated for 15 minutes, with a pause at 8 minutes for gentle trituration. Following incubation, 500 µL of HI FBS was added to each tube to stop the tissue digestion. The conical tubes were then nutated for an additional 5 minutes at 37 °C. Prepared digestions were centrifuged at 200 x *g* for 5 minutes at room temperature. Following centrifugation, supernatants were aspirated and the pellets were resuspended in 5 mL of 37 °C astrocyte medium (as previously defined) followed by trituration in order to obtain a single cell suspension. Each suspension was initially triturated with a 5 mL transfer pipette, followed by an 18-gauge blunt-tipped needle attached to a 5 mL syringe, and

lastly a 21-gauge blunt-tipped needle. The prepared suspensions were then passed through a sterile 70 μm strainer into a 50 mL conical tube and centrifuged at 200 x *g* for 5 minutes. Supernatants were aspirated, pellets were carefully resuspended in 12 mL of astrocyte medium and transferred to a T75 flask for incubation at 37 °C with 5% CO_2. The following day, astrocyte medium was carefully removed to preserve the monolayer and replaced with 12 mL of fresh pre-warmed astrocyte medium. On day 3 and 6 following the initial culture preparation, two-thirds of the medium in each flask was replaced with fresh pre-warmed astrocyte medium. Cultures present initially as a mixture of intermingled astrocytes and microglia, however, as confluency progresses, microglia additionally establish a loosely attached monolayer on top of the mixed culture.

The previously described cultures were further used to obtain purified microglia. Depending on the confluency of microglia, isolation occurred on days 10 – 14 following culture preparation. Following the observation of sufficient microglia on the surface of the cultures, flasks were shaken at 200 rpm for 1 hour in a standing incubator at 37 °C to detach the microglia. Medium from each flask was then collected and centrifuged at 400 x *g* for 10 minutes at room temperature. Pellets were resuspended in 1 mL of astrocyte-conditioned medium and 10 μL was added to 10 μL of trypan blue for cell counting. Purified microglia were then plated at 2.5 x 10^5 cells/mL in the appropriate experimental vessel(s). Microglia stimulation experiments were performed within 3-5 days of plating.

Following isolation of the loosely attached microglia on the surface of the cultures, 12 mL of fresh astrocyte medium was added to each flask and the remaining mixture of intermingled microglia and astrocytes were returned to the 37 °C, 5% CO_2 incubator, grown to

confluency, collected, and plated at 2.5 x 10^5 cells/mL for use in experiments pertaining to mixed glial cultures.

3.3 Human Primary Peripheral Blood Mononuclear Cells & Monocyte-Derived Macrophages

All studies involving human samples received institutional review board approval at Memorial University of Newfoundland (Health Research Ethics Authority) and strictly followed Canadian Institutes of Health Research (CIHR) guidelines (Study numbers: HREB#2014.182, HREB#2014.216, HREB#2014.181, HREB#2019.190, HREB#2015.103). Following informed consent, whole peripheral blood was collected from MS patients, non-inflammatory neurological disorder (NIND) patients, and healthy study participants (Tables 1 – 3) in EDTA-coated tubes. Blood was nutated at room temperature while preparing for the isolation protocol. The following solutions were prepared: Peripheral blood mononuclear cell (PBMC) medium consisting of RPMI (pH = 7.4), 10% HI-FBS, 1x penicillin/streptomycin , and 1x GlutaMAX; macrophage medium consisting of RPMI (pH = 7.4), 10% HI-FBS, 1x penicillin/streptomycin , 1x GlutaMAX, and 25 ng/mL M-CSF; magnetic-activated cell sorting (MACS) buffer (pH = 7.4) consisting of sterile PBS, 2 mM EDTA and 0.5 % FBS. Whole blood from the same donor was pooled from two 10 mL BD Vacutainer® into a 50 mL conical tube. The original tubes were then rinsed with 5 mL of 1x PBS, and the contents were added to the corresponding 50 mL conical tube. The conical tube was then filled to 35 mL with additional 1x PBS. SepMate™ tubes (StemCell Technologies) were used to isolate PBMCs. The lower chamber of the SepMate™ tube was filled with 15 mL of Ficol-Hypaque (ThermoFisher/Life Technologies) and the 35 mL of blood/PBS mixture was carefully added to the upper chamber with a 25 mL serological pipette. Each SepMate™ tube was centrifuged at 1200 x *g* for 10 minutes to separate the contents of the

tube. PBMCs were carefully scraped from the side of the tube and the entire top layer was transferred into a 50 mL conical tube, which was then brought up to 50 mL with 1x PBS. PBMCs were then centrifuged at 300 x *g* for 15 minutes and the supernatant aspirated. From here, the PBMC pellet was either resuspended in PBMC medium and counted prior to cryopreservation or resuspended in 20 mL of MACS buffer and counted prior to monocyte isolation. Counting following trypan blue staining was conducted as previously described.

Table 3.1: Study participant demographic data (*TAAR1* expression in whole PBMC cohort)

	Number of participants	Age (Years)	Female:Male Ratio
*NIND	10	47 ± 1	2.67
MS	14	44 ± 9	1.85
Controls	15	51 ± 7	1.16

*NIND: Non-inflammatory neurological disorders

Table 3.2: Non-inflammatory neurological disorder (NIND) diagnoses of participants

*NIND	Number of participants (10)
Idiopathic intracranial hypertension	5
Upper motor neuron disease	1
Visual migraine phenomenon	1
Spasticity	1
Ataxia	1
Neurogenic bladder	1

*NIND: Non-inflammatory neurological disorders

Table 3.3: Study participant demographic data (TAAR1 expression in CD14+ monocytes cohort)

	Number of participants	Age (Years)	Female:Male Ratio
MS	11	42 ± 11	1.75
Controls	9	38 ± 11	2

For monocyte isolation, the sample was brought to 50 mL with MACS buffer and centrifuged at 300 x *g* for 10 minutes. The supernatant was aspirated and the pellet resuspended in 80 µL of MACS buffer for every 1 x 10^7 cells. Anti-CD14 antibody coated magnetic beads (20 µL; Miltenyi Biotec) were added and the samples were incubated at 4°C for 15 minutes. During the 15-minute incubation, the MACS column was washed with 3 mL of MACS buffer. Following incubation, the samples were washed with 20 mL of MACS buffer and centrifuged at 300 x *g* for 10 minutes. The supernatant was aspirated and the PBMCs were resuspended in MACS buffer to 1 x 10^7 cells/mL (1 mL minimum). The prepared cell suspension was then poured directly through the MACS column and flow through collected in a new 15 mL conical tube. The column was washed three times with 3 mL of MACS buffer and each wash flow through discarded. The MACS column was then carefully removed from the magnet and placed into a fresh 15 mL conical tube. MACS buffer was added to the column up to a volume of 5 mL and quickly expelled to remove the separated CD14+ monocyte cells from the column. A cell count was conducted as previously described and the sample was centrifuged at 300 x *g* for 15 minutes. CD14+ monocytes were either collected for RNA extraction (Section 3.5) or resuspended to 5 x 10^5 cells/mL in macrophage medium and plated in the appropriate experimental vessel. Following incubation at 37°C with 5% CO_2 for 3 days, a half medium change was performed to replenish nutrients including M-CSF. The cells were then used for experimentation within 3-4 days.

3.4 Human Primary Fetal Microglia

Fetal microglia were isolated and cultured according to the protocol developed by Durafort and colleagues (118). Isolation and culturing of human microglia was conducted by Dr.

Craig Moore. Briefly, human microglia were isolated from CNS tissue obtained from fetuses provided by consenting and informed donors (Health Sciences Centre – General Hospital, St. John's, NL). Culture medium consisting of DMEM (pH = 7.4), 5% HI-FBS, 1x penicillin/streptomycin, and 1x GlutaMAX was prepared and pre-warmed in a 37°C water bath. CNS dissection was carried out with sterilized surgical instruments and a stereomicroscope. Brain and/or spinal cord tissue was isolated and transferred to a sterile 15 mm petri dish containing sterile 1x PBS. The meninges were carefully removed with forceps and the tissue was transferred to a 15 mL conical tube along with a digestion solution consisting of 0.625 % trypsin (Thermofisher/Life Technologies) and 0.05 mg/mL DNase I (Sigma Aldrich) in 1x PBS. Samples were triturated with a P-1000 pipette and then incubated at 37°C for 15 minutes on a nutator. Following incubation, 1 mL of HI-FBS was added to stop the digestion and the sample triturated and passed through a 70 µm filter into a 50 mL conical tube. The filter was rinsed with an additional 5 mL of 1x PBS and total run-through was then centrifuged at 300 x g for 10 minutes at 4°C. The supernatant was then aspirated, and the pellet resuspended in 5 mL of culture medium for another centrifugation at 300 x *g* for 10 minutes. The supernatant was aspirated, the pellet was resuspended in 4 mL of culture medium, and the cell suspension transferred to a T12.5 flask.

3.5 RNA Isolation, Reverse Transcription, and Quantitative Polymerase Chain Reaction

Mr. Brad Williams and Mrs. Neva Fudge of the Moore Lab had previously collected cell lysates, stored in QIAzol® reagent (Qiagen) at -80ºC, and isolated RNA with the RNeasy® Micro Kit (Qiagen) to generate an extensive RNA library of whole PBMC and CD14+ monocyte samples. The RNA concentration was determined by measuring the absorbance at 260 nm and 280 nm using a Nanodrop 1000 Spectrophotometer (Fisher Scientific). The High Capacity cDNA Reverse Transcription Kit (Applied Biosystems) was used to generate cDNA from 200 ng of RNA per sample. The M-MLV reverse transcriptase (RT) solution was prepared by heating a mixture of 5X first strand buffer, 0.1 M dithiothreitol, RNaseOUT™ recombinant ribonuclease inhibitor, and M-MLV RT to 65ºC for 5 minutes and quickly chilling on ice. The following contents were gently mixed in a nuclease-free microcentrifuge tube and incubated at 37ºC for 2 minutes: 200 ng of RNA, 250 ng of random primers, a 10 mM dNTP mix (containing dATP, dGTP, dTTP, and dCTP), and sterile distilled water at volumes indicated in the manufacturers protocol. The M-MLV RT solution was added to the mixture and the reaction solution was incubated for 50 minutes at 37 ºC. To inactivate the reaction mixture, the solution was heated to 70 ºC for 15 minutes. After this step, cDNA was ready for amplification via polymerase chain reaction.

TaqMan® Fast Universal PCR Master Mix (Applied Biosystems) was used to conduct the polymerase chain reaction (PCR). The proprietary human TaqMan® FAM-*TAAR1* (Hs00373229_s1) and VIC-*hGAPDH* (glyceraldehyde 3-phosphate dehydrogenase; Hs02786624_g1) probes and primers (Applied Biosystems) were used to assess *TAAR1* expression in human cells of interest. Each reaction contained 5 µL of TaqMan® Master Mix, 0.25 µL of each of the previously defined probes and primers, 3.5 µL of RNase-free water

(Applied Biosystems) and 1 µL of prepared cDNA and reactions performed in a sealed 96-well qPCR plate. A no-template control and another lacking reverse transcriptase were included. RT-qPCR was performed with the Applied Biosystems® ViiA 7 Real-Time PCR System using the following cycling parameters: heat to 50ºC and hold for 2 minutes, heat to 95ºC and hold for 2 minutes, then 40 cycles between 95ºC (3 seconds) and 60ºC (30 seconds). Amplification analysis was conducted on QuantStudio™ Software (Applied Biosystems). Fold changes were determined using the ΔΔCT method (119).

3.6 Flow Cytometry

Flow cytometry was performed in order to assess TAAR1 protein expression in T cells, B cells, and monocytes from human PBMC samples by a modification of the protocol described by Pitts et al. (2019). Fluorescence-activated cell sorting (FACS) buffer containing 1% FBS in 1x PBS was prepared and stored at 4°C. Human PBMCs were taken from cryopreservation, washed with RPMI, resuspended in 1 mL of FACS buffer, and counted in the presence of trypan blue as previously described. PBMCs were seeded at 500,000 cells/well in a round-bottom 96-well plate (Thermofisher). Single stain, no-primary antibody, and isotype controls were included in addition to the test sample in all experiments. Zombie Aqua Live/Dead™ (Invitrogen; L34966) was added to the appropriate wells at 1:1000 and the plate was incubated at 4 °C for 30 minutes. All incubations were protected from light from this point forward. Next, the samples were washed with 200 µL of FACS buffer, centrifuged at 200 x g for 5 minutes, and resuspended in 100 µL of fixation buffer (Invitrogen). The plate was then incubated at 4°C for 35 minutes. Following fixation, the samples were centrifuged at 200 x g for 5 minutes, supernatants discarded, and pellets washed twice with 200 µL of 1x permeabilization buffer (Invitrogen).

Next, all samples were resuspended in Human SeroBock™ (1:10 in FACS buffer; Bio-rad; BUFD70B) and incubated at room temperature for 15 minutes. Next 81 µg/mL of mouse anti-human TAAR1 antibody solution (a generous gift from Hoffmann-La Roche, Switzerland (85)) or normal mouse IgG_1 (eBioscience; 16-4714-85; isotype control) was added to the appropriate samples and incubated at 4 °C for 35 minutes. Following incubation, samples were centrifuged at 200 x g for 5 minutes, supernatants discarded, and pellets resuspended in 5 µg/mL R-phycoerythrin-conjugated Affinipure donkey anti-mouse IgG (Jackson; 715-116-150) in permeabilization buffer and incubated at 4 °C for 35 minutes. Samples were then washed twice with 200 µL of FACS buffer and resuspended in primary-conjugated antibody solutions containing either a single antibody or a combination of all three diluted in permeabilization buffer. Antibodies used were AF-488 conjugated mouse anti-human CD20 (1.25 µg/mL; BD Biosciences; 558056), allophycocyanin-conjugated mouse anti-human CD14 (1 µg/mL; BD Biosciences; 561383) and/or PE-Cy7 conjugated mouse anti-human CD3 (0.2 µg/mL; BD Biosciences; 557851). Additionally, a solution containing AF488 (BD Biosciences; 558055), allophycocyanin (BD Biosciences; 555745), and PE-Cy7 (BD Biosciences; 557907) mouse isotype antibodies with matching concentrations were included in one sample in place of the cell-marker targeting antibodies. All samples were then incubated at 4 °C for 35 minutes. Samples were washed twice with FACS buffer and resuspended in 200 µL of FACS buffer. Finally, samples were transferred to appropriately labelled FACS tubes (Thermofisher) and wrapped in aluminum foil.

Analysis of cell marker/TAAR1 expression was measured by FACS analysis. Events (10,000) were recorded using a Beckman Coulter CytoFLEX Analyser with the appropriate laser and detector settings for each fluorophore (Table 4). Data was analyzed using FlowJo version 9.

Table 3.4: Beckman Coulter CytoFLEX flow cytometer settings for chosen fluorophores

Laser	Detector	Range	Channel	Fluorochrome/dye*
405 nm Violet	450/45	505-545	KO525	Zombie Aqua™*
488 nm Blue	525/40	505-545	FITC	Alexa Fluor 488®
	585/42	564-606	PE	Phycoerythrin
	780/60	750-810	PC7	Phycoerythrin-Cy™7
638 nm Red	660/10	655-665	APC	Allophycocyanin

3.7 Measurement of Effects of TAAR1 Agonists on Pro-inflammatory Stimulation of Mouse and Human Macrophages and Microglia

Pro-inflammatory stimulation was conducted in mouse and human macrophages (24-well plate; 1.25 x 10^5 cells/well) and microglia (48-well plate; 3 x 10^4 cells/well). Initially, medium was changed to a serum-free environment (DMEM or RPMI, 1x GlutaMAX, and 1x penicillin/streptomycin). Depending on the experiment, one of the following pro-inflammatory stimuli was utilized: LPS (Sigma Aldrich; L2880; 100 ng/mL; 6 hours), the DAMPs: ATP (30 μM – 3 mM; 6 hours) (Sigma Aldrich) or ADP (30 μM – 3 mM; 24 hours) (Sigma Aldrich), or the synthetic P2X receptor agonist 2-methylthio-ADP (Tocris; 1 – 300 μM; 24 hours). Optimal concentration and time-points for inducing pro-inflammatory activation were determined empirically as described in the corresponding figures.

For assessment of the effects of TAAR1 agonism, cells were treated with either RO5256390 or RO5263397 (both generous gifts from Hoffman La Roche, Switzerland) at a concentration range of 1-300 nM in the absence or presence of optimized pro-inflammatory stimulation. Following stimulation, the medium from each replicate was collected and centrifuged at 300 x g for 5 minutes. Supernatants were then frozen at - 80 °C until assayed for cytokine secretion (See Section 3.11).

3.8 Propidium Iodide Uptake Assay

Propidium iodide (PI; ThermoFisher/Life Technologies) is a fluorescent DNA stain internalized by permeabilized cells that was used to quantify the extent of cell death occurring during ATP pro-inflammatory activation experiments. Mouse bone marrow-derived macrophages (BMDMs) were plated (96-well plate; 1 x 10^6 cells/well) using serum/phenol-red-

free DMEM. To account for background fluorescence, one column of the 96-well plate did not contain cells. Triton X-100 (1%) was used as a positive control for cell permeabilization in addition to a no treatment condition to account for background cell death.

ATP (1 mM, 6hrs) with and without RO5256390 (100 mM) treatments were conducted as previously described. Prior to treatment, the medium was replaced with serum/phenol-red-free DMEM containing 1 μg/mL propidium iodide. Following treatments, the plate was incubated for 3 minutes (37°C, 5% CO_2), and then transferred to a Cytation™ 5 Cell Imaging Multi-Mode Reader (BioTek) (37 ± 2°C, 5% CO_2). Fluorescence intensity was determined at 533/617 nm (excitation/emission) every 3 minutes for 6 hours. The relative propidium iodide uptake at each reading was determined with the following equation:

$$Relative\ Propidium\ Iodide\ Uptake = \frac{Sample - Background}{Triton\ X - Background}$$

3.9 Immunocytochemistry

Human CD14+ monocytes were seeded at 100,000 cells/well in 8-well Permanox® Chamber slides (Lab-Tek®) and grown under standard culture conditions as previously described (see Section 3.3). Following pro-inflammatory stimulation with LPS (see section 3.7), macrophages were fixed with 2% formalin for 15 minutes at room temperature. Macrophages were then washed with 500 μL of 1x PBS and permeabilized with 500 μL of 0.3% triton X-100 (ThermoFisher) in 1x PBS for 10 minutes at room temperature. During this incubation the following solutions were prepared: immunofluorescence (IF) buffer (pH = 7.4) consisting of 1x PBS with 0.1% bovine serum albumin (ThermoFisher), 0.3% triton X-100 (ThermoFisher), and 0.05% TWEEN-20® (ThermoFisher), as well as blocking buffer consisting of 10% goat serum

(ThermoFisher) in IF buffer. Following permeabilization, cells were blocked with 500 µL of blocking buffer for 1 hour with shaking (Fisher Scientific Platform Rocker set to low) at room temperature. Next, the monoclonal mouse anti-human TAAR1 antibody (previously described) was used as a primary antibody to stain for TAAR1. The antibody was diluted to a working concentration of 16.2 µg/mL in IF buffer and incubated with the cells for 16-18 hours at 4°C in the dark. IF buffer without the antibody was used as a "no-primary" negative control. Following primary staining, macrophages were washed 3 times for 15 minutes each with 500 µL of 1x PBS. During this period, a secondary antibody solution was prepared containing a goat anti-mouse IgG AlexaFluor™ 594-congugated secondary antibody (Life Technologies; A11005; 1:500), AlexaFluor™ 488-conjugated phalloidin (Invitrogen™; 2 drops/mL). and 4',6-diamidino-2-phenylindole (DAPI; 1:1000) diluted in 1x PBS. Following washing, macrophages were stained with 500 µL of the secondary antibody solution for 1 hour at room temperature in the dark. Following secondary staining, macrophages were washed 3 times for 5 minutes with 500 µL of 1x PBS. Next, the chambers were carefully removed, and the slide was coated with 2 drops of Fluoromount – G (Cedarlane) before applying a coverslip. The slide was then sealed with nail polish and stored in the dark at 4°C until imaging with a Zeiss AX10 fluorescent microscope at 40X and 63X magnification.

3.10 Histology and Immunohistochemistry

Formalin-fixed paraffin-embedded human brain sections from mixed active/inactive MS lesions were used for *in situ* studies following a next-of-kin consented autopsy and with the approval of the Newfoundland Health Research Ethics Board. Adjacent sections were used for four staining protocols. Three of these protocols had previously been completed by the Moore

lab (120,121): hematoxylin and eosin (H&E), luxol fast blue, and CD68 staining, where adjacent sections were stained and stored at room temperature and protected from light, to characterize regions of interest surrounding and within an MS lesion via bright-field imaging with a Cytation™ 5 Cell Imaging Multi-Mode Reader (BioTek). The fourth protocol consisted of utilizing an adjacent unstained section for immunohistochemistry to observe TAAR1 protein expression within the identified regions of interest.

For immunohistochemical analysis of TAAR1 expression, paraffin-embedded sections were subjected to heat-induced antigen retrieval (microwave at full power, 20 minutes) using sodium citrate buffer (10mM, pH = 6.0), washed twice with PBS, and blocked (room temperature, 1 hour) with PBS containing 10% horse serum (ThermoFisher). For primary antibody incubation, sections were incubated overnight at 4-8°C with an antibody solution containing the TAAR1 antibody (16.2 μg/mL) and a chicken anti-human IBA-1 antibody (20 μg/mL, Ares Labs, AIF101) in PBS with 10% horse serum. Following overnight incubation, sections were washed five times with PBS for 5 minutes. For secondary antibody incubation, sections were incubated at 4-8°C for 1 hour with a secondary antibody solution containing a goat anti-mouse IgG AlexaFluor™ 594-conjugated antibody (1:500, Life, A11005), a goat anti-chicken IgG AlexaFluor™ 488-conjugated antibody (1:500, Invitrogen, A32931), and DAPI (1:1000) diluted in PBS. Following the secondary antibody incubation, sections were washed five times for 5 minutes with PBS and coated with 2 drops of Fluoromount – G (Cedarlane) before applying a coverslip. The sections were stored in the dark at 4°C prior to imaging with a Zeiss AX10 fluorescent microscope at 10X and 40X magnification.

3.11 Enzyme-Linked Immunosorbent Assay

TNF and IL-6 OptEIA enzyme-linked immunosorbent assay (ELISA) kits (BD Biosciences) were used. All ELISAs followed a standard protocol, however, concentrations of antibodies differed based on the manufacturer's instruction with the specific kit. ELISA microplates (96-well; ThermoFisher) were loaded with capture antibody diluted in coating buffer (0.1 M Sodium Carbonate, pH = 9.5) and sealed for overnight incubation at 4 – 8 ºC. Following incubation, wells were carefully aspirated and washed 3 times with wash buffer (PBS with 0.05% TWEEN-20®, pH = 7.0). Next the plates were blocked with assay diluent (PBS with 10% FBS, pH = 7.0) for 1 hour at room temperature. During this incubation, the recombinant protein standard solutions were prepared via serial dilution (1:2) in assay diluent (1000 pg/mL to 7.8 pg/mL, protein dependent on kit). Additionally, samples were diluted with assay diluent or not to ensure that absorbance readings fell within the standard curve, where dilution values had previously been determined by the Moore lab and differed based on the species and protein of interest (human TNF 1:10, mouse TNF 1:20, IL-6 undiluted). Solutions were aspirated from the plate and each well washed as previously described, prior to loading in duplicate with the standard and sample solutions. The plate was then sealed and incubated at room temperature for 2 hours. Following this incubation, the wells were aspirated, washed, and loaded with the working detector solution (kit-specific detection antibody (1:250) and streptavidin-horseradish peroxidase conjugate (1:250) in assay diluent). The plate was then sealed for an additional incubation for 2 hours at room temperature. Following aspiration and washing, wells were loaded with substrate solution (1:1 mixture of tetramethylbenzidine and hydrogen peroxide; Substrate Reagent Set®, BD Biosciences) for a 20 minute incubation (protected from light, room temperature, unsealed). Lastly, the stop solution (2N H_2SO_4) was added to each well and the

absorbance readings were recorded within 30 minutes of stopping the reaction. Absorbance readings were obtained using a Cytation™ 5 Cell Imaging Multi-Mode Reader (BioTek; 450 nm measurement, subtracting 570 nm reference readings) and concentrations were determined accounting for dilution using the standard curve interpolation analysis feature in GraphPad Prism Version 9.1.1.

3.12 Real-Time ATP Rate Assay

The Seahorse™ XFe24 Analyzer (Agilent) was used to assess glycolytic and mitochondrial ATP production in pro-inflammatory macrophages. Prior to beginning the assay, each well of the Seahorse XFe24 cell culture microplate (Agilent) was coated with 50 µL of poly-L-lysine (Sigma Aldrich; 22.4 µg/mL) for 1 hour, rinsed with deionized water, sealed with parafilm, and stored at 4 – 8 °C for up to one week. Two days prior to the planned assay, mouse macrophages were taken from cryopreservation and grown in a non-tissue culture treated petri dish for 24 hours with macrophage medium as previously described. After 24 hours, macrophages were scraped off the plate with a sterile cell lifter (Thermofisher/Life Technologies) and centrifuged at 300 x *g* for 5 minutes. Following centrifugation, the supernatant was aspirated, and the cells resuspended in 1 mL of macrophage medium for counting. Following counting, 100 µL of single cell suspension at required cell densities was added to each well of the poly-L-lysine-coated microplate. Initial studies empirically determined optimal cell density for all future experiments. The plate was then incubated at 37 °C for 1 hour, to allow cells to settle to the bottom of the wells. Next, 150 µL of macrophage medium was added to each well and the plate incubated overnight to allow the macrophages to firmly adhere. During this incubation, the Seahorse™ XFe24 cartridge (Agilent) was hydrated using Seahorse

Calibrant (Agilent) as recommended by the supplier. Following overnight incubation, the macrophage medium was carefully replaced with serum-free DMEM and macrophages were stimulated with ATP (1 mM) and RO5256390 (100 nM) for 2 hours. Preliminary studies empirically determined the optimal ATP incubation time for subsequent experiments. During the stimulation, the ATP rate assay medium was prepared containing 10 mM glucose (Agilent), 1 mM pyruvate (Agilent), and 2 mM glutamine (Agilent) in phenol red/sodium bicarbonate-free DMEM (Agilent). After stimulation, the cells were washed and the medium was carefully replaced with assay medium, ensuring the monolayer remained intact. From here, the plate was transferred to the Seahorse XFe24 (Agilent) to record oxygen consumption rate (OCR) and extracellular acidification rate (ECAR) in order to deduce rates of glycolysis and oxidative phosphorylation, respectively. Over a 1 hour and 24 minute recording time, nine measurements were taken: three to observe basal rates following the treatments, three to record the effect of the ATP-synthase inhibitor oligomycin (1.5 μM; Agilent), and three to record the effects of a mixture of electron transport chain inhibitors (rotenone and antimycin A; 0.5 μM; Agilent). With these recorded rates, the extent of ATP production from either the mitochondria or glycolysis is computed and generated by the Seahorse XFe24 software. Data were transferred to GraphPad Prism (version 9.1.1) software for further analysis.

3.13 Statistical Analysis

Statistical analyses were performed using GraphPad Version Prism 9.1.1. All data is presented in the form of mean ± standard error of the mean (SEM). Data were analyzed by either t-test, normal, or non-parametric one-way analyses of variance (ANOVA) with post-hoc tests as appropriate as described in figure legends. If the initial ANOVA indicated a non-normal

distribution of the data, a non-parametric ANOVA used. $P < 0.05$ was considered significant in all instances.

Log concentration-response curves were fit using a nonlinear regression for a variable slope (four parameter) sigmoid curve fit, as recommended by GraphPad Version 9.1.1 and IC_{50} or EC_{50} values determined. Where available, the 95% confidence intervals and R^2 values are provided for log concentration-response curves and the determined IC_{50} or EC_{50} values.

IV. RESULTS

4.1 TAAR1 mRNA expression in whole PBMCs from MS patients and in MS CD14+ monocytes.

RT-qPCR was used to measure *TAAR1* expression levels in whole PBMCs and CD14+ monocytes. A sample amplification curve is shown in Figure 4.1A. TAAR1 amplification required around 32 cycles, suggesting TAAR1 transcript levels are relatively low. Results were normalized to the mean of the healthy volunteer samples to determine mean fold change in relative *TAAR1* expression. In PBMCs, a significant increase in variance was seen in the MS and NIND patients when compared to the healthy controls (Figure 4.1B; Brown-Forsythe test; $P = 0.03$). While there was no significant change seen in the MS patients, TAAR1 levels were significantly higher in the NIND patients than the healthy controls (Kruskal-Wallis Test; $P = 0.03$, with Dunn's post-hoc multiple comparison test; $P = 0.02$). RT-qPCR was also used to measure *TAAR1* levels in CD14+ monocytes from a different cohort of MS patients and healthy volunteers (Figure 4.1C) a significant decrease in relative *TAAR1* expression was seen in MS patients ($P = 0.04$). In both whole PBMCs and CD14+ monocytes, cohorts were age- and sex-matched, and no significant effect of sex was observed in either case.

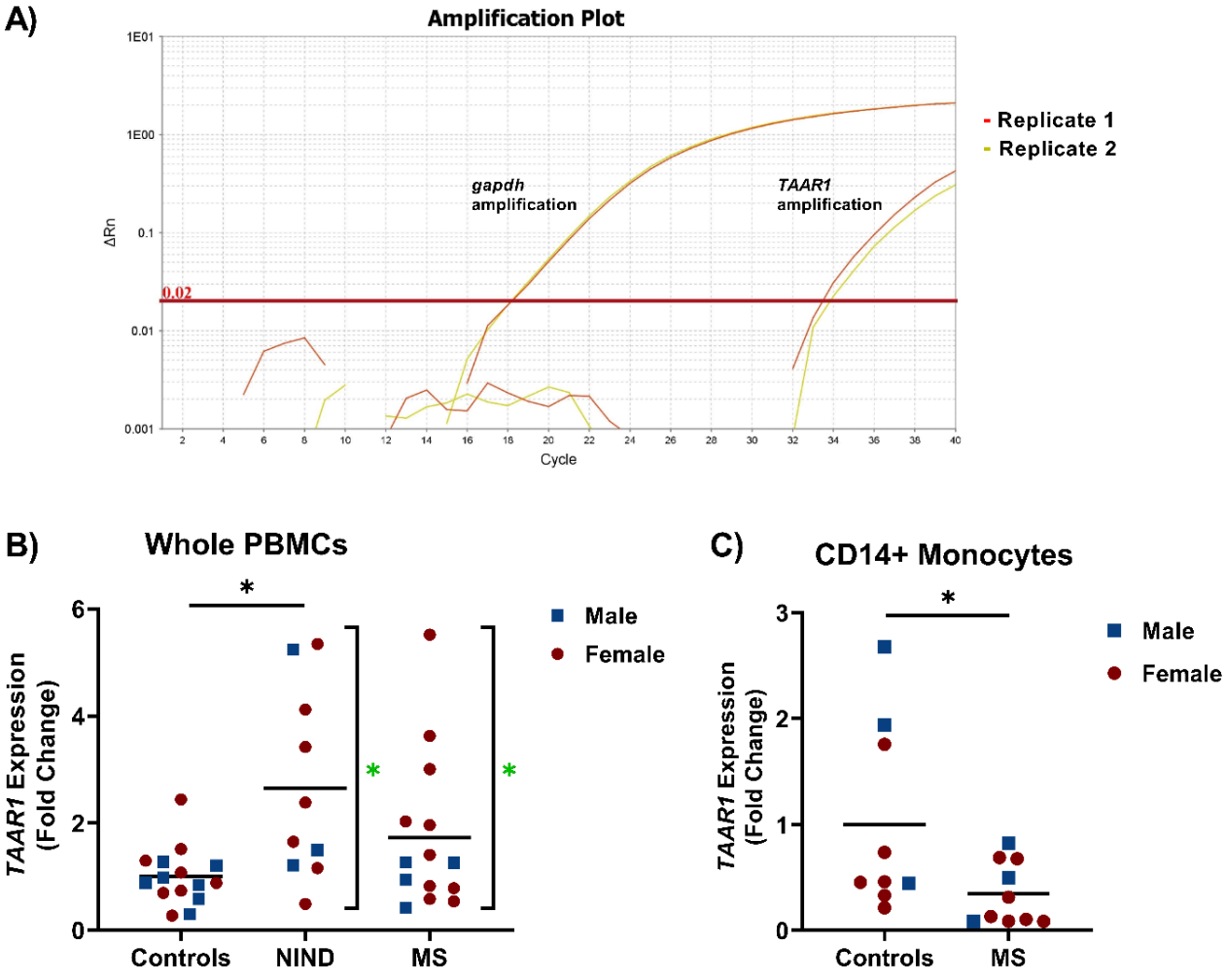
A)
Amplification Plot
1E01
1E00
0.1
0.01
0.001
ΔRn
0.02
gapdh
amplification
TAAR1
amplification
Replicate 1
Replicate 2
Cycle
B)
Whole PBMCs
TAAR1 Expression
(Fold Change)
Male
Female
Controls
NIND
MS
C)
CD14+ Monocytes
TAAR1 Expression
(Fold Change)
Male
Female
Controls
MS

Figure 4.1: TAAR1 expression in MS whole PBMCs, CD14+ monocytes, and the respective controls. A) A representative amplification curve following RT-qPCR analysis of one control whole PBMC sample, plated in technical duplicate. Both *gapdh* (VIC™ dye) and *TAAR1*(FAM™ dye) were multiplexed to observe amplification in each technical replicate. Following analysis, the ΔΔCT method was used to compare *TAAR1* expression to the *gapdh* housekeeping gene. B) Brown-Forsythe test showed significant differences between group variances (*$P < 0.05$). ANOVA comparisons were therefore determined via non-parametric Kruskal-Wallis test with Dunn's post-hoc multiple comparison test between groups (*$P < 0.05$). C) Two-tailed unpaired t test showed a significant difference between the groups (*$P < 0.05$).

4.2 TAAR1 protein expression in human PBMC subsets.

Intracellular flow cytometry analysis was utilized to assess TAAR1 expression in healthy human PBMC subsets. A gating protocol was utilized to select single, viable, and either CD14+ (monocytes), CD3+ (T cells), or CD20+ (B cells) cells (Figure 4.2). The percentage of TAAR1 expressing cells was highest within the B cell population (Figure 4.3B; 46%). While monocytes were also shown to express TAAR1 (Figure 4.3C; 31.8%), T cells did not (Figure 4.3A). In all cases, the isotype control samples (in blue) presented with high fluorescence levels relative to the no-stain controls (in green), indicating non-specific binding of the IgG_1 isotype. Additionally, the samples containing only the secondary antibody also presented with higher fluorescence levels than expected, indicating further non-specific binding. Extensive troubleshooting of antibody concentrations was unable to address the observed non-specific binding.

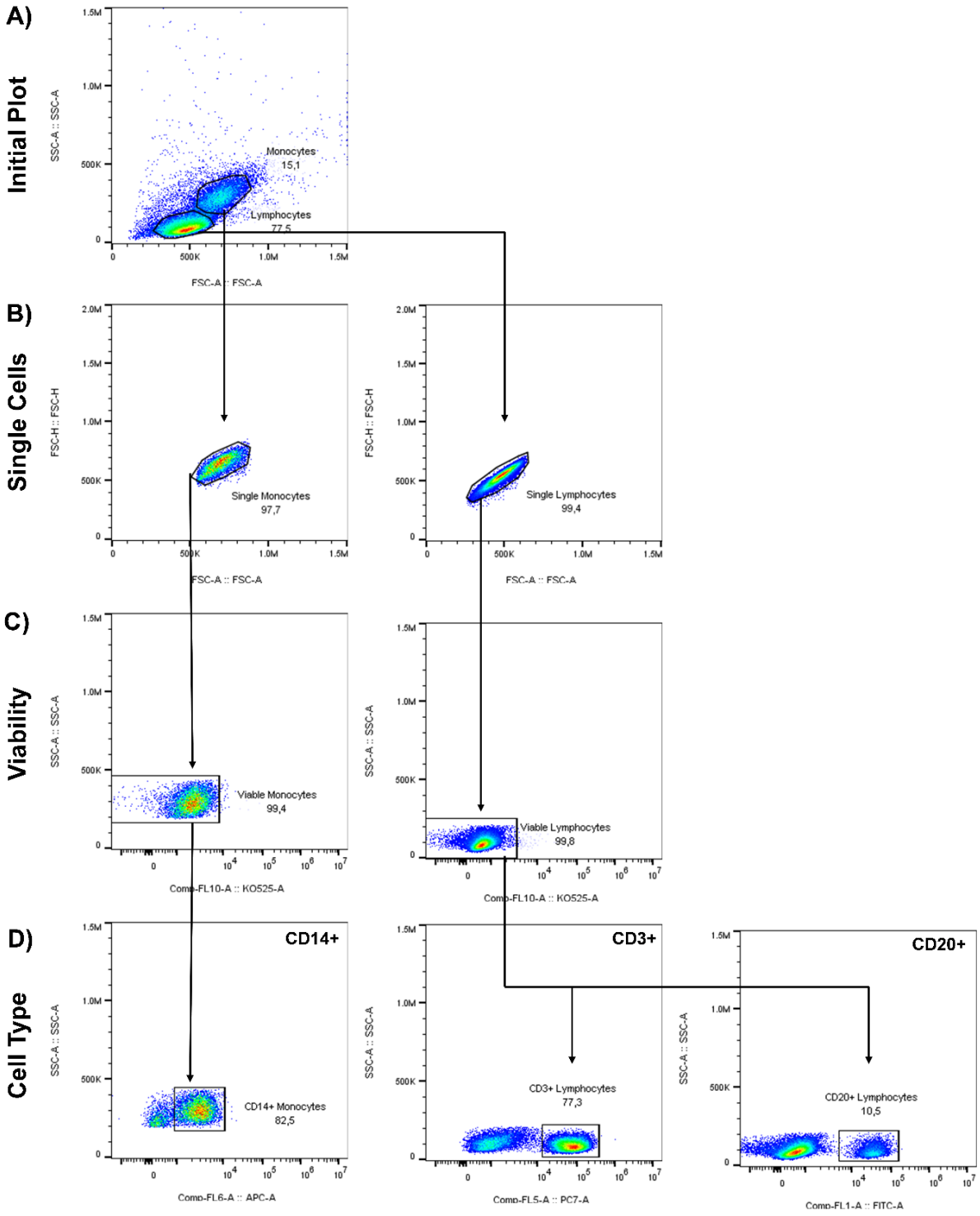
A)
Initial Plot
SSC-A :: SSC-A
FSC-A :: FSC-A
Monocytes
15,1
Lymphocytes
77,5
B)
Single Cells
FSC-H :: FSC-H
FSC-A :: FSC-A
Single Monocytes
97,7
Single Lymphocytes
99,4
C)
Viability
SSC-A :: SSC-A
Comp-FL10-A :: KO525-A
Viable Monocytes
99,4
Viable Lymphocytes
99,8
D)
Cell Type
CD14+
CD14+ Monocytes
82,5
Comp-FL6-A :: APC-A
CD3+
CD3+ Lymphocytes
77,3
Comp-FL5-A :: PC7-A
CD20+
CD20+ Lymphocytes
10,5
Comp-FL1-A :: FITC-A

Figure 4.2: Flow cytometry gating for human PBMCs.

A) 10,000 events were collected and plotted for side scatter (cell granularity; y-axis) versus forward scatter (cell size; x-axis) B) Monocyte and lymphocyte populations selected from A were plotted on height of scatter (y-axis) versus area of scatter (x-axis) to allow populations of single cells to be selected. C) Single cell populations selected from B were plotted on granularity (y-axis) versus fluorescence intensity (x-axis) on the Zombie Aqua channel to allow viable single cell selection. D) Viable single cells selected from C were plotted on cell granularity (y-axis) versus fluorescence intensity (x-axis) for the fluorophore corresponding to the marker of choice (APC for CD14, PE-Cy7 for CD3, and AF488 for CD20). Single, and viable, monocytes, CD3+ lymphocytes, and CD20+ lymphocytes were selected from D and used for further analyses.

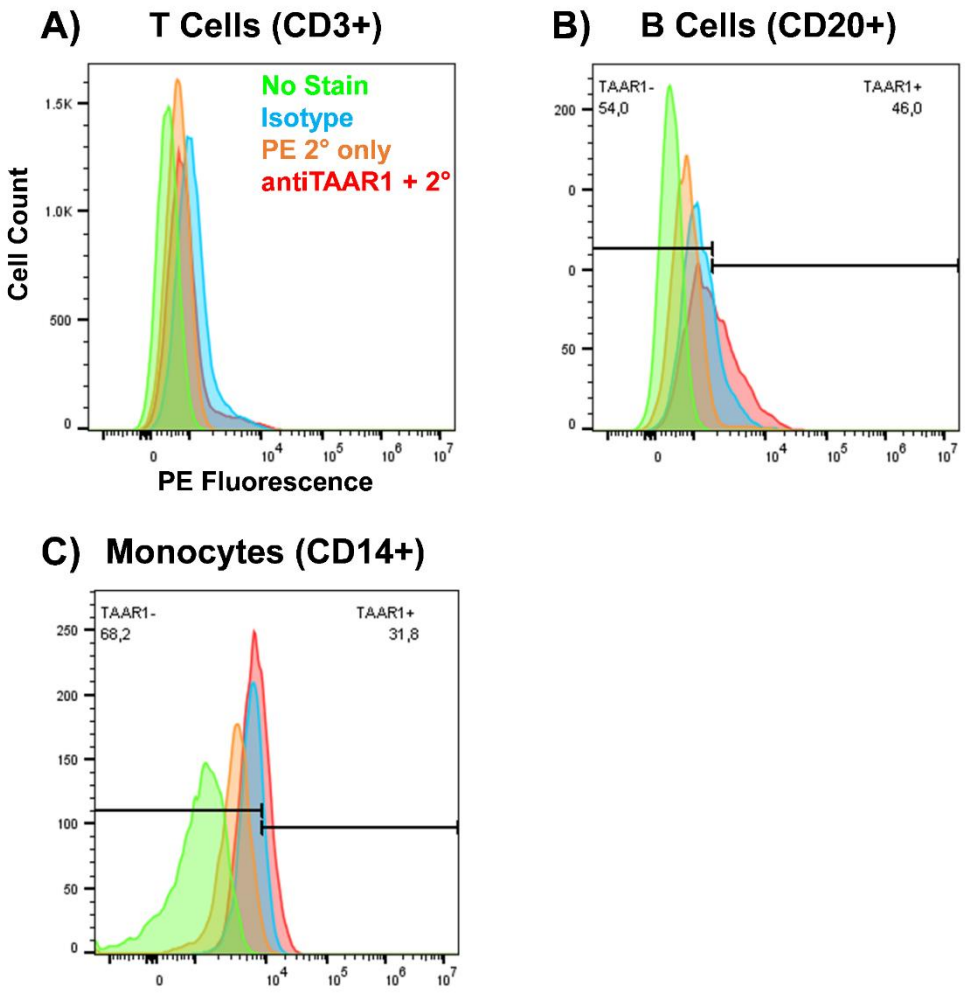

Figure 4.3: TAAR1 expression in human PBMC subsets.

Gated populations (See Figure 4.2D) of CD3+ T cells (A), CD20+ B cells (B), and CD14+ monocytes (C) within the four sample groups (no stain, isotype control, no primary control, and anti-TAAR1 antibody plus secondary antibody) were plotted on number of cells (y-axis) versus fluorescence intensity (x-axis) of PE. Percentage of cells expressing TAAR1 at higher fluorescence intensity than the isotype is provided for the anti-TAAR1 antibody plus secondary antibody sample where relevant.

4.3 TAAR1 is expressed in CD14+ monocyte-derived macrophages and displays a pronounced shift out of the nucleus following stimulation.

Initially, the anti-TAAR1 antibody and chosen secondary antibody combination were validated using healthy human CD14+ monocyte-derived macrophages (Figure 4.4). No non-specific binding was observed in the no-primary antibody control sample compared to the sample containing the anti-TAAR1 primary antibody (Figure 4.4, top row), further supporting previously established validation of the antibody in other cell types (85,101). TAAR1 staining highlighted an apparent nuclear localization (Figure 4.4, bottom row). The antibody was then used to assess TAAR1 protein expression and localization within healthy CD14+ monocyte-derived macrophages under basal and LPS-stimulated conditions.

TAAR1 staining was observed almost exclusively within the nucleus under basal conditions (Figure 4.5, top row). Following a 24-hour LPS stimulation, phalloidin staining confirmed cellular contraction consistent with the established amoeboid characteristics of macrophages (122). In these LPS-stimulated cells, TAAR1 expression showed a pronounced expansion out of the nucleus to also include prominent cytoplasmic staining (Figure 4.5, bottom row).

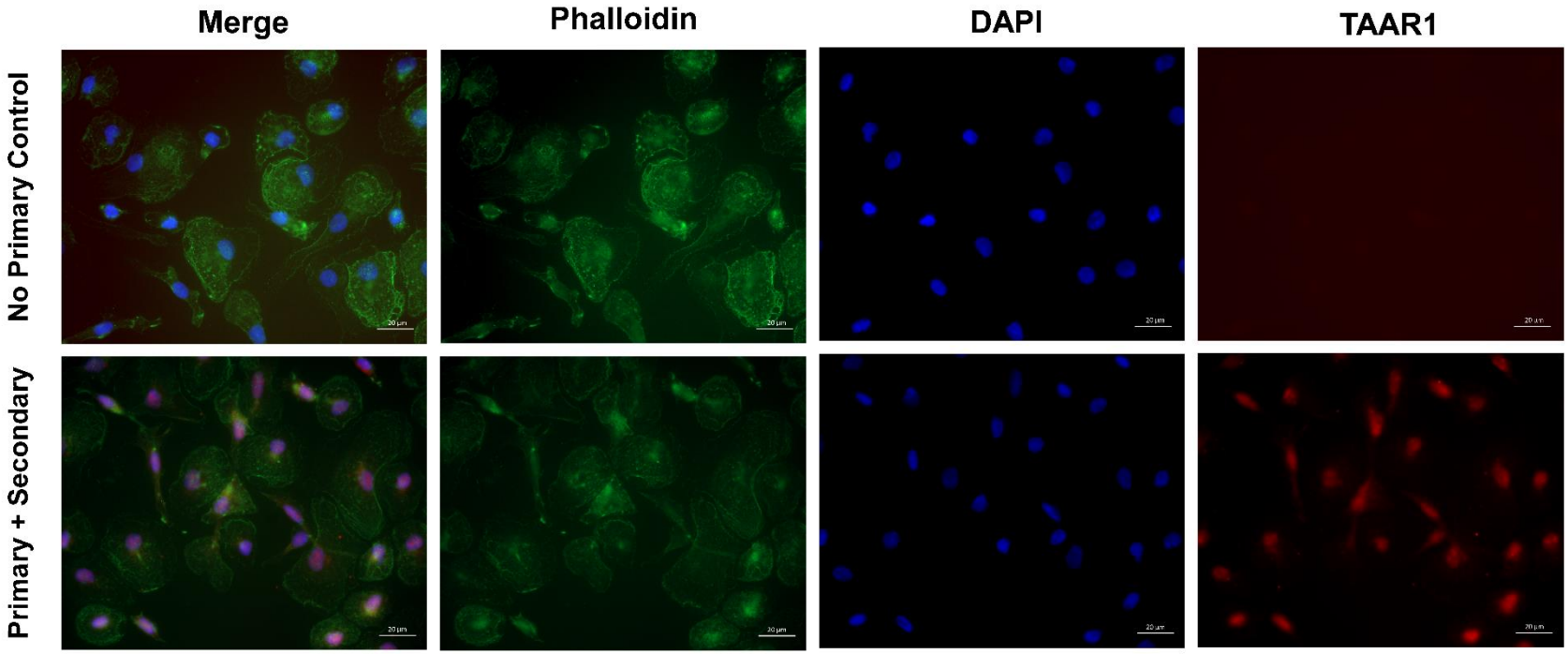
Merge
Phalloidin
DAPI
TAAR1
No Primary Control
Primary + Secondary

Figure 4.4: Anti-TAAR1 antibody selectivity validation in basal CD14+ monocyte-derived macrophages from healthy volunteers.

TAAR1 protein was visualized using a previously validated anti-human TAAR1 mouse primary antibody combined with a goat anti-mouse IgG AlexaFluor™ 594-conjugated secondary antibody (red). Nuclei were visualized via DAPI staining (blue) and actin with AlexaFluor™ 488-conjugated phalloidin (green). The top row contains macrophages stained with an antibody solution lacking the primary anti-TAAR1 antibody. The lower row contains macrophages stained with both the primary and secondary antibody. Scale bar represents 20 µm. All images were taken with a Zeiss AX10 fluorescence microscope at 63X magnification generated with the built-in Zeiss software.

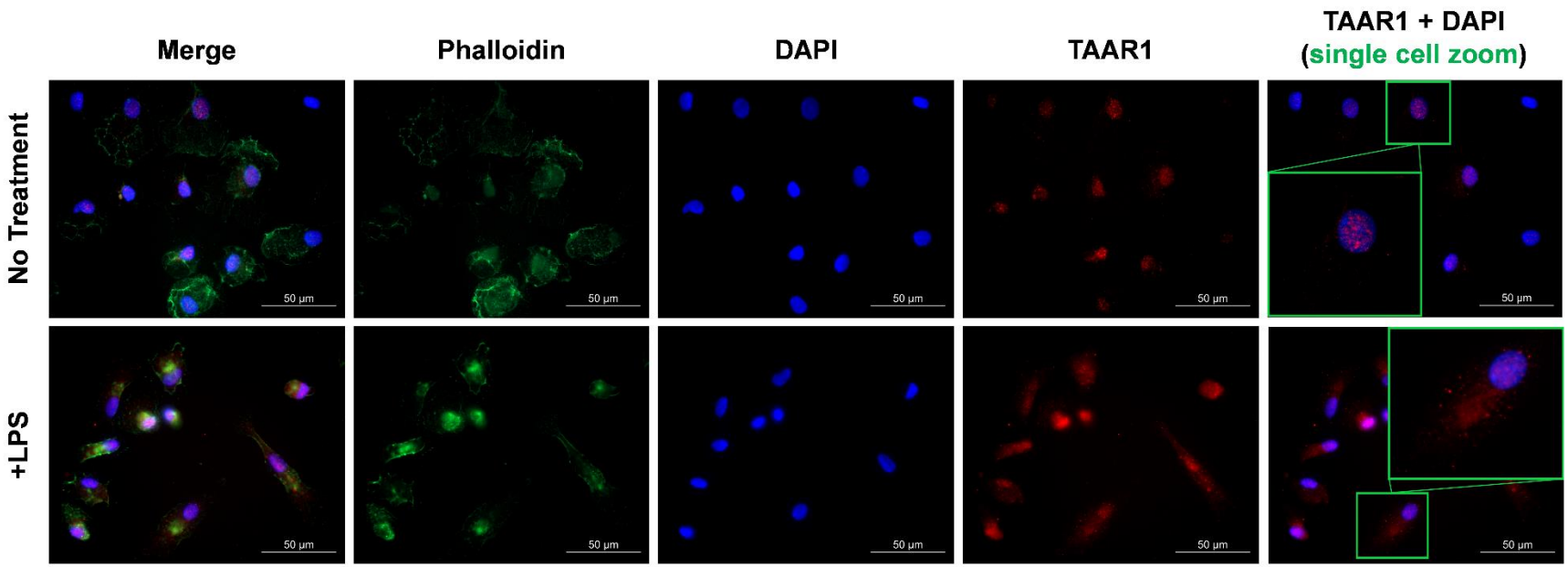
Merge
Phalloidin
DAPI
TAAR1
TAAR1 + DAPI
(single cell zoom)
No Treatment
+LPS
50 µm

Figure 4.5: TAAR1 localization in basal and LPS-stimulated CD14+ monocyte-derived macrophages from healthy volunteers.

TAAR1 protein in resting (N/T) or LPS stimulated (LPS) human monocyte-derived macrophages was visualized with a validated anti-human TAAR1 mouse primary antibody (as described in Figure 4.4; red). Nuclei were visualized via DAPI staining (blue) and actin with AlexaFluor™ 647-conjugated phalloidin (green). The last column contains the DAPI and anti-TAAR1 channels featuring a zoom via Microsoft© Paint 3D™ Version 6.2203 on a single cell (green boxes). Scale bar represents 50 μM. All images were taken with a Zeiss AX10 fluorescence microscope at 63X magnification generated with the built-in Zeiss software.

4.4 TAAR1 protein expression in the inflamed area of a mixed active/inactive MS lesion.

A mixed active/inactive MS lesion was identified using hematoxylin and eosin (Figure 4.6A), luxol fast blue (Figure 4.6B) and CD68 (Figure 4.6C) staining via bright-field microscopy, as previously described by the Moore lab (120). CD68 was used as a marker for microglia/macrophages *in situ*, while LFB stained intact myelin bordering and surrounding the lesion. Primary antibodies for TAAR1 and IBA-1 were then used to visualize TAAR1 expression within the corresponding microglia/macrophage populations (Figure 4.6D-I). TAAR1 expression was most visible in the normal appearing white matter (NAWM) and at the border of the MS lesion (Figure 4.6D&E). Co-staining for IBA-1 and TAAR1 was primarily observed near the lesion border (yellow; Figure 4.6H&I), with TAAR1 staining particularly prominent in macrophages/microglia surrounding a blood vessel, possibly in the process of extravasation (BV; Figure 4.6H). Notably, TAAR1 sub-cellular distribution was diffuse in these macrophages/microglia, similar to *in vitro* LPS-activated macrophages (Figure 4.5). Although IBA-1 positive cells were mostly TAAR1 negative in the NAWM near the lesion, TAAR1 expression was still visible in this area (Figure 4.6G). When examining the lesion center, there was less TAAR1 staining and macrophages/microglia than the other regions examined (Figure 4.6F).

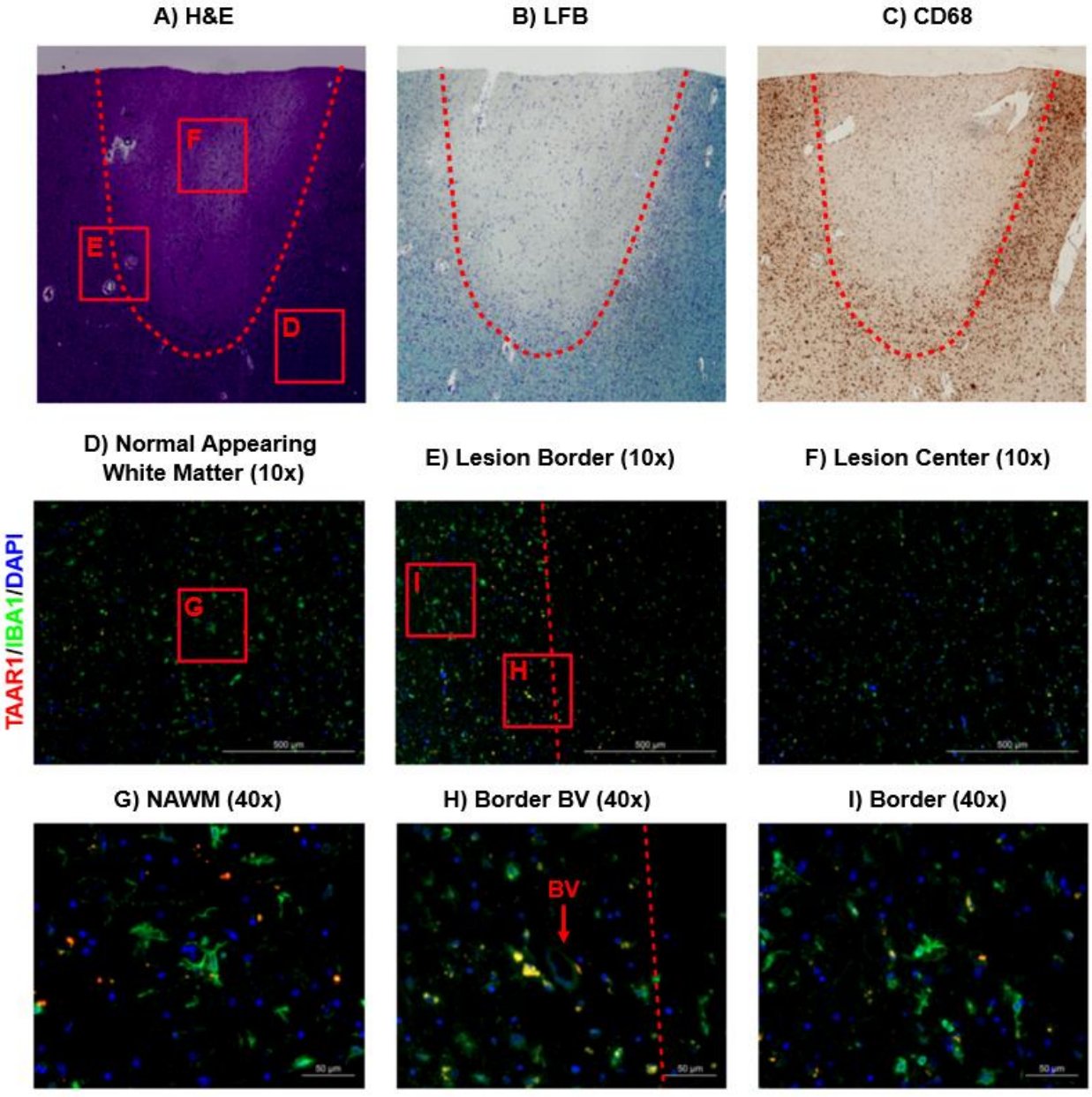
A) H&E
B) LFB
C) CD68
F
E
D
D) Normal Appearing White Matter (10x)
E) Lesion Border (10x)
F) Lesion Center (10x)
TAAR1/IBA1/DAPI
G
I
H
G) NAWM (40x)
H) Border BV (40x)
I) Border (40x)
BV

Figure 4.6: TAAR1 expression profile within and surrounding a mixed active/inactive MS lesion.

Bright field images of a mixed active/inactive MS lesion were visualized using hematoxylin and eosin (H&E: A), luxol fast blue (LFB; B), and CD68 (C) staining. Primary antibodies for TAAR1 and IBA-1 were used in combination with AlexaFluor™ 594 (red) and AlexaFluor™ 647 (green) conjugated secondary antibodies to visualize TAAR1 expression and microglia/macrophage localization, respectively. DAPI staining was used to identify nucleated cells (blue). Co-localization of IBA-1 and TAAR1 can be seen in yellow. Bright-field images were taken with a Cytation™ 5 Cell Imaging Multi-Mode Reader (BioTek). Scale bar represents 500 μm (D – F) or 50 μm (G – I). Fluorescence imaging was conducted with a Zeiss AX10 fluorescent microscope at 10X and 40X magnification and images generated with the built-in Zeiss software.

4.5 Determination of optimal mouse macrophage cell density for metabolic profile assays.

Next, this study aimed to elucidate TAAR1 function in macrophages through a variety of assays, first of which assessed metabolic profile following inflammatory stimulation. Cell density for mouse macrophage metabolic profile experiments (1×10^5 cells/well) was validated using previously established density values from the literature in addition to experimentation (Figure 4.7A & B). Drops in oxygen consumption and increases in extracellular acidification rates following the addition of rotenone and oligomycin/antimycin A are used to deduce the pathway preference of ATP production in later experiments. Based on the observed oxygen consumption and extracellular acidification rates, 1×10^5 cells/well was chosen as the cell density for future metabolic profile experiments such that sufficient ranges were observed to allow for deduction of ATP production pathway preference. Additionally, LPS clearly induced a functionally detectable glycolytic shift at this density (Figure 4.7C & D) consistent with pro-inflammatory activation of mouse macrophages, as previously established in the literature (16).

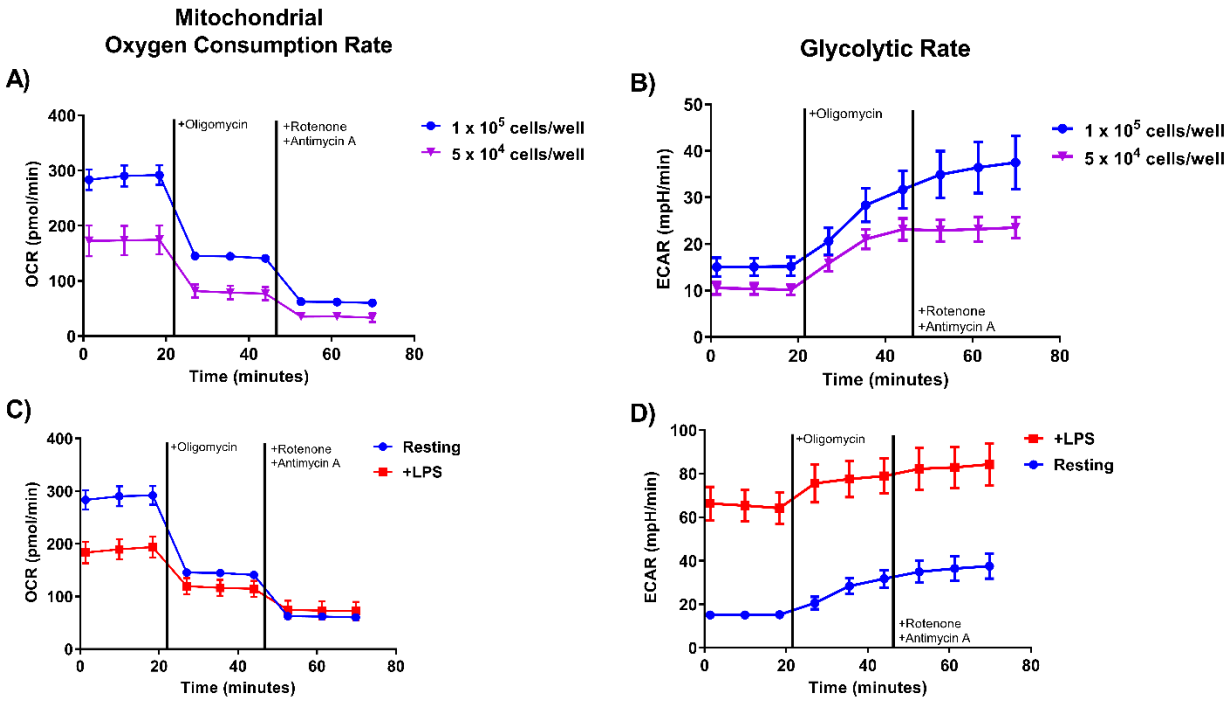

Figure 4.7: Seahorse assay cell density and glycolytic shift validation with mouse BMDMs.

Resting mouse BMDMs were seeded at 1 x 10^5 cells/well and 5 x 10^4 cells/well to compare the effect of density (A and B). BMDMs (1 x 10^5 cells/well) were treated with LPS for 24 hours(+LPS) to validate pro-inflammatory induced glycolytic shift (C and D). The extent of oxidative phosphorylation (A and C) and glycolysis (B and D) were measured through monitoring oxygen consumption rate (OCR) and extracellular acidification rate (ECAR), respectively. Data represents the mean ± SEM of 5 cultures from a single experiment.

4.6 LPS-induced TNF secretion is unaffected by TAAR1 agonism in human and mouse macrophages.

To assess the effects of TAAR1 agonism on pro-inflammatory cytokine secretion, LPS was used as a pro-inflammatory stimulus to induce TNF secretion in both human CD14+ monocyte-derived macrophages (MDMs) and mouse BMDMs (Figure 4.8). Optimal treatment conditions for LPS had been previously determined by the Moore Lab to be 100 ng/mL for 6 hours (121,123). In both mouse (Figure 4.8A & B) and human (Figure 4.8C &D) macrophages, neither the full TAAR1 agonist RO5256390 (Figure 4.8A & C) nor the partial TAAR1 agonist RO5263397 had any effect on LPS-induced TNF secretion.

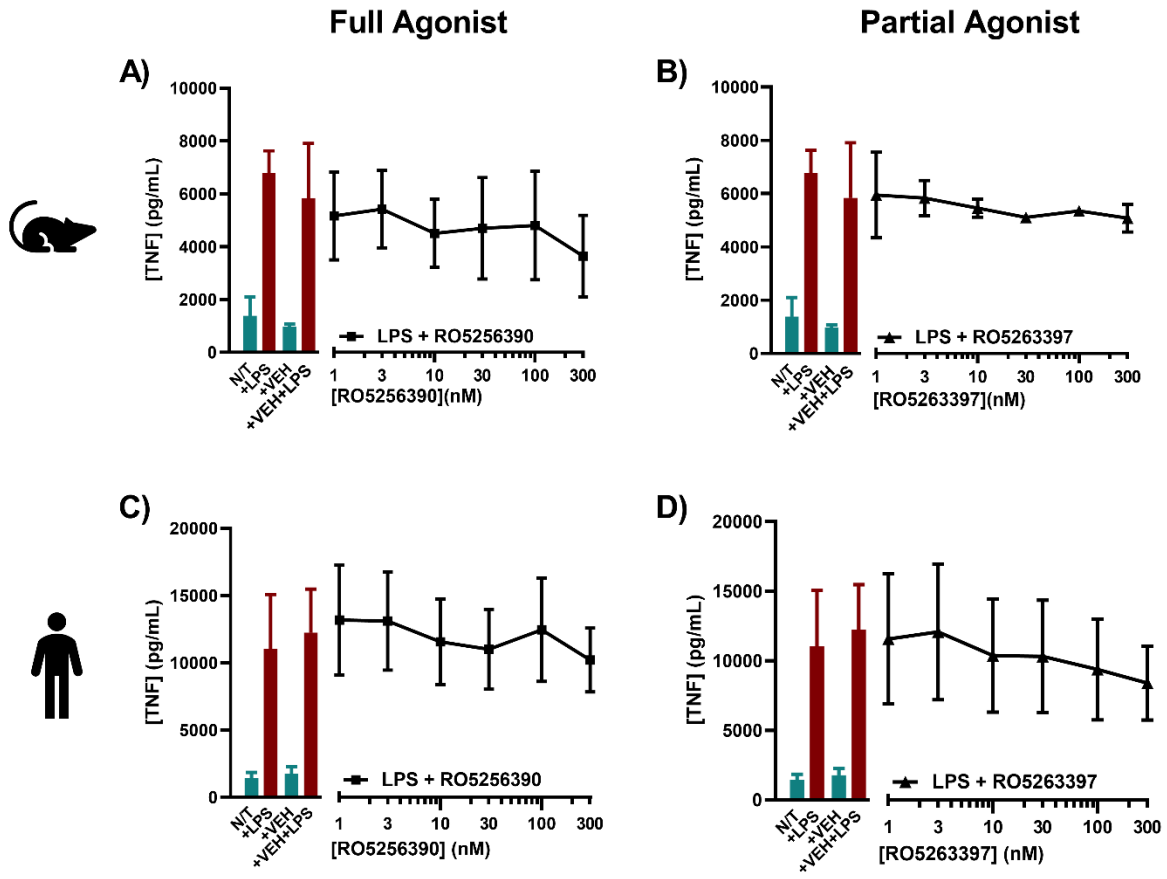

Figure 4.8: LPS-induced TNF secretion from mouse and human macrophages is unaffected by TAAR1 agonism. Mouse BMDMs (A and B) and healthy human MDMs (C and D) were treated with a single administration of LPS (100 ng/mL; 6 hours) in the absence and presence of varying concentrations of either the TAAR1 full agonist RO5256390 (A and C) or partial agonist RO5263397 (B and D). TNF secretion was measured under basal and DMSO-treated (0.1 %; 6 hours) conditions as no treatment (N/T) and drug vehicle (VEH) controls, respectively. Data represents the mean ± SEM of 3 independent experiments.

4.7 ATP is a pro-inflammatory stimulus for induction of cytokine secretion and glycolytic shift in mouse BMDMs.

ATP was next explored as an alternative, physiologically more relevant, pro-inflammatory stimulus. ATP treatment induced significant low-level TNF secretion in a concentration-dependent manner (Figure 4.9A, EC_{50} = 606.1 μM, $\log EC_{50}$ = 2.8, 95% C.I: 2.4 to 3.0, R^2 = 0.7) and 1 mM ATP was chosen for all future experiments (Figure 4.9A). This concentration of ATP was confirmed to induce a time-dependent glycolytic shift (Figure 4.9B - E) clearly decreasing OCR (Figure 4.9B) and increasing ECAR (Figure 4.9C), indicating a clear shift towards glycolytic ATP-production (Figure 4.9D & E), an attribute of pro-inflammatory macrophages (16). Similar to section 4.5, 2 hours was chosen for future Seahorse assays with ATP as the pro-inflammatory stimulus to allow sufficient ranges in OCR and ECAR for deduction of ATP production pathway preference and to minimize potential death from prolonged stimulation.

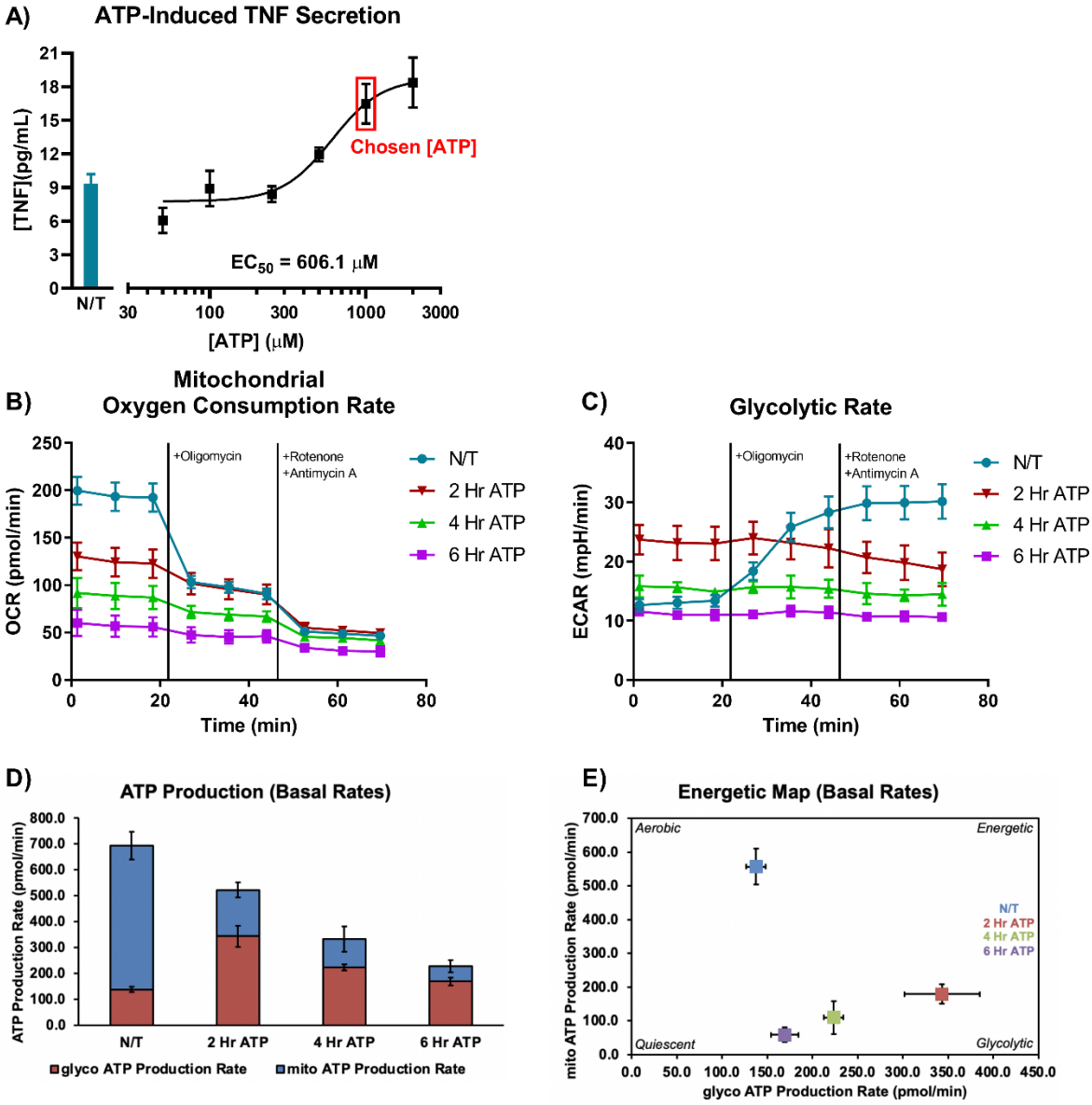
A)
ATP-Induced TNF Secretion
[TNF](pg/mL)
Chosen [ATP]
EC50 = 606.1 μM
N/T
[ATP] (μM)
B)
Mitochondrial
Oxygen Consumption Rate
OCR (pmol/min)
+Oligomycin
+Rotenone
+Antimycin A
N/T
2 Hr ATP
4 Hr ATP
6 Hr ATP
Time (min)
C)
Glycolytic Rate
ECAR (mpH/min)
Time (min)
D)
ATP Production (Basal Rates)
ATP Production Rate (pmol/min)
glyco ATP Production Rate
mito ATP Production Rate
E)
Energetic Map (Basal Rates)
Aerobic
Energetic
Quiescent
Glycolytic
mito ATP Production Rate (pmol/min)
glyco ATP Production Rate (pmol/min)

Figure 4.9: ATP induces low level TNF secretion and glycolytic shift in mouse BMDMs.

TNF secretion (A) was measured from mouse BMDMs treated with a single administration of ATP (6 hrs) at a range of concentrations via ELISA. Following treatment with ATP (1 mM) for either 2, 4, or 6 hrs, the extent of oxidative phosphorylation (C) and glycolysis (D) were measured through monitoring oxygen consumption rate (OCR) and extracellular acidification rate (ECAR), respectively. ATP production due to oxidative phosphorylation or glycolysis was then deduced following sequential administration of oligomycin and rotenone/antimycin A (D and E). ELISA data (A) represents the mean ± SEM of 3 – 5 independent experiments. ATP rate assay data (B - E) represents the mean ± SEM of 3 cultures from a single experiment.

4.8 TAAR1 agonism inhibits ATP-induced TNF secretion from mouse BMDMs, independent of IL-6 secretion or glycolytic shift.

Following administration of ATP and RO5256390, the full TAAR1 agonist inhibited ATP-induced TNF secretion in a concentration-dependent manner (Figure 4.10A, IC_{50} = 19.8 nM, $logIC_{50}$ = 1.3, 95% C.I: could not be determined, R^2 = 0.3). ATP alone or in the presence of RO5256390 had no effect on IL-6 secretion (Figure 4.10B). A propidium iodide uptake assay was used to assess the influence of the treatments on cell viability (Figure 4.10C). No significant difference in propidium iodide uptake was observed under any treatment condition compared to the no-treatment control. Likewise, RO5256390 did not affect the ATP-induced glycolytic shift (Figure 4.11). While the ATP-induced shift towards glycolysis was significant (Figure 4.11C, $P < 0.005$), RO5256390 had no effect on this ATP-induced shift (Figure 4.11C & D).

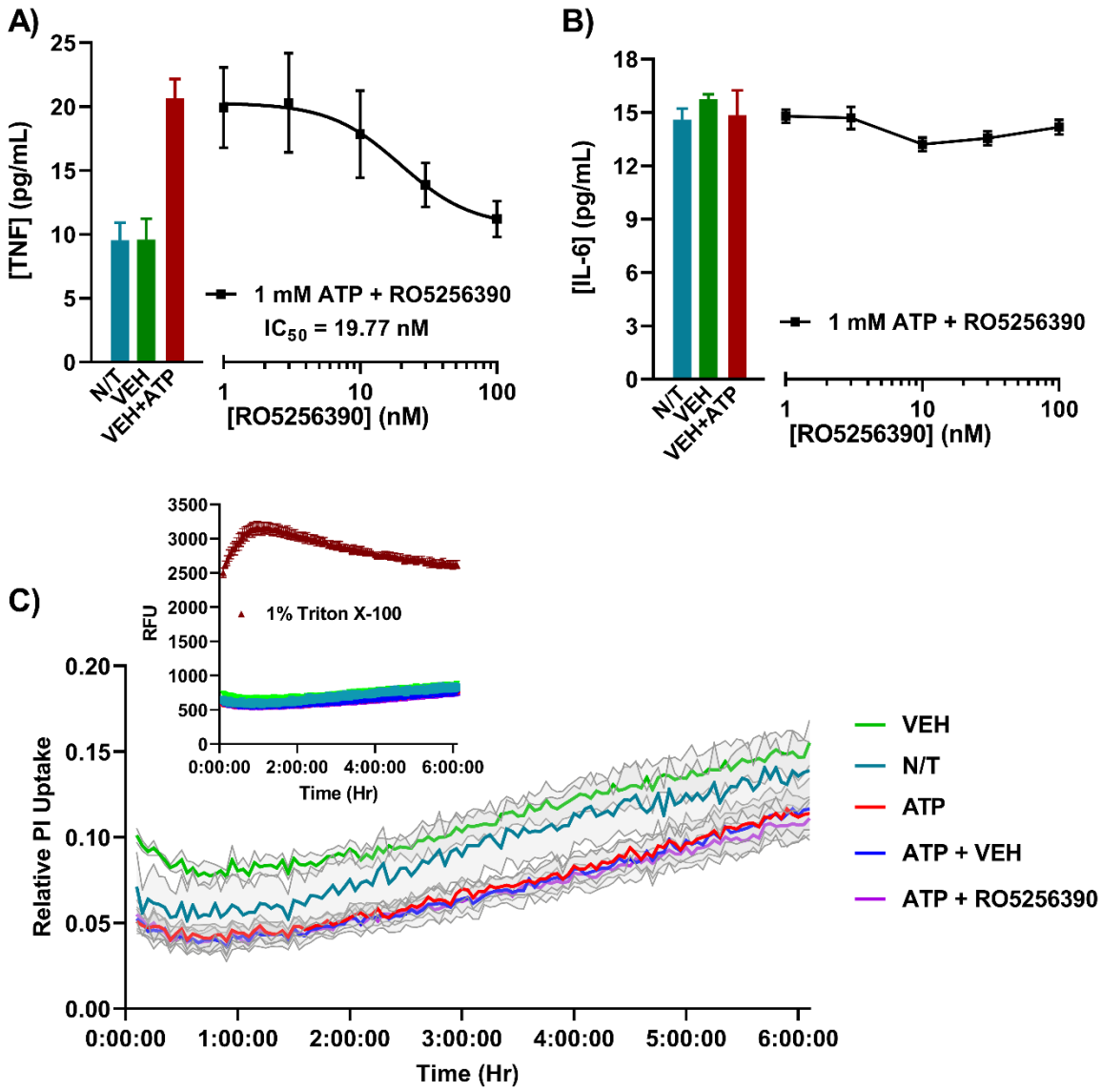
A)
[TNF] (pg/mL)
25
20
15
10
5
0
N/T
VEH
VEH+ATP
1 mM ATP + RO5256390
IC50 = 19.77 nM
1
10
100
[RO5256390] (nM)
B)
[IL-6] (pg/mL)
18
15
12
9
6
3
0
N/T
VEH
VEH+ATP
1 mM ATP + RO5256390
1
10
100
[RO5256390] (nM)
C)
RFU
3500
3000
2500
2000
1500
1000
500
0
1% Triton X-100
0:00:00
2:00:00
4:00:00
6:00:00
Time (Hr)
Relative PI Uptake
0.20
0.15
0.10
0.05
0.00
0:00:00
1:00:00
2:00:00
3:00:00
4:00:00
5:00:00
6:00:00
Time (Hr)
VEH
N/T
ATP
ATP + VEH
ATP + RO5256390

Figure 4.10: ATP-induced TNF secretion from mouse BMDMs is inhibited by TAAR1 agonism and is independent of cell death and IL-6 secretion. TNF (A) and IL-6 (B) secretion from mouse BMDMs treated with ATP (1 mM; 6 hrs) in the absence and presence of varying RO5256390 concentrations were measured via ELISA. The propidium iodide (PI) uptake (C) was measured for mouse BMDMs treated with ATP (1 mM; 6 hrs) ± RO5256390 (100 nM) relative to the maximum value observed from the positive control (1% Triton X-100; inset). Data represents the mean ± SEM of 3-6 independent experiments.

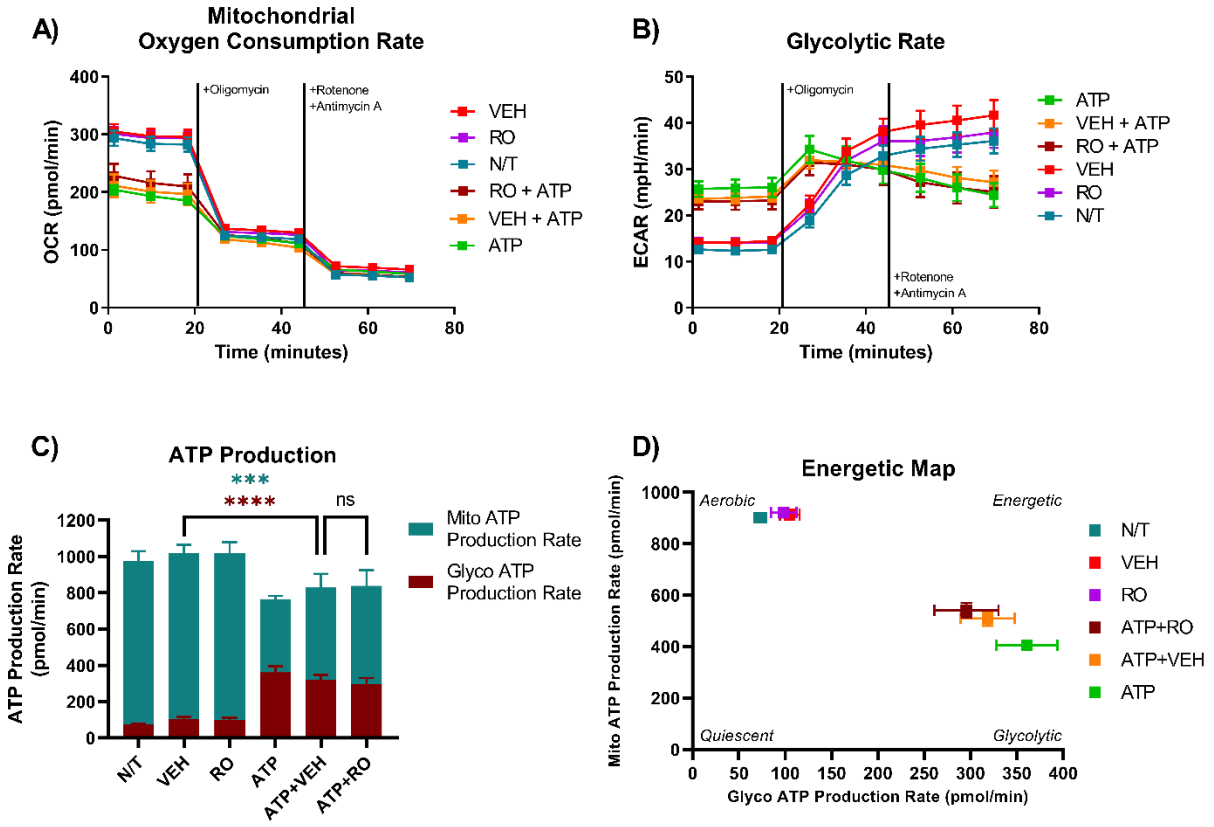

Figure 4.11: ATP-induced glycolytic shift in mouse BMDMs is unaffected by TAAR1 agonism. Following treatment with ATP (1 mM) ± RO5256390 (100 nM) for 2 hours, the extent of oxidative phosphorylation (A) and glycolysis (B) in mouse BMDMs was measured through monitoring oxygen consumption rate (OCR) and extracellular acidification rate (ECAR), respectively. The rate of mitochondrial and glycolytic ATP production was then deduced (C & D) following sequential administration of oligomycin followed by rotenone/antimycin A. Data represents the mean ± SEM of 3 independent experiments. Statistical analysis (C) consisted of an ordinary one-way ANOVA (mito ATP production rate; $P < 0.0001$, glyco ATP production rate $P < 0.0001$) with Turkey's multiple comparisons test between indicated treatment conditions and the vehicle control (VEH) (***$P < 0.0005$, ****$P < 0.0001$).

4.9 ATP does not induce TNF secretion from human MDMs or mouse microglia.

In contrast to the effects in mouse BMDMs, ATP did not induce TNF secretion in either human MDMs (Figure 4.12) or mouse microglia (Figure 4.13). There was an apparent decrease in TNF secretion at 1 mM ATP in pure microglia cultures (Figure 4.13A) that was not seen in mixed glia. The lack of increased TNF secretion in microglia was not affected by the presence of astrocytes (Figure 4.13B).

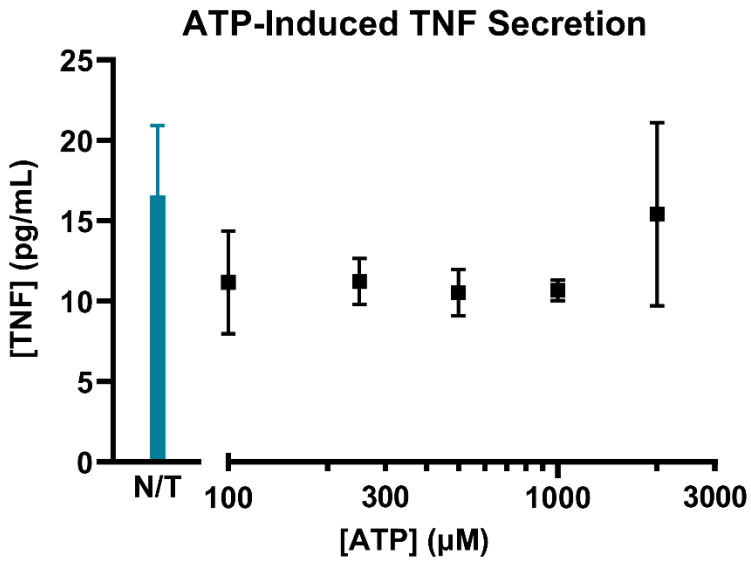

Figure 4.12: ATP does not induce TNF secretion from human MDMs. TNF secretion was measured via ELISA from human MDMs treated with a single administration of ATP (6 hrs) at a range of concentrations. Data represents the mean ± SEM of 3 independent experiments.

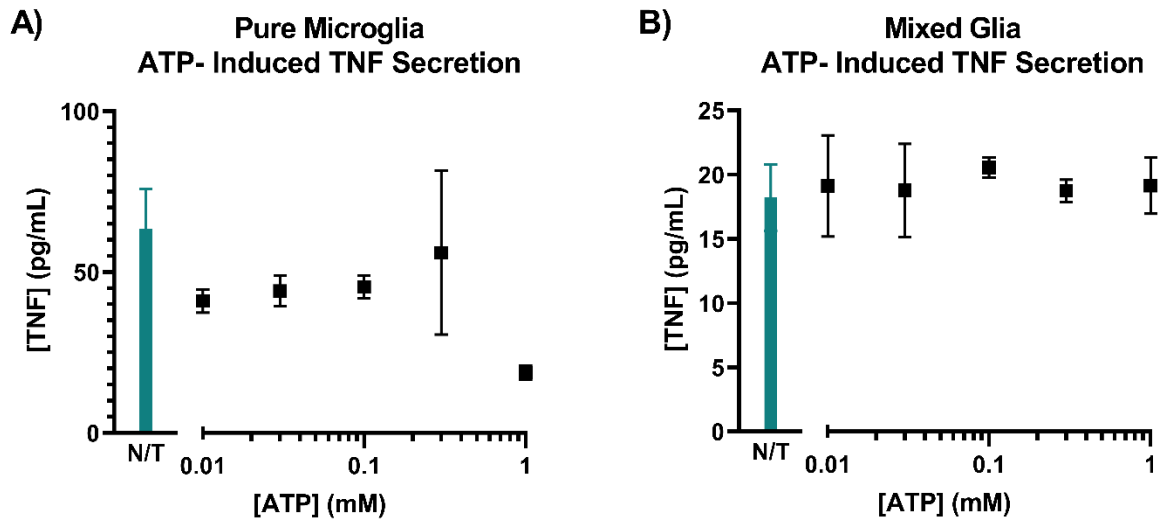

Figure 4.13: ATP does not induce TNF secretion from mouse pure microglia or mixed glia cultures. TNF secretion was measured via ELISA from mouse microglia cultured in the absence (A) or presence (B) of astrocytes and treated with a single administration of ATP (6 hrs) at a range of concentrations. Data represents the mean ± SEM of 3 independent experiments.

4.10 TAAR1 agonism does not affect ADP-induced cytokine secretion from mouse microglia in either the absence or presence of astrocytes.

ADP was validated as an alternative pro-inflammatory stimulus for both pure mouse microglia and mouse microglia co-cultured with astrocytes (Figure 4.14). In pure microglia, 24 hour ADP treatment induced minor TNF secretion in a concentration-dependent manner (Figure 4.14A; Table 4.1) and IL-6 (Figure 4.14C; Table 4.1) secretion at the highest concentration of ADP used (10 mM). In mixed glial cultures, ADP induced a far more pronounced concentration-dependent secretion of both TNF (Figure 4.14B; Table 4.1) and IL-6 (Figure 4.14D; Table 4.1). Notably, the basal levels of TNF were higher in the purified microglia cultures (Figure 4.14A) compared to the mixed glial cultures (Figure 4.14B) and the amount of IL-6 secreted as a result of ADP stimulation was roughly 40-fold higher in the cultures containing astrocytes (Figure 4.14D), compared to those without (Figure 4.14C). To minimize cell death from over-stimulation while still ensuring an effect, a concentration of 3 mM was selected for all future experiments with ADP stimulation.

Next, levels of ADP-induced TNF and IL-6 secretion were measured following treatment of purified and mixed microglia cultures with the full TAAR1 agonist RO5256390 (Figure 4.15). In all cases, RO5256390 had no effect on ADP-induced cytokine secretion (Figure 4.15A - D).

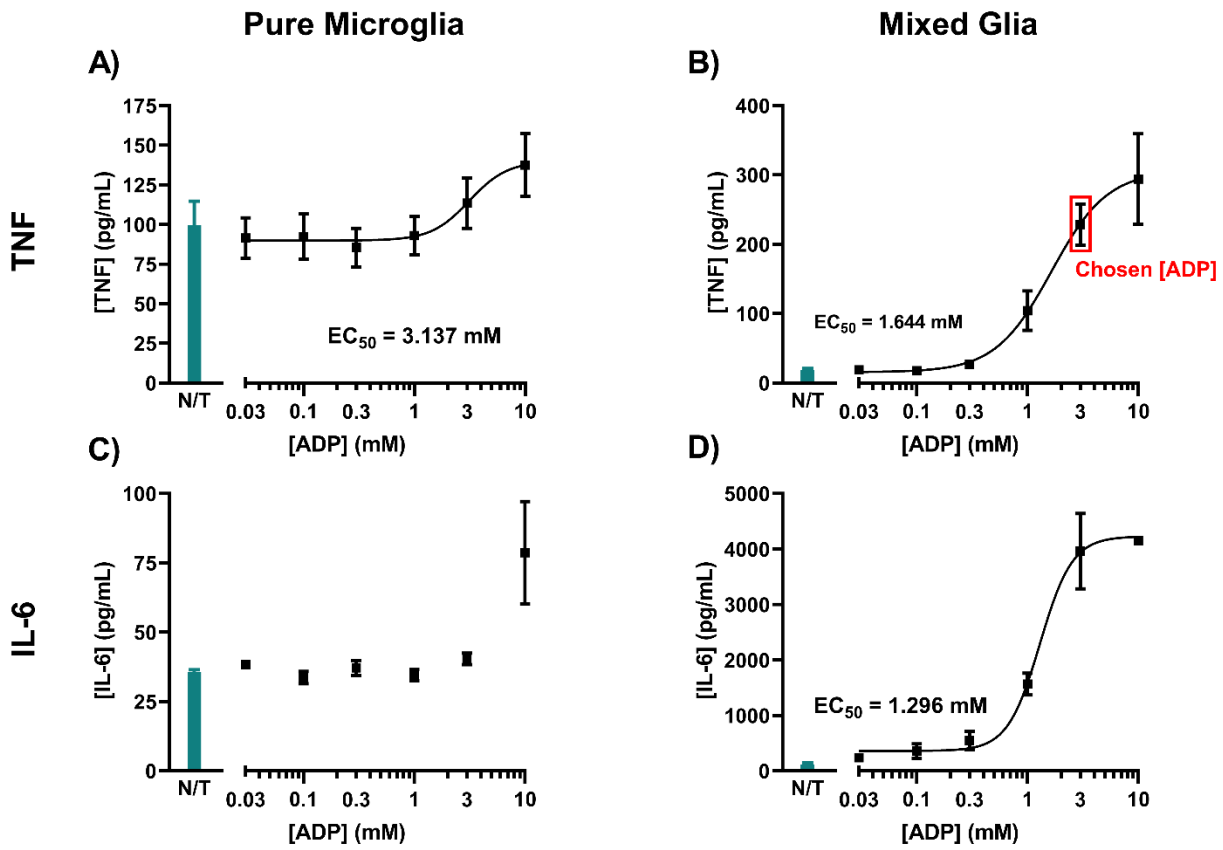

Figure 4.14: ADP induces TNF and IL-6 secretion from mouse pure microglia and mixed glia cultures. TNF (A & B) and IL-6 (C & D) secretion from mouse microglia cultured in the absence (A & C) or presence (B & D) of astrocytes was measured via ELISA in the absence or presence of a single administration of ADP (24 hrs) at a range of concentrations. A concentration of 3 mM was selected for ADP treatment in future experiments (red). Data represents the mean ± SEM of 3 independent experiments.

Table 4.1: TNF and IL-6 Secretion from Pure Microglia and Mixed Glia Cultures Treated with ADP

		EC_{50} (mM)	$logEC_{50}$	95% C.I.
TNF	Pure Microglia	3.1	0.5	n.d.
	Mixed Glia	1.6	0.2	-0.3 – 0.4
IL-6	Pure Microglia	n.d.*	n.d.	n.d.
	Mixed Gia	1.3	0.11	-0.02 – 0.35

*IL-6 secretion only observed at highest concentration of ADP.

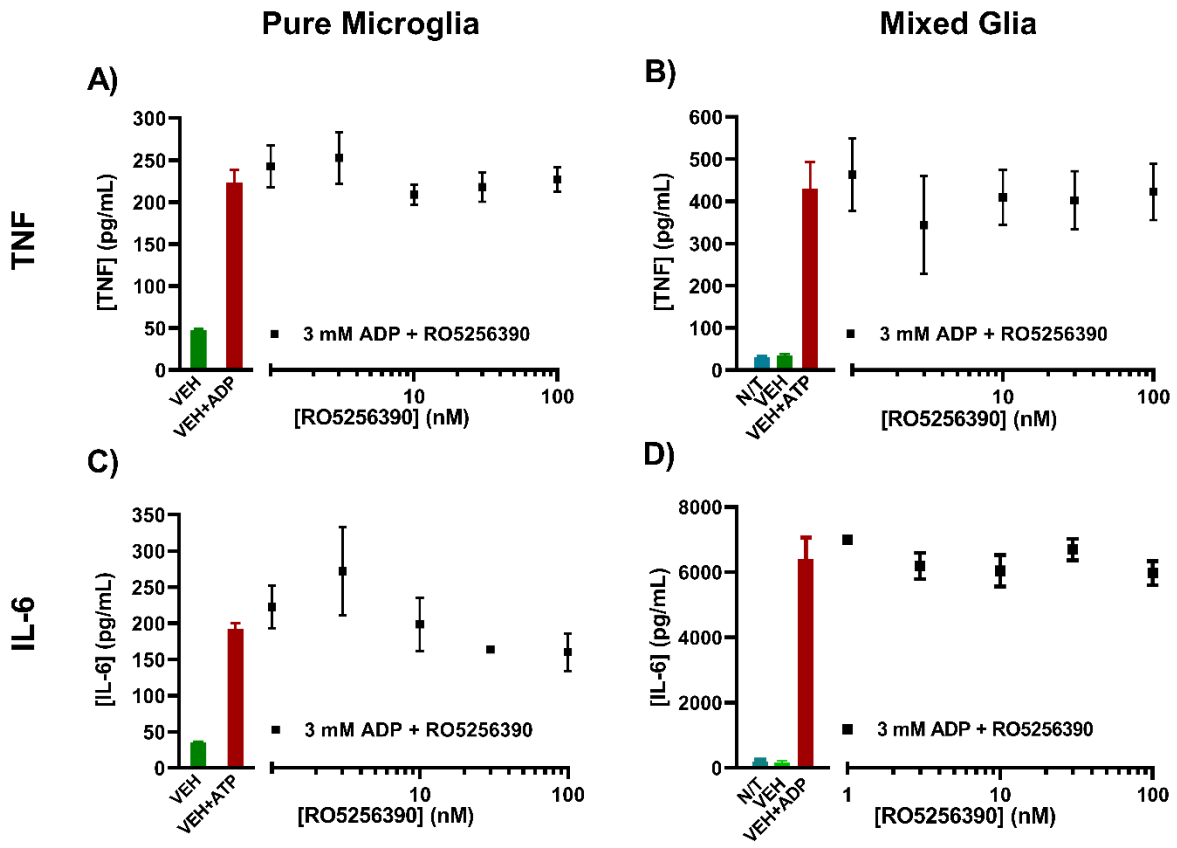

Figure 4.15: ADP-induced TNF and IL-6 secretion from mouse pure microglia and mixed glia cultures is unaffected by TAAR1 agonism. TNF (A & B) and IL-6 (C & D) secretion was measured via ELISA from mouse microglia cultured in the absence (A & C) or presence (B & D) of astrocytes treated with 3 mM ADP (24 hrs) ± RO5256390 at a range of concentrations. Data represents the mean ± SEM of 3 independent experiments.

4.11 ADP induces TNF secretion from human fetal microglia.

To investigate ADP as a possible pro-inflammatory stimulus for human microglia, TNF secretion from purified human fetal microglia was measured following treatment with either ADP or the selective P2Y receptor agonist 2-methylthio-ADP (Figure 4.16). ADP induced TNF secretion, while 2-methylthio-ADP did not (Figure 4.16), suggesting the observed response is not due to P2Y receptor stimulation. The observed TNF secretion was approximately 10-fold lower than that of the LPS-treated positive control (red bar).

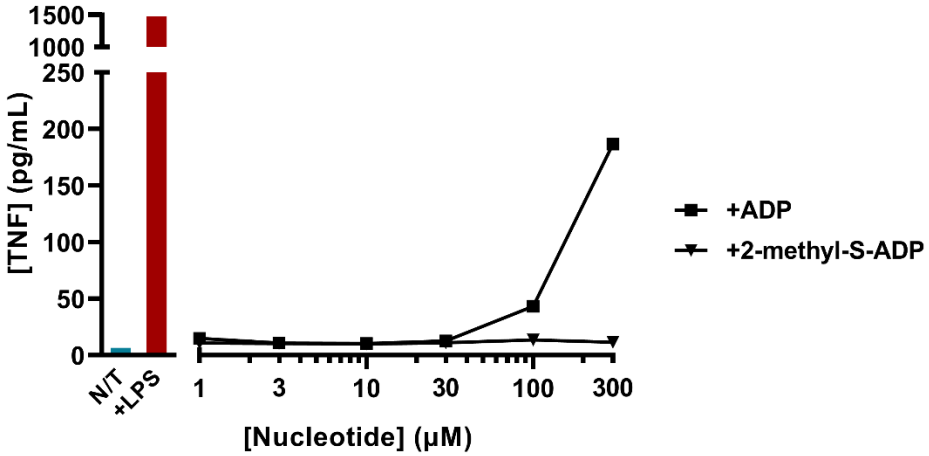

4.16: ADP induces TNF secretion from human fetal microglia while 2-methylthio-ADP does not. TNF secretion was measured via ELISA from human fetal microglia treated with a single administration of ADP or 2-methylthio-ADP (2-methyl-S-ADP) at a range of concentrations. Data represents the mean of two independent cultures within a single experiment.

*4.12 *Published Results Disclosure*

The following publications feature the listed data:

Barnes DA, Galloway DA, Hoener MC, Berry MD, Moore CS (2021). TAAR1 Expression in Human Macrophages and Brain Tissue: A Potential Novel Facet of MS Neuroinflammation. *Int J Mol Sci.* **22**(21):11576.

- Includes data from figures 4.1, 4.4, 4.5, and 4.6.
- Includes data from tables 3.1, 3.2, and 3.3.

V. DISCUSSION

Based on the established neuroregulatory (67) and emerging immunomodulatory properties of TAAR1 (65), I aimed to investigate whether TAAR1 could be a novel protein of interest in the pathophysiology of MS. Herein, I have provided the first systematic analysis of TAAR1 expression at both the mRNA and protein level in primary MS patient samples, from both the periphery and within the CNS. Additionally, I have provided the initial characterization of function for TAAR1 agonism within myeloid-derived immune cells relevant to MS pathophysiology. With an increasing interest in the myeloid cell compartment in the context of MS pathogenesis (124), this study focused on macrophages and their peripheral precursors, monocytes. RT-qPCR analyses of both MS patient whole PBMCs and CD14+ monocytes provided evidence of a potential clinical relevance for TAAR1 in MS and the basis for future examination of the role of TAAR1 in human monocytes and macrophages.

Analyses of relative *TAAR1* expression demonstrated no significant difference in *TAAR1* mRNA levels in MS patient whole PBMCs compared to controls, however, in both the NIND and MS patient groups, there was a significant increase in variance compared to controls (Figure 4.1B). The multiple subtypes and fluidity associated with MS progression and relapse (39) could be related to this observed increase in variance, raising the possibility that increased *TAAR1* expression is a biomarker of disease subtypes. Additionally, MS is prevalent in the global population at a female to male ratio of 3:1 (39), which was represented within my study cohort, however, participant numbers were insufficient to conclude that there was any significant effect of sex in either whole PBMCs or CD14+ monocytes. With an increased sample size, the basis of any sex component to the increased variation could be further investigated.

When assessing CD14+ monocytes, a significant decrease was observed when comparing *TAAR1* mRNA levels in MS patients to healthy volunteers (Figure 4.1C). That whole PBMCs trended towards an increase in TAAR1 mRNA is potentially indicative of different functions of TAAR1 in different leukocyte populations. The MS patient monocytes and PBMCs used for this study were collected from treatment-naïve patients early in their disease course and, as such, there was no confounding factor relating to treatment status. In MS, altered polarization of peripherally-derived and CNS-resident macrophages is directly involved in the periods of inflammatory demyelination and anti-inflammatory remyelination associated with relapse and remission periods (124,125). Sample numbers did not allow analysis of whether expression levels were related to relapse or remission status at the time of blood sampling and would be an area worth considering in future studies. Previous reports have associated TAAR1 activation with anti-inflammatory T cell differentiation (91). If TAAR1 has a similar function in monocytes and monocyte-derived macrophages, lower *TAAR1* mRNA could be indicative of decreased anti-inflammatory differentiation which could lead to the pro-inflammatory state causing the increased demyelination in MS.

Having found evidence for altered *TAAR1* mRNA expression, the next step was to analyze TAAR1 protein expression in human immune cells, given that target mRNA and protein levels can vary greatly because of the many different variations in post-transcriptional and translational regulation. To assess TAAR1 protein expression in human PBMCs, I first aimed to validate a selective anti-human TAAR1 antibody (85) for flow cytometric analyses using primary samples (Figure 4.2 & 4.3). Healthy human PBMCs were gated (Figure 4.2) to assess TAAR1 expression within CD14+ (monocyte), CD3+ (T cell), and CD20+ (B cell) populations. I observed that TAAR1 expression was most associated with B cells (46% of cells selected; Figure 4.3B), also

present in monocytes (31.6% of cells selected; Figure 4.3C), but absent from T cells (Figure 4.3A). More prominent expression levels in B cells supports previous studies which established *TAAR1* mRNA as abundantly expressed in B cells (91-93), while the moderate expression observed in monocytes is also in line with a previous study (91). The established research in the field suggests TAAR1 is expressed at both the mRNA and protein level in human T cells and is functionally relevant to T cell differentiation (91), however, no TAAR1 expression was observed. This observation could be due to TAAR1 upregulation following T cell stimulation or co-stimulatory interaction, in keeping with observed changes in TAAR1 expression following stimulation in macrophages (Figure 4.5).When taken in combination with the observed overlap in signal with the isotype (Figure 4.3), however, the lack of observed expression could suggest that the antibody used in this study may not have had suitable sensitivity for effectively detecting TAAR1 in human PBMCs. Although vigorous troubleshooting was attempted through adjusting antibody and isotype concentrations, the results shown (Figure 4.3) reflect the most successful attempt. Instead of committing further resources to developing this protocol, I shifted focus towards supplementing my TAAR1 mRNA analyses with protein analyses using immunocytochemistry, a technique that had been previously used to validate the specificity of the antibody and for other studies (85,101).

Using macrophages derived from human CD14+ peripheral monocytes, I observed TAAR1 localization under standard cell culture conditions and following pro-inflammatory stimulation. In contrast to the archetypal localization of GPCRs within the plasma membrane, reports of TAAR1 expression primarily describe an intracellular localization (75,79,85,88,91,101,126). Under standard conditions, resting macrophages showed TAAR1 protein expression primarily localized to the nucleus, with pro-inflammatory stimulation inducing a shift to a diffuse intracellular distribution (Figure 4.5), presumably associated with membrane structures throughout the

cytoplasm. With regards to TAAR1, nuclear sub-cellular distribution has previously been seen in some, but not all, breast cancer cell lines (101), although the functional relevance of this has yet to be determined. Nuclear functions of GPCRs are an emerging area of therapeutic interest, with established functions in regulation of transcription, cell proliferation, cell migration, apoptosis, and angiogenesis (127). Altered sub-cellular localization of GPCRs has been previously reported to occur during immune cell activation (128). For example, the sphingosine-1-phosphate receptor was reported to show altered expression, localization, and function in stimulated and unstimulated T cells (128). The altered sub-cellular localization of TAAR1 following stimulation suggests variable TAAR1 function that may be dependent on the state of macrophage polarization, thereby implicating TAAR1 as a novel component of inflammatory cellular processes such as migration and proliferation, both of which are associated with the neuroinflammation occurring in an active MS lesion.

Interestingly, there has been no consensus as to the exact location of TAAR1 within the cell. A recent study has shown that following serum-starvation, TAAR1 shifts from a perinuclear localization to the cilia of mouse thyroid epithelial cells, a re-localization proposed to facilitate TAAR1 interaction with the extracellular environment (126), indicating that TAAR1 sub-cellular localization may be dependent on environmental (extracellular) signals. A similar situation could be occurring in macrophages, where the function of TAAR1 under pro-inflammatory conditions requires trafficking to the cytosol. Other studies have primarily associated TAAR1 localization with intracellular membrane structures such as the Golgi apparatus (85,129). Co-localization studies with organelle markers or higher resolution, real-time imaging studies could further clarify the precise localization and consequences of variable sub-localization of TAAR1 and the signals mediating such receptor trafficking.

For the next portion of the study, I provided the first visualization of TAAR1 protein in human brain tissue with immunohistochemical analysis of a post-mortem MS patient brain section (Figure 4.6). As previously performed in our lab, I first identified mixed active/inactive MS lesions with hematoxylin and eosin (Figure 4.6A), luxol fast blue (Figure 4.6B), and CD68 (Figure 4.6C) staining via brightfield microscopy (120). A mixed active/inactive lesion features an "active," and expanding, border region rich with pro-inflammatory peripheral macrophages and CNS-resident microglia, in addition to an inactive and demyelinated center composed of glial scar tissue (130). The area surrounding the mixed active/inactive lesion is classified as NAWM on the basis of normal appearing myelination and lack of immune cell aggregation (130). In the identified lesion, the center region showed little staining for TAAR1 and is consistent with noticeably fewer macrophages/microglia and a predominance of metabolically inactive scar tissue (Figure 4.6F). Meanwhile the NAWM had clear TAAR1 staining (Figure 4.6D), however virtually no co-localization with the macrophage/microglia marker IBA-1 was observed (Figure 4.6G). Interestingly, within the inflamed border region of the identified MS lesion, pronounced colocalization of IBA-1 with TAAR1 was observed (Figure 4.6E). More specifically, I observed IBA-1 positive cells (macrophages and/or microglia) with particularly prominent TAAR1 staining associated in close proximity with blood vessels within this region (Figure 4.6H). This raises the intriguing possibility that TAAR1 protein is up-regulated in macrophages (perhaps in contrast to microglia) during the active phase of extravasation and CNS invasion. This would be consistent with previous reports that TAAR1 plays a role in immune cell chemotaxis (91), and could also suggest that TAAR1 ligands serve as a new family of DAMPs. In these cells TAAR1 exhibited a diffuse intracellular localization, similar to that observed in pro-inflammatory stimulated peripherally-derived macrophages (Figure 4.5). Within the defined border region, but more distant

from the blood vessel, a combination of macrophages/microglia with and without TAAR1 staining was observed (Figure 4.6I). This further supports my hypothesis that TAAR1 protein is increased in extravasating pro-inflammatory peripheral macrophages within the border of an MS lesion and should be an area of focus for future investigations.

Following successful demonstration of TAAR1 mRNA and protein in myeloid cells relevant to MS pathophysiology, I next aimed to elucidate the function of TAAR1 agonism in these cells through analyzing the effect of TAAR1 activation on pro-inflammatory-induced cytokine secretion and metabolic shift. Initially, the established pro-inflammatory stimulus LPS (131) was used to induce a robust pro-inflammatory response in primary mouse (Figure 4.7 & 9) and human macrophages (Figure 4.8), polarizing them towards an M1-like phenotype. Administration of selective and potent TAAR1 full (RO5256390) or partial (RO5263397) agonists had no effect on LPS-induced TNF secretion in either mouse or human primary macrophages (Figure 4.8). The oligodendrocyte and neuronal death associated with MS pathophysiology results in the release of nucleotides such as ATP and ADP that induce purinergic signaling in surrounding immune cells, seen as a DAMP-mediated pro-inflammatory response (132). I therefore examined extracellular purines as a pro-inflammatory stimulus that would induce a response that is more physiologically-relevant to MS. Extracellular ATP exposure to mouse BMDMs resulted in low level TNF secretion (Figure 4.9A) and a shift in metabolic profile towards glycolysis as the primary source of energy production (Figure 4.9B-E), both of which are consistent with pro-inflammatory activation (14,16).

Purinergic signaling in macrophages and microglia occurs through two main classes of receptor: P2X receptors which act as ligand-gated cation channels (25) and P2Y receptors which are G_i protein-coupled receptors (26). The observed EC_{50} value of 606 μM is most consistent with

the activation of the $P2X_7$ purinoceptor, which has a reported EC_{50} value of 100 μM. In contrast, reported EC_{50} values for ATP binding at various other purinoceptors lie within the range of 0.5 to 10 μM (25). $P2X_7$-mediated pro-inflammatory polarization of mouse BMDMs is also consistent with the established designation of $P2X_7$ as a pro-inflammatory receptor (25). Although high concentration ATP is known to facilitate inflammatory cell death when in combination with other pro-inflammatory compounds (133), a PI-uptake assay confirmed mouse BMDMs maintained viability throughout treatment, ruling out cell-death as the cause of the low-level TNF secretion (Figure 4.10C).

TNF and IL-6 are both transcriptionally regulated by the induction of the transcription factor NF-κB (134), however, they differ in their secretory pathway (135). TNF is produced and trafficked to the outer membrane, where it is cleaved from its transmembrane form to its soluble form by the enzyme TNFα cleaving enzyme (TACE; EC 3.4.24.86), whereas IL-6 is produced in its soluble form and secreted via exocytosis (135). Since there was no evidence of ATP-induced secretion of IL-6, we can conclude that NF-κB expression is not being induced by extracellular ATP, and that the low level TNF secretion observed may be the product of interplay between purinergic signaling and the unique secretory pathway components for TNF.

There exist a number of pathways for TAAR1 signalling in macrophages. Treatment with RO5256390 inhibited the low level TNF secretion induced by extracellular ATP (Figure 4.10A) from mouse BMDMs, with no effect on IL-6 secretion (Figure 4.10B) suggesting an opposition between purinergic signaling and TAAR1 signaling in the macrophage inflammatory response. Since TAAR1 is an established G_s protein-coupled receptor (70) and is also known to signal through opening GirK channels via activation (105), there exist multiple opportunities for competition with purinergic signaling. As previously discussed, the observed EC_{50} for ATP

suggests $P2X_7$ is inducing the pro-inflammatory activation in mouse BMDMs, and since $P2X_7$ functions as a ligand-gated ion channel (25), perhaps TAAR1-mediated GirK channels counteract $P2X_7$ signaling and the TNF secretion downstream. Teasing out the precise interaction between these vast signaling networks represents an area of future study for TAAR1 signaling in macrophages.

In assessing the metabolic profile of mouse BMDMs following ATP stimulation, I observed that ATP induced a significant shift towards glycolysis for energy production. TAAR1 has been implicated in metabolic reconfiguration in mice via the trace amine 3-iodothyronamine, an endogenous TAAR1 agonist (67), inducing a switch from glucose to lipid utilization (136). As previously described, in terms of macrophage metabolic profile, utilization of glycolysis for energy production is associated with an M1 phenotype and pro-inflammatory stimulation, whereas M2 macrophages switch towards using β oxidation to fuel the electron transport chain within the mitochondria for energy production (16). The ATP induced a pro-inflammatory metabolic switch (Figure 4.11C) which was unaffected by RO5256390 (Figure 4.11C & D) at a concentration that was previously observed to significantly inhibit TNF secretion (Figure 4.10A). This suggests that TAAR1 agonism interacts with macrophage pro-inflammatory signaling down-stream of glycolytic shift, but upstream of TNF secretion. In addition to fueling antioxidant pathways, the principle reason for the glycolytic shift in M1 macrophages is to allow the use of Kreb's cycle intermediates, pentose phosphate pathway intermediates, and the mitochondria for cytokine production (16). Given this, we can assume that TNF is still being produced and prepared for secretion in pro-inflammatory BMDMs, and that TAAR1-mediated inhibition is not due to decreased TNF synthesis. This also raises the possibility that the observed change in expression pattern from primarily within the nucleus to a diffuse pattern throughout the cytoplasm following

pro-inflammatory stimulation (Figure 4.5), could relate to interplay between TAAR1 signaling and the TNF secretory pathway.

Having demonstrated TAAR1-mediuated regulation of pro-inflammatory signaling in mouse macrophages, I sought to confirm a similar effect in human cells. Extracellular ATP, however, did not induce the same low-level TNF secretion in human MDMs (Figure 4.12). I therefore examined the effects of TAAR1 agonism on pro-inflammatory stimulation and cytokine secretion from microglia and astrocytes, CNS-resident myeloid-derived cell types also relevant to MS neuroinflammation. ATP again failed to produce a TNF response (Figure 4.13A & B). Since microglia highly express the $P2Y_{12}$ purinergic receptor subtype (26), and it is established that ADP is a preferential agonist for this receptor (26), the effects of ADP treatment were investigated. ADP successfully induced TNF secretion from mouse microglia in both the absence and presence of astrocytes (Figure 4.14A & B). The reported EC_{50} for ADP at $P2Y_{12}$, however, is 60 nM (26), which makes the observed millimolar responses observed here unlikely to be $P2Y_{12}$-mediated (Figure 4.14).

Intriguingly, basal extracellular TNF levels were higher in the purified microglia cultures (Figure 4.14A) than the co-cultures containing astrocytes (Figure 4.14B), however, following pro-inflammatory activation secreted TNF levels were markedly higher in the co-cultures, implying that astrocytes help maintain the resting phenotype of microglia but facilitate polarization towards the pro-inflammatory phenotype in the presence of DAMPs. This lends further support towards the established cross-talk between microglia and astrocytes during events of damage or disease (137). Additionally, two different levels of IL-6 response were observed: low level secretion from pure microglia (Figure 4.14C) and a robust IL-6 response in the presence of astrocytes (Figure 4.14D), in which levels of secreted IL-6 were 40-fold higher than in pure microglia cultures. This

is again consistent with previous evidence for cross-talk between microglia and astrocytes (137). In this instance it could be the case that either low-level IL-6 secretion from microglia stimulates astrocytic IL-6 production or astrocyte-released factors communicate towards microglia to produce profoundly higher levels of IL-6 in the event of CNS damage.

While the research surrounding TAAR1 in microglia is limited to a meta-analysis suggesting very low-level expression (117), TAAR1 has been previously implicated in regulating astrocytic processes such as glutamate clearance in response to viral infection (114,115). In the current study, no effect of RO5256390 on the stimulated TNF or IL-6 secretion was seen in either the presence or absence of astrocytes (Figure 4.15A-D). The lack of inhibition seen with TNF secretion in this case, compared to the effect seen with peripherally-derived mouse BMDMs (Figure 4.9A) suggests that TAAR1 function may differ in CNS resident macrophages compared to those of the periphery. The previously described analyses of TAAR1 expression bordering human MS lesions supports differing function in CNS-resident and peripherally-derived macrophages, where TAAR1 expression was heterogeneous, with preference towards those near a peripheral interface (Figure 4.6H). Further analyses of the expression and immunological function of TAAR1 in peripheral and CNS-resident macrophage pools could help elucidate whether TAAR1-mediated effects within the immune system are strictly peripheral or not.

In the final experiments of this study, purified human fetal microglia cultures (118) were examined. Due to limited sample availability, only a single experiment could be performed. Similar to the response seen in pure mouse microglia cultures (Figure 4.14A), ADP induced a TNF response (Figure 4.16) only at high concentrations. The P2Y receptor agonist 2-methylthio-ADP (138), however, did not induce the same effect (Figure 4.16). As previously discussed, the observed responses from purinergic activation with mouse BMDMs were not consistent with P2Y

receptor activation (Figure 4.9 & 11), and since 2-methylthio-ADP did not induce a response, this may be the case with mouse microglia as well. This brings to question whether the effects seen on cytokine secretion are truly P2Y-mediated as previously stated in the literature (26), or if the effects are due to the activation of a different purinergic receptor. In the case of further studies with ADP and human microglia, investigation into metabolic profile as conducted with ATP and mouse BMDMs (Figure 4.11) could yield results that help verify pro-inflammatory activation.

VI. CONCLUSIONS & FUTURE DIRECTIONS

In conclusion, this study demonstrates the potential for a novel link between TAAR1 and MS pathophysiology and establishes critical preliminary research towards elucidating the function of TAAR1 in peripheral and CNS-resident macrophages. I observed a statistically significant decrease in TAAR1 mRNA in MS patient monocytes compared to controls, a pronounced shift in sub-cellular localization following pro-inflammatory stimulation in peripheral macrophages, and TAAR1 colocalization with the macrophage and microglia marker IBA-1 within the inflamed border region of an MS lesion. Taken together, these observations suggest TAAR1 function is both cell-type and stimulation-status dependent. Additionally, I observed TAAR1-mediated inhibition of ATP-induced TNF secretion in mouse macrophages and determined that this effect was independent of transcriptional regulation and shift in metabolic profile. Finally, I determined that while ADP can be used as a robust pro-inflammatory stimulus for microglia in the presence and absence of astrocytes, this pro-inflammatory response is unaffected by TAAR1 agonism.

These findings support further study towards elucidating the role of TAAR1 in immune cell populations, and the pharmacological investigation of selective TAAR1 agonists (103,139) in animal models of MS (46). Future directions for this project should include further investigation of TAAR1 mRNA expression levels in MS patients in other immune cell subsets such as T cells or B cells or longitudinal analysis of TAAR1 mRNA levels throughout the MS disease course and within disease sub-types. Expanding cohorts and analysis of TAAR1 mRNA levels in MS patients could also support sex-dependent differences in expression as well. For further elucidation of the function of TAAR1 in monocytes and macrophages, chemotaxis assays utilizing a TAAR1 agonist chemokine gradient could further investigate the proposed links between immune cell extravasation and TAAR1 expression. Lastly, assessment of TAAR1 agonism in an animal model

such as induced EAE (46) could provide valuable information towards the potential for TAAR1 agonists in MS treatment.

VII. REFERENCES

1. Stephen, B., and Hajjar, J. (2018) Overview of Basic Immunology and Translational Relevance for Clinical Investigators. *Adv Exp Med Biol* **995**, 1-41
2. Marshall, J. S., Warrington, R., Watson, W., and Kim, H. L. (2018) An introduction to immunology and immunopathology. *Allergy Asthma Clin Immunol* **14**, 49
3. Hoffman, W., Lakkis, F. G., and Chalasani, G. (2016) B Cells, Antibodies, and More. *Clin J Am Soc Nephrol* **11**, 137-154
4. Kumar, B. V., Connors, T. J., and Farber, D. L. (2018) Human T Cell Development, Localization, and Function throughout Life. *Immunity* **48**, 202-213
5. Wan, Y. Y. (2010) Multi-tasking of helper T cells. *Immunology* **130**, 166-171
6. Berry, S. P. D., Dossou, C., Kashif, A., Sharifinejad, N., Azizi, G., Hamedifar, H., Sabzvari, A., and Zian, Z. (2021) The role of IL-17 and anti-IL-17 agents in the immunopathogenesis and management of autoimmune and inflammatory diseases. *Int Immunopharmacol*, 108402
7. Tang, D., Kang, R., Coyne, C. B., Zeh, H. J., and Lotze, M. T. (2012) PAMPs and DAMPs: signal 0s that spur autophagy and immunity. *Immunol Rev* **249**, 158-175
8. Hart, G. T., Tran, T. M., Theorell, J., Schlums, H., Arora, G., Rajagopalan, S., Sangala, A. D. J., Welsh, K. J., Traore, B., Pierce, S. K., Crompton, P. D., Bryceson, Y. T., and Long, E. O. (2019) Adaptive NK cells in people exposed to Plasmodium falciparum correlate with protection from malaria. *J Exp Med* **216**, 1280-1290
9. Guilliams, M., Mildner, A., and Yona, S. (2018) Developmental and Functional Heterogeneity of Monocytes. *Immunity* **49**, 595-613

10. Zanoni, I., Ostuni, R., Marek, L. R., Barresi, S., Barbalat, R., Barton, G. M., Granucci, F., and Kagan, J. C. (2011) CD14 controls the LPS-induced endocytosis of Toll-like receptor 4. *Cell* **147**, 868-880

11. Koenderman, L. (2019) Inside-Out Control of Fc-Receptors. *Front Immunol* **10**, 544

12. Zhao, Y., Zou, W., Du, J., and Zhao, Y. (2018) The origins and homeostasis of monocytes and tissue-resident macrophages in physiological situation. *J Cell Physiol* **233**, 6425-6439

13. Chazaud, B. (2020) Inflammation and Skeletal Muscle Regeneration: Leave It to the Macrophages! *Trends Immunol* **41**, 481-492

14. Mosser, D. M., and Edwards, J. P. (2008) Exploring the full spectrum of macrophage activation. *Nat Rev Immunol* **8**, 958-969

15. Murray, P. J., Allen, J. E., Biswas, S. K., Fisher, E. A., Gilroy, D. W., Goerdt, S., Gordon, S., Hamilton, J. A., Ivashkiv, L. B., Lawrence, T., Locati, M., Mantovani, A., Martinez, F. O., Mege, J. L., Mosser, D. M., Natoli, G., Saeij, J. P., Schultze, J. L., Shirey, K. A., Sica, A., Suttles, J., Udalova, I., van Ginderachter, J. A., Vogel, S. N., and Wynn, T. A. (2014) Macrophage activation and polarization: nomenclature and experimental guidelines. *Immunity* **41**, 14-20

16. Galvan-Pena, S., and O'Neill, L. A. (2014) Metabolic reprograming in macrophage polarization. *Front Immunol* **5**, 420

17. Ajami, B., Bennett, J. L., Krieger, C., Tetzlaff, W., and Rossi, F. M. (2007) Local self-renewal can sustain CNS microglia maintenance and function throughout adult life. *Nat Neurosci* **10**, 1538-1543

18. Varol, C., Mildner, A., and Jung, S. (2015) Macrophages: development and tissue specialization. *Annu Rev Immunol* **33**, 643-675

19. Michell-Robinson, M. A., Touil, H., Healy, L. M., Owen, D. R., Durafourt, B. A., Bar-Or, A., Antel, J. P., and Moore, C. S. (2015) Roles of microglia in brain development, tissue maintenance and repair. *Brain* **138**, 1138-1159

20. Leidi, M., Gotti, E., Bologna, L., Miranda, E., Rimoldi, M., Sica, A., Roncalli, M., Palumbo, G. A., Introna, M., and Golay, J. (2009) M2 macrophages phagocytose rituximab-opsonized leukemic targets more efficiently than m1 cells in vitro. *J Immunol* **182**, 4415-4422

21. Ponce-Regalado, M. D., Perez-Sanchez, G., Rojas-Espinosa, O., Arce-Paredes, P., Giron-Perez, M. I., Pavon-Romero, L., and Becerril-Villanueva, E. (2022) NeuroImmunoEndocrinology: A brief historic narrative. *J Leukoc Biol*

22. Burnstock, G. (2018) Purine and purinergic receptors. *Brain Neurosci Adv* **2**, 2398212818817494

23. Abbracchio, M. P., and Ceruti, S. (2007) P1 receptors and cytokine secretion. *Purinergic Signal* **3**, 13-25

24. Vultaggio-Poma, V., Falzoni, S., Salvi, G., Giuliani, A. L., and Di Virgilio, F. (2022) Signalling by extracellular nucleotides in health and disease. *Biochim Biophys Acta Mol Cell Res* **1869**, 119237

25. Illes, P., Muller, C. E., Jacobson, K. A., Grutter, T., Nicke, A., Fountain, S. J., Kennedy, C., Schmalzing, G., Jarvis, M. F., Stojilkovic, S. S., King, B. F., and Di Virgilio, F. (2021) Update of P2X receptor properties and their pharmacology: IUPHAR Review 30. *Br J Pharmacol* **178**, 489-514

26. Jacobson, K. A., Delicado, E. G., Gachet, C., Kennedy, C., von Kugelgen, I., Li, B., Miras-Portugal, M. T., Novak, I., Schoneberg, T., Perez-Sen, R., Thor, D., Wu, B., Yang, Z., and Muller, C. E. (2020) Update of P2Y receptor pharmacology: IUPHAR Review 27. *Br J Pharmacol* **177**, 2413-2433

27. Cai, X., Yao, Y., Teng, F., Li, Y., Wu, L., Yan, W., and Lin, N. (2021) The role of P2X7 receptor in infection and metabolism: Based on inflammation and immunity. *Int Immunopharmacol* **101**, 108297

28. Debom, G. N., Rubenich, D. S., and Braganhol, E. (2021) Adenosinergic Signaling as a Key Modulator of the Glioma Microenvironment and Reactive Astrocytes. *Front Neurosci* **15**, 648476

29. Beaulieu, J. M., Espinoza, S., and Gainetdinov, R. R. (2015) Dopamine receptors - IUPHAR Review 13. *Br J Pharmacol* **172**, 1-23

30. Basu, S., and Dasgupta, P. S. (2000) Dopamine, a neurotransmitter, influences the immune system. *J Neuroimmunol* **102**, 113-124

31. Papa, I., Saliba, D., Ponzoni, M., Bustamante, S., Canete, P. F., Gonzalez-Figueroa, P., McNamara, H. A., Valvo, S., Grimbaldeston, M., Sweet, R. A., Vohra, H., Cockburn, I. A., Meyer-Hermann, M., Dustin, M. L., Doglioni, C., and Vinuesa, C. G. (2017) TFH-derived dopamine accelerates productive synapses in germinal centres. *Nature* **547**, 318-323

32. Arce-Sillas, A., Sevilla-Reyes, E., Alvarez-Luquin, D. D., Guevara-Salinas, A., Boll, M. C., Perez-Correa, C. A., Vivas-Almazan, A. V., Rodriguez-Ortiz, U., Castellanos Barba, C., Hernandez, M., Fragoso, G., Sciutto, E., Cardenas, G., and Adalid-Peralta, L. V.

(2019) Expression of Dopamine Receptors in Immune Regulatory Cells. *Neuroimmunomodulation* **26**, 159-166

33. Besser, M. J., Ganor, Y., and Levite, M. (2005) Dopamine by itself activates either D2, D3 or D1/D5 dopaminergic receptors in normal human T-cells and triggers the selective secretion of either IL-10, TNFalpha or both. *J Neuroimmunol* **169**, 161-171

34. Levite, M., Chowers, Y., Ganor, Y., Besser, M., Hershkovits, R., and Cahalon, L. (2001) Dopamine interacts directly with its D3 and D2 receptors on normal human T cells, and activates beta1 integrin function. *Eur J Immunol* **31**, 3504-3512

35. Nakano, K., Higashi, T., Takagi, R., Hashimoto, K., Tanaka, Y., and Matsushita, S. (2009) Dopamine released by dendritic cells polarizes Th2 differentiation. *Int Immunol* **21**, 645-654

36. Han, X., Ni, J., Wu, Z., Wu, J., Li, B., Ye, X., Dai, J., Chen, C., Xue, J., Wan, R., Wen, L., Wang, X., and Hu, G. (2020) Myeloid-specific dopamine D2 receptor signalling controls inflammation in acute pancreatitis via inhibiting M1 macrophage. *Br J Pharmacol* **177**, 2991-3008

37. Arreola, R., Alvarez-Herrera, S., Perez-Sanchez, G., Becerril-Villanueva, E., Cruz-Fuentes, C., Flores-Gutierrez, E. O., Garces-Alvarez, M. E., de la Cruz-Aguilera, D. L., Medina-Rivero, E., Hurtado-Alvarado, G., Quintero-Fabian, S., and Pavon, L. (2016) Immunomodulatory Effects Mediated by Dopamine. *J Immunol Res* **2016**, 3160486

38. Melnikov, M., Rogovskii, V., Boyksmall o, C. A., and Pashenkov, M. (2020) Dopaminergic Therapeutics in Multiple Sclerosis: Focus on Th17-Cell Functions. *J Neuroimmune Pharmacol* **15**, 37-47

39. MSIF. (2020) Atlas of MS 3rd Edition. in *MSIF*

40. Lublin, F. D., and Reingold, S. C. (1996) Defining the clinical course of multiple sclerosis: results of an international survey. National Multiple Sclerosis Society (USA) Advisory Committee on Clinical Trials of New Agents in Multiple Sclerosis. *Neurology* **46**, 907-911

41. Larochelle, C., Uphaus, T., Prat, A., and Zipp, F. (2016) Secondary Progression in Multiple Sclerosis: Neuronal Exhaustion or Distinct Pathology? *Trends Neurosci* **39**, 325-339

42. Faissner, S., Plemel, J. R., Gold, R., and Yong, V. W. (2019) Progressive multiple sclerosis: from pathophysiology to therapeutic strategies. *Nat Rev Drug Discov* **18**, 905-922

43. Liddelow, S. A., Guttenplan, K. A., Clarke, L. E., Bennett, F. C., Bohlen, C. J., Schirmer, L., Bennett, M. L., Munch, A. E., Chung, W. S., Peterson, T. C., Wilton, D. K., Frouin, A., Napier, B. A., Panicker, N., Kumar, M., Buckwalter, M. S., Rowitch, D. H., Dawson, V. L., Dawson, T. M., Stevens, B., and Barres, B. A. (2017) Neurotoxic reactive astrocytes are induced by activated microglia. *Nature* **541**, 481-487

44. Mishra, M. K., and Yong, V. W. (2016) Myeloid cells - targets of medication in multiple sclerosis. *Nat Rev Neurol* **12**, 539-551

45. Attfield, K. E., Jensen, L. T., Kaufmann, M., Friese, M. A., and Fugger, L. (2022) The immunology of multiple sclerosis. *Nat Rev Immunol*

46. Constantinescu, C. S., Farooqi, N., O'Brien, K., and Gran, B. (2011) Experimental autoimmune encephalomyelitis (EAE) as a model for multiple sclerosis (MS). *Br J Pharmacol* **164**, 1079-1106

47. Lodygin, D., Hermann, M., Schweingruber, N., Flugel-Koch, C., Watanabe, T., Schlosser, C., Merlini, A., Korner, H., Chang, H. F., Fischer, H. J., Reichardt, H. M., Zagrebelsky, M., Mollenhauer, B., Kugler, S., Fitzner, D., Frahm, J., Stadelmann, C., Haberl, M., Odoardi, F., and Flugel, A. (2019) beta-Synuclein-reactive T cells induce autoimmune CNS grey matter degeneration. *Nature* **566**, 503-508

48. Baecher-Allan, C., Kaskow, B. J., and Weiner, H. L. (2018) Multiple Sclerosis: Mechanisms and Immunotherapy. *Neuron* **97**, 742-768

49. Hauser, S. L., Bhan, A. K., Gilles, F., Kemp, M., Kerr, C., and Weiner, H. L. (1986) Immunohistochemical analysis of the cellular infiltrate in multiple sclerosis lesions. *Ann Neurol* **19**, 578-587

50. Traugott, U., Reinherz, E. L., and Raine, C. S. (1983) Multiple sclerosis. Distribution of T cells, T cell subsets and Ia-positive macrophages in lesions of different ages. *J Neuroimmunol* **4**, 201-221

51. Panitch, H. S., Hirsch, R. L., Haley, A. S., and Johnson, K. P. (1987) Exacerbations of multiple sclerosis in patients treated with gamma interferon. *Lancet* **1**, 893-895

52. Havrdova, E., Belova, A., Goloborodko, A., Tisserant, A., Wright, A., Wallstroem, E., Garren, H., Maguire, R. P., and Johns, D. R. (2016) Activity of secukinumab, an anti-IL-17A antibody, on brain lesions in RRMS: results from a randomized, proof-of-concept study. *J Neurol* **263**, 1287-1295

53. Simpson, D., Noble, S., and Perry, C. (2002) Glatiramer acetate: a review of its use in relapsing-remitting multiple sclerosis. *CNS Drugs* **16**, 825-850

54. Li, R., Rezk, A., Miyazaki, Y., Hilgenberg, E., Touil, H., Shen, P., Moore, C. S., Michel, L., Althekair, F., Rajasekharan, S., Gommerman, J. L., Prat, A., Fillatreau, S., Bar-Or, A.,

and Canadian, B. c. i. M. S. T. (2015) Proinflammatory GM-CSF-producing B cells in multiple sclerosis and B cell depletion therapy. *Sci Transl Med* **7**, 310ra166

55. Dong, Y., and Yong, V. W. (2019) When encephalitogenic T cells collaborate with microglia in multiple sclerosis. *Nat Rev Neurol* **15**, 704-717

56. Zrzavy, T., Hametner, S., Wimmer, I., Butovsky, O., Weiner, H. L., and Lassmann, H. (2017) Loss of 'homeostatic' microglia and patterns of their activation in active multiple sclerosis. *Brain* **140**, 1900-1913

57. Mack, C. L., Vanderlugt-Castaneda, C. L., Neville, K. L., and Miller, S. D. (2003) Microglia are activated to become competent antigen presenting and effector cells in the inflammatory environment of the Theiler's virus model of multiple sclerosis. *J Neuroimmunol* **144**, 68-79

58. Marik, C., Felts, P. A., Bauer, J., Lassmann, H., and Smith, K. J. (2007) Lesion genesis in a subset of patients with multiple sclerosis: a role for innate immunity? *Brain* **130**, 2800-2815

59. Ajami, B., Bennett, J. L., Krieger, C., McNagny, K. M., and Rossi, F. M. (2011) Infiltrating monocytes trigger EAE progression, but do not contribute to the resident microglia pool. *Nat Neurosci* **14**, 1142-1149

60. Yamasaki, R., Lu, H., Butovsky, O., Ohno, N., Rietsch, A. M., Cialic, R., Wu, P. M., Doykan, C. E., Lin, J., Cotleur, A. C., Kidd, G., Zorlu, M. M., Sun, N., Hu, W., Liu, L., Lee, J. C., Taylor, S. E., Uehlein, L., Dixon, D., Gu, J., Floruta, C. M., Zhu, M., Charo, I. F., Weiner, H. L., and Ransohoff, R. M. (2014) Differential roles of microglia and monocytes in the inflamed central nervous system. *J Exp Med* **211**, 1533-1549

61. Voge, N. V., and Alvarez, E. (2019) Monoclonal Antibodies in Multiple Sclerosis: Present and Future. *Biomedicines* **7**

62. Prado, C., Gaiazzi, M., Gonzalez, H., Ugalde, V., Figueroa, A., Osorio-Barrios, F. J., Lopez, E., Lladser, A., Rasini, E., Marino, F., Zaffaroni, M., Cosentino, M., and Pacheco, R. (2018) Dopaminergic Stimulation of Myeloid Antigen-Presenting Cells Attenuates Signal Transducer and Activator of Transcription 3-Activation Favouring the Development of Experimental Autoimmune Encephalomyelitis. *Front Immunol* **9**, 571

63. Dijkstra, C. D., van der Voort, E. R., De Groot, C. J., Huitinga, I., Uitdehaag, B. M., Polman, C. H., and Berkenbosch, F. (1994) Therapeutic effect of the D2-dopamine agonist bromocriptine on acute and relapsing experimental allergic encephalomyelitis. *Psychoneuroendocrinology* **19**, 135-142

64. Bissay, V., De Klippel, N., Herroelen, L., Schmedding, E., Buisseret, T., Ebinger, G., and De Keyser, J. (1994) Bromocriptine therapy in multiple sclerosis: an open label pilot study. *Clin Neuropharmacol* **17**, 473-476

65. Christian, S. L., and Berry, M. D. (2018) Trace Amine-Associated Receptors as Novel Therapeutic Targets for Immunomodulatory Disorders. *Front Pharmacol* **9**, 680

66. Boulton, A. A. (1974) Letter: Amines and theories in psychiatry. *Lancet* **2**, 52-53

67. Gainetdinov, R. R., Hoener, M. C., and Berry, M. D. (2018) Trace Amines and Their Receptors. *Pharmacol Rev* **70**, 549-620

68. Coutts, R. H., Baker, G. S., and Pasutto, F. M. (1986) Foodstuffs as sources of psychoactive amines and their precursors: content, significance and identification. *Adv. Drug Res.* **15**, 169-232

69. Berry, M. D. (2004) Mammalian central nervous system trace amines. Pharmacologic amphetamines, physiologic neuromodulators. *J Neurochem* **90**, 257-271

70. Borowsky, B., Adham, N., Jones, K. A., Raddatz, R., Artymyshyn, R., Ogozalek, K. L., Durkin, M. M., Lakhlani, P. P., Bonini, J. A., Pathirana, S., Boyle, N., Pu, X., Kouranova, E., Lichtblau, H., Ochoa, F. Y., Branchek, T. A., and Gerald, C. (2001) Trace amines: identification of a family of mammalian G protein-coupled receptors. *Proc Natl Acad Sci U S A* **98**, 8966-8971

71. Lindemann, L., and Hoener, M. C. (2005) A renaissance in trace amines inspired by a novel GPCR family. *Trends Pharmacol Sci* **26**, 274-281

72. Ferrero, D. M., Wacker, D., Roque, M. A., Baldwin, M. W., Stevens, R. C., and Liberles, S. D. (2012) Agonists for 13 trace amine-associated receptors provide insight into the molecular basis of odor selectivity. *ACS Chem Biol* **7**, 1184-1189

73. Li, Q., Tachie-Baffour, Y., Liu, Z., Baldwin, M. W., Kruse, A. C., and Liberles, S. D. (2015) Non-classical amine recognition evolved in a large clade of olfactory receptors. *Elife* **4**, e10441

74. Scanlan, T. S., Suchland, K. L., Hart, M. E., Chiellini, G., Huang, Y., Kruzich, P. J., Frascarelli, S., Crossley, D. A., Bunzow, J. R., Ronca-Testoni, S., Lin, E. T., Hatton, D., Zucchi, R., and Grandy, D. K. (2004) 3-Iodothyronamine is an endogenous and rapid-acting derivative of thyroid hormone. *Nat Med* **10**, 638-642

75. Bunzow, J. R., Sonders, M. S., Arttamangkul, S., Harrison, L. M., Zhang, G., Quigley, D. I., Darland, T., Suchland, K. L., Pasumamula, S., Kennedy, J. L., Olson, S. B., Magenis, R. E., Amara, S. G., and Grandy, D. K. (2001) Amphetamine, 3,4-methylenedioxymethamphetamine, lysergic acid diethylamide, and metabolites of the

catecholamine neurotransmitters are agonists of a rat trace amine receptor. *Mol Pharmacol* **60**, 1181-1188

76. Sotnikova, T. D., Beaulieu, J. M., Espinoza, S., Masri, B., Zhang, X., Salahpour, A., Barak, L. S., Caron, M. G., and Gainetdinov, R. R. (2010) The dopamine metabolite 3-methoxytyramine is a neuromodulator. *PLoS One* **5**, e13452

77. Liberles, S. D., and Buck, L. B. (2006) A second class of chemosensory receptors in the olfactory epithelium. *Nature* **442**, 645-650

78. Hussain, A., Saraiva, L. R., Ferrero, D. M., Ahuja, G., Krishna, V. S., Liberles, S. D., and Korsching, S. I. (2013) High-affinity olfactory receptor for the death-associated odor cadaverine. *Proc Natl Acad Sci U S A* **110**, 19579-19584

79. Lindemann, L., Ebeling, M., Kratochwil, N. A., Bunzow, J. R., Grandy, D. K., and Hoener, M. C. (2005) Trace amine-associated receptors form structurally and functionally distinct subfamilies of novel G protein-coupled receptors. *Genomics* **85**, 372-385

80. Kalinina, D. S., Ptukha, M. A., Goriainova, A. V., Merkulyeva, N. S., Kozlova, A. A., Murtazina, R. Z., Shemiakova, T. S., Kuvarzin, S. R., Vaganova, A. N., Volnova, A. B., Gainetdinov, R. R., and Musienko, P. E. (2021) Role of the trace amine associated receptor 5 (TAAR5) in the sensorimotor functions. *Sci Rep* **11**, 23092

81. Efimova, E. V., Kozlova, A. A., Razenkova, V., Katolikova, N. V., Antonova, K. A., Sotnikova, T. D., Merkulyeva, N. S., Veshchitskii, A. S., Kalinina, D. S., Korzhevskii, D. E., Musienko, P. E., Kanov, E. V., and Gainetdinov, R. R. (2021) Increased dopamine transmission and adult neurogenesis in trace amine-associated receptor 5 (TAAR5) knockout mice. *Neuropharmacology* **182**, 108373

82. Vaganova, A. N., Murtazina, R. Z., Shemyakova, T. S., Prjibelski, A. D., Katolikova, N. V., and Gainetdinov, R. R. (2021) Pattern of TAAR5 Expression in the Human Brain Based on Transcriptome Datasets Analysis. *Int J Mol Sci* **22**

83. Berry, M. D., Gainetdinov, R. R., Hoener, M. C., and Shahid, M. (2017) Pharmacology of human trace amine-associated receptors: Therapeutic opportunities and challenges. *Pharmacol Ther* **180**, 161-180

84. Loftis, J. M., Lasarev, M., Shi, X., Lapidus, J., Janowsky, A., Hoffman, W. F., and Huckans, M. (2019) Trace amine-associated receptor gene polymorphism increases drug craving in individuals with methamphetamine dependence. *PLoS One* **14**, e0220270

85. Raab, S., Wang, H., Uhles, S., Cole, N., Alvarez-Sanchez, R., Kunnecke, B., Ullmer, C., Matile, H., Bedoucha, M., Norcross, R. D., Ottaway-Parker, N., Perez-Tilve, D., Conde Knape, K., Tschop, M. H., Hoener, M. C., and Sewing, S. (2016) Incretin-like effects of small molecule trace amine-associated receptor 1 agonists. *Mol Metab* **5**, 47-56

86. Regard, J. B., Kataoka, H., Cano, D. A., Camerer, E., Yin, L., Zheng, Y. W., Scanlan, T. S., Hebrok, M., and Coughlin, S. R. (2007) Probing cell type-specific functions of Gi in vivo identifies GPCR regulators of insulin secretion. *J Clin Invest* **117**, 4034-4043

87. Regard, J. B., Sato, I. T., and Coughlin, S. R. (2008) Anatomical profiling of G protein-coupled receptor expression. *Cell* **135**, 561-571

88. Revel, F. G., Moreau, J. L., Pouzet, B., Mory, R., Bradaia, A., Buchy, D., Metzler, V., Chaboz, S., Groebke Zbinden, K., Galley, G., Norcross, R. D., Tuerck, D., Bruns, A., Morairty, S. R., Kilduff, T. S., Wallace, T. L., Risterucci, C., Wettstein, J. G., and Hoener, M. C. (2013) A new perspective for schizophrenia: TAAR1 agonists reveal

antipsychotic- and antidepressant-like activity, improve cognition and control body weight. *Mol Psychiatry* **18**, 543-556

89. Kidd, M., Gustafsson, B. I., Drozdov, I., and Modlin, I. M. (2009) IL1beta- and LPS-induced serotonin secretion is increased in EC cells derived from Crohn's disease. *Neurogastroenterol Motil* **21**, 439-450

90. Ito, J., Ito, M., Nambu, H., Fujikawa, T., Tanaka, K., Iwaasa, H., and Tokita, S. (2009) Anatomical and histological profiling of orphan G-protein-coupled receptor expression in gastrointestinal tract of C57BL/6J mice. *Cell Tissue Res* **338**, 257-269

91. Babusyte, A., Kotthoff, M., Fiedler, J., and Krautwurst, D. (2013) Biogenic amines activate blood leukocytes via trace amine-associated receptors TAAR1 and TAAR2. *J Leukoc Biol* **93**, 387-394

92. Nelson, D. A., Tolbert, M. D., Singh, S. J., and Bost, K. L. (2007) Expression of neuronal trace amine-associated receptor (Taar) mRNAs in leukocytes. *J Neuroimmunol* **192**, 21-30

93. Wasik, A. M., Millan, M. J., Scanlan, T., Barnes, N. M., and Gordon, J. (2012) Evidence for functional trace amine associated receptor-1 in normal and malignant B cells. *Leuk Res* **36**, 245-249

94. Dinter, J., Muhlhaus, J., Wienchol, C. L., Yi, C. X., Nurnberg, D., Morin, S., Gruters, A., Kohrle, J., Schoneberg, T., Tschop, M., Krude, H., Kleinau, G., and Biebermann, H. (2015) Inverse agonistic action of 3-iodothyronamine at the human trace amine-associated receptor 5. *PLoS One* **10**, e0117774

95. Espinoza, S., Salahpour, A., Masri, B., Sotnikova, T. D., Messa, M., Barak, L. S., Caron, M. G., and Gainetdinov, R. R. (2011) Functional interaction between trace amine-associated receptor 1 and dopamine D2 receptor. *Mol Pharmacol* **80**, 416-425

96. Lindemann, L., Meyer, C. A., Jeanneau, K., Bradaia, A., Ozmen, L., Bluethmann, H., Bettler, B., Wettstein, J. G., Borroni, E., Moreau, J. L., and Hoener, M. C. (2008) Trace amine-associated receptor 1 modulates dopaminergic activity. *J Pharmacol Exp Ther* **324**, 948-956

97. Liu, J., Johnson, B., Wu, R., Seaman, R., Jr., Vu, J., Zhu, Q., Zhang, Y., and Li, J. X. (2020) TAAR1 agonists attenuate extended-access cocaine self-administration and yohimbine-induced reinstatement of cocaine-seeking. *Br J Pharmacol* **177**, 3403-3414

98. Venken, T., Claes, S., Sluijs, S., Paterson, A. D., van Duijn, C., Adolfsson, R., Del-Favero, J., and Van Broeckhoven, C. (2005) Genomewide scan for affective disorder susceptibility Loci in families of a northern Swedish isolated population. *Am J Hum Genet* **76**, 237-248

99. Sotnikova, T. D., Zorina, O. I., Ghisi, V., Caron, M. G., and Gainetdinov, R. R. (2008) Trace amine associated receptor 1 and movement control. *Parkinsonism Relat Disord* **14 Suppl 2**, S99-102

100. Schwartz, M. D., Black, S. W., Fisher, S. P., Palmerston, J. B., Morairty, S. R., Hoener, M. C., and Kilduff, T. S. (2017) Trace Amine-Associated Receptor 1 Regulates Wakefulness and EEG Spectral Composition. *Neuropsychopharmacology* **42**, 1305-1314

101. Pitts, M. S., McShane, J. N., Hoener, M. C., Christian, S. L., and Berry, M. D. (2019) TAAR1 levels and sub-cellular distribution are cell line but not breast cancer subtype specific. *Histochem Cell Biol* **152**, 155-166

102. Galley, G., Beurier, A., Decoret, G., Goergler, A., Hutter, R., Mohr, S., Pahler, A., Schmid, P., Turck, D., Unger, R., Zbinden, K. G., Hoener, M. C., and Norcross, R. D. (2016) Discovery and Characterization of 2-Aminooxazolines as Highly Potent, Selective, and Orally Active TAAR1 Agonists. *ACS Med Chem Lett* **7**, 192-197

103. Koblan, K. S., Kent, J., Hopkins, S. C., Krystal, J. H., Cheng, H., Goldman, R., and Loebel, A. (2020) A Non-D2-Receptor-Binding Drug for the Treatment of Schizophrenia. *N Engl J Med* **382**, 1497-1506

104. Heffernan, M. L. R., Herman, L. W., Brown, S., Jones, P. G., Shao, L., Hewitt, M. C., Campbell, J. E., Dedic, N., Hopkins, S. C., Koblan, K. S., and Xie, L. (2022) Ulotaront: A TAAR1 Agonist for the Treatment of Schizophrenia. *ACS Med Chem Lett* **13**, 92-98

105. Bradaia, A., Trube, G., Stalder, H., Norcross, R. D., Ozmen, L., Wettstein, J. G., Pinard, A., Buchy, D., Gassmann, M., Hoener, M. C., and Bettler, B. (2009) The selective antagonist EPPTB reveals TAAR1-mediated regulatory mechanisms in dopaminergic neurons of the mesolimbic system. *Proc Natl Acad Sci U S A* **106**, 20081-20086

106. Leo, D., Mus, L., Espinoza, S., Hoener, M. C., Sotnikova, T. D., and Gainetdinov, R. R. (2014) Taar1-mediated modulation of presynaptic dopaminergic neurotransmission: role of D2 dopamine autoreceptors. *Neuropharmacology* **81**, 283-291

107. Espinoza, S., Ghisi, V., Emanuele, M., Leo, D., Sukhanov, I., Sotnikova, T. D., Chieregatti, E., and Gainetdinov, R. R. (2015) Postsynaptic D2 dopamine receptor supersensitivity in the striatum of mice lacking TAAR1. *Neuropharmacology* **93**, 308-313

108. Wolinsky, T. D., Swanson, C. J., Smith, K. E., Zhong, H., Borowsky, B., Seeman, P., Branchek, T., and Gerald, C. P. (2007) The Trace Amine 1 receptor knockout mouse: an animal model with relevance to schizophrenia. *Genes Brain Behav* **6**, 628-639

109. Asif-Malik, A., Hoener, M. C., and Canales, J. J. (2017) Interaction Between the Trace Amine-Associated Receptor 1 and the Dopamine D2 Receptor Controls Cocaine's Neurochemical Actions. *Sci Rep* **7**, 13901

110. Harmeier, A., Obermueller, S., Meyer, C. A., Revel, F. G., Buchy, D., Chaboz, S., Dernick, G., Wettstein, J. G., Iglesias, A., Rolink, A., Bettler, B., and Hoener, M. C. (2015) Trace amine-associated receptor 1 activation silences GSK3beta signaling of TAAR1 and D2R heteromers. *Eur Neuropsychopharmacol* **25**, 2049-2061

111. D'Andrea, G., Terrazzino, S., Fortin, D., Farruggio, A., Rinaldi, L., and Leon, A. (2003) HPLC electrochemical detection of trace amines in human plasma and platelets and expression of mRNA transcripts of trace amine receptors in circulating leukocytes. *Neurosci Lett* **346**, 89-92

112. Panas, M. W., Xie, Z., Panas, H. N., Hoener, M. C., Vallender, E. J., and Miller, G. M. (2012) Trace amine associated receptor 1 signaling in activated lymphocytes. *J Neuroimmune Pharmacol* **7**, 866-876

113. Bugda Gwilt, K., Olliffe, N., Hoffing, R. A., and Miller, G. M. (2019) Trace amine associated receptor 1 (TAAR1) expression and modulation of inflammatory cytokine production in mouse bone marrow-derived macrophages: a novel mechanism for inflammation in ulcerative colitis. *Immunopharmacol Immunotoxicol* **41**, 577-585

114. Cisneros, I. E., and Ghorpade, A. (2014) Methamphetamine and HIV-1-induced neurotoxicity: role of trace amine associated receptor 1 cAMP signaling in astrocytes. *Neuropharmacology* **85**, 499-507

115. Dave, S., Chen, L., Yu, C., Seaton, M., Khodr, C. E., Al-Harthi, L., and Hu, X. T. (2019) Methamphetamine decreases K(+) channel function in human fetal astrocytes by activating the trace amine-associated receptor type-1. *J Neurochem* **148**, 29-45

116. Cisneros, I. E., Ghorpade, A., and Borgmann, K. (2020) Methamphetamine Activates Trace Amine Associated Receptor 1 to Regulate Astrocyte Excitatory Amino Acid Transporter-2 via Differential CREB Phosphorylation During HIV-Associated Neurocognitive Disorders. *Front Neurol* **11**, 593146

117. Fleischer, L. M., Somaiya, R. D., and Miller, G. M. (2018) Review and Meta-Analyses of TAAR1 Expression in the Immune System and Cancers. *Front Pharmacol* **9**, 683

118. Durafourt, B. A., Moore, C. S., Blain, M., and Antel, J. P. (2013) Isolating, culturing, and polarizing primary human adult and fetal microglia. *Methods Mol Biol* **1041**, 199-211

119. Schmittgen, T. D., and Livak, K. J. (2008) Analyzing real-time PCR data by the comparative C(T) method. *Nat Protoc* **3**, 1101-1108

120. Blandford, S. N., Galloway, D. A., Williams, J. B., Arsenault, S., Brown, J., MacLean, G., Moore, G. R. W., Barron, J., Ploughman, M., Clift, F., Stefanelli, M., and Moore, C. S. (2021) Interleukin-1 receptor antagonist: An exploratory plasma biomarker that correlates with disability and provides pathophysiological insights in relapsing-remitting multiple sclerosis. *Mult Scler Relat Disord* **52**, 103006

121. Galloway, D. A., Blandford, S. N., Berry, T., Williams, J. B., Stefanelli, M., Ploughman, M., and Moore, C. S. (2019) miR-223 promotes regenerative myeloid cell phenotype and function in the demyelinated central nervous system. *Glia* **67**, 857-869

122. McWhorter, F. Y., Davis, C. T., and Liu, W. F. (2015) Physical and mechanical regulation of macrophage phenotype and function. *Cell Mol Life Sci* **72**, 1303-1316

123. Galloway, D. A., Carew, S. J., Blandford, S. N., Benoit, R. Y., Fudge, N. J., Berry, T., Moore, G. R. W., Barron, J., and Moore, C. S. (2022) Investigating the NLRP3 inflammasome and its regulator miR-223-3p in multiple sclerosis and experimental demyelination. *J Neurochem*

124. Prinz, M., and Priller, J. (2014) Microglia and brain macrophages in the molecular age: from origin to neuropsychiatric disease. *Nat Rev Neurosci* **15**, 300-312

125. Peterson, J. W., and Trapp, B. D. (2005) Neuropathobiology of multiple sclerosis. *Neurol Clin* **23**, 107-129, vi-vii

126. Qatato, M., Venugopalan, V., Al-Hashimi, A., Rehders, M., Valentine, A. D., Hein, Z., Dallto, U., Springer, S., and Brix, K. (2021) Trace Amine-Associated Receptor 1 Trafficking to Cilia of Thyroid Epithelial Cells. *Cells* **10**

127. Goncalves-Monteiro, S., Ribeiro-Oliveira, R., Vieira-Rocha, M. S., Vojtek, M., Sousa, J. B., and Diniz, C. (2021) Insights into Nuclear G-Protein-Coupled Receptors as Therapeutic Targets in Non-Communicable Diseases. *Pharmaceuticals (Basel)* **14**

128. Liao, J. J., Huang, M. C., Graler, M., Huang, Y., Qiu, H., and Goetzl, E. J. (2007) Distinctive T cell-suppressive signals from nuclearized type 1 sphingosine 1-phosphate G protein-coupled receptors. *J Biol Chem* **282**, 1964-1972

129. Barak, L. S., Salahpour, A., Zhang, X., Masri, B., Sotnikova, T. D., Ramsey, A. J., Violin, J. D., Lefkowitz, R. J., Caron, M. G., and Gainetdinov, R. R. (2008) Pharmacological characterization of membrane-expressed human trace amine-associated receptor 1 (TAAR1) by a bioluminescence resonance energy transfer cAMP biosensor. *Mol Pharmacol* **74**, 585-594

130. Kuhlmann, T., Ludwin, S., Prat, A., Antel, J., Bruck, W., and Lassmann, H. (2017) An updated histological classification system for multiple sclerosis lesions. *Acta Neuropathol* **133**, 13-24

131. Huang, X., Li, Y., Fu, M., and Xin, H. B. (2018) Polarizing Macrophages In Vitro. *Methods Mol Biol* **1784**, 119-126

132. Amadio, S., Apolloni, S., D'Ambrosi, N., and Volonte, C. (2011) Purinergic signalling at the plasma membrane: a multipurpose and multidirectional mode to deal with amyotrophic lateral sclerosis and multiple sclerosis. *J Neurochem* **116**, 796-805

133. Zha, Q. B., Wei, H. X., Li, C. G., Liang, Y. D., Xu, L. H., Bai, W. J., Pan, H., He, X. H., and Ouyang, D. Y. (2016) ATP-Induced Inflammasome Activation and Pyroptosis Is Regulated by AMP-Activated Protein Kinase in Macrophages. *Front Immunol* **7**, 597

134. Li, H., Jiang, T., Li, M. Q., Zheng, X. L., and Zhao, G. J. (2018) Transcriptional Regulation of Macrophages Polarization by MicroRNAs. *Front Immunol* **9**, 1175

135. Murray, R. Z., and Stow, J. L. (2014) Cytokine Secretion in Macrophages: SNAREs, Rabs, and Membrane Trafficking. *Front Immunol* **5**, 538

136. Braulke, L. J., Klingenspor, M., DeBarber, A., Tobias, S. C., Grandy, D. K., Scanlan, T. S., and Heldmaier, G. (2008) 3-Iodothyronamine: a novel hormone controlling the balance between glucose and lipid utilisation. *J Comp Physiol B* **178**, 167-177

137. Matejuk, A., and Ransohoff, R. M. (2020) Crosstalk Between Astrocytes and Microglia: An Overview. *Front Immunol* **11**, 1416

138. Macfarlane, D. E., Srivastava, P. C., and Mills, D. C. (1983) 2-Methylthioadenosine[beta-32P]diphosphate. An agonist and radioligand for the receptor that inhibits the accumulation of cyclic AMP in intact blood platelets. *J Clin Invest* **71**, 420-428

139. Hopkins, S. C., Dedic, N., and Koblan, K. S. (2021) Effect of TAAR1/5-HT1A agonist SEP-363856 on REM sleep in humans. *Transl Psychiatry* **11**, 228